ISTANBUL TECHNICAL UNIVERSITY ★ GRADUATE SCHOOL

A MOLECULAR DYNAMICS STUDY OF THE PRION PROTEIN

Ph.D. THESIS

Ayşenaz TAVŞANLI

Department of Molecular Biology-Genetics and Biotechnology

Molecular Biology-Genetics and Biotechnology Programme

MAY 2023

ISTANBUL TECHNICAL UNIVERSITY ★ GRADUATE SCHOOL

A MOLECULAR DYNAMICS STUDY OF THE PRION PROTEIN

Ph.D. THESIS

Ayşenaz TAVŞANLI
(521152101)

Department of Molecular Biology-Genetics and Biotechnology

Molecular Biology-Genetics and Biotechnology Programme

Thesis Advisor: Asst. Prof. Dr. Bülent BALTA

MAY 2023

ISTANBUL TEKNİK ÜNİVERSİTESİ ★ LİSANSÜSTÜ EĞİTİM ENSTİTÜSÜ

PRION PROTEİNİN MOLEKÜLER DİNAMİK SİMÜLASYONLARI İLE ARAŞTIRILMASI

DOKTORA TEZİ

Ayşenaz TAVŞANLI
(521152101)

Moleküler Biyoloji-Genetik ve Biyoteknoloji Anabilim Dalı

Moleküler Biyoloji-Genetik ve Biyoteknoloji Programı

Tez Danışmanı: Dr. Öğretim Üyesi Bülent BALTA

MAYIS 2023

Ayşenaz TAVŞANLI, a Ph.D. student of İTU Graduate School of Science Engineering and Technology student ID 521152101, successfully defended the thesis/dissertation entitled "A MOLECULAR DYNAMICS STUDY OF THE PRION PROTEIN", which she prepared after fulfilling the requirements specified in the associated legislations, before the jury whose signatures are below.

Thesis Advisor :	**Asst. Prof. Dr. Bülent BALTA** İstanbul Technical University	.....
Jury Members :	**Prof. Dr. Mine YURTSEVER** Istanbul Technical University	.....
	Prof. Dr. Canan ATILGAN Sabancı University	.....
	Asst. Prof. Dr. Sefer BADAY Istanbul Technical University	.....
	Prof. Dr. Serdar DURDAĞI Bahçeşehir University	.....

Date of Submission : 26 January 2023
Date of Defense : 12 May 2023

To my beloved family,

FOREWORD

I would like to express my deep gratidute to my advisor Asst. Prof. Dr. Bülent BALTA for giving the opportunity to meet the world of molecular dynamics and giving a chance to improve myself on a subject that I had zero experince on. I would like to thank him for believing in me, his advices, support and guidance.

I would like to thank Prof. Dr. Mine YURTSEVER and Prof. Dr. Canan ATILGAN for their support, ideas and directions.

I would like to thank TRUBA (Turkish National e-Science e-Infrastructure) and UHeM (The National Center for High Performance Computing) for providing computational facilities and CPU time.

I also would like to thank my dearest friends for their enormous support and encourage through these years.

Lastly but not leastly, I would like to thank my parents for believing in me, for their endless love, support and patience.

May 2023

Ayşenaz TAVŞANLI
(M.Sc.)

TABLE OF CONTENTS

Page

FOREWORD ..... **ix**
TABLE OF CONTENTS ..... **xi**
ABBREVIATIONS ..... **xiii**
SYMBOLS ..... **xv**
LIST OF TABLES ..... **xvii**
LIST OF FIGURES ..... **xix**
SUMMARY ..... **xxiii**
ÖZET ..... **xxv**
1. INTRODUCTION **1**
1.1 Structure of Prion Protein 1
1.2 Function of Prion Protein 4
1.3 Prion Diseases 4
1.4 Prion Protein and Endosome Pathway 10
1.5 Prion Protein Conversion and PrP^{Sc} Models 10
1.6 Prion Protein Gene (PRNP) and Mutations 14
1.7 Computational Studies 17
1.8 Aim of the Study 23
2. MATERIALS AND METHODS **25**
3. RESULTS AND DISCUSSION **27**
3.1 MD Simulations Result 27
3.1.1 ARQ simulation-1 at 310K 27
3.1.2 ARQ simulation-2 at 310K 29
3.1.3 VRQ simulation-1 at 310K 31
3.1.4 VRQ simulation-2 at 310K 32
3.1.5 ARR simulation-1 at 310K 34
3.1.6 ARR simulation-2 at 310K 35
3.2 Restrained Simulations 36
3.2.1 TPX-ARQ helix restrain 37
3.2.2 TPX-ARQ β-sheet restrain 38
3.2.3 TQB-VRQ helix restrain 40
3.2.4 TQB-VRQ β-sheet restrain 40
3.2.5 TQC-ARR helix restrain 42
3.2.6 TQC-ARR β-sheet restrain 43
3.3 ARQ, VRQ and ARR Simulations at 330K 44
3.4 VRR Simulations at 310K 47
3.5 Unfolding of H1 47
3.5.1 H1-H1 dimer formation 48
3.5.2 H1-Polybasic dimer formation 48
3.5.3 H1-Polyvaline dimer formation 50
3.5.4 N-terminal-H1 intramolecular complex formation 51
3.5.5 H1-Cl- and H1-K+ interaction 51
3.5.6 Different protonation states of H1 52

3.5.7 Potential Mean Force Energy calculations to unfold H1 54
3.5.8 H1 and adjacent sequences 57
3.5.8.1 Standard MD simulations 58
3.5.8.2 Replica exchange simulations of H1 and charged sequences 63
3.6 REMD of H2-H3 Results 70
4. CONCLUSION 79
REFERENCES 83
CURRICULUM VITAE 91

ABBREVIATIONS

Ab : Amyloid β
CD : Circular Dichroism
CJD : Creutzfeldt-Jakob Disease
CNS : Central Nervous System
fCJD : Familial Creutzfeldt-Jakob Disease
FFI : Fatal Familial Insomnia
FTIR : Fourier-transform Infrared
gCJD : Genetic Creutzfeldt-Jakob Disease
GPI : Glycosylphosphatidy-linositol
GSS : Gerstmann–Straussler–Scheinker Disease
huPrP : Human Prion Protein
iCJD : Iatrogenic Creutzfeldt-Jakob Disease
ILVs : Intraluminal Vesicles
MC/MD : Monte Carlo/Molecular Dynamics
moPrP : Mouse Prion Protein
MD : Molecular Dynamics
NMR : Nuclear Magnetic Resonance
ovPrP : Ovine Prion Protein
PDB : Protein Data Bank
PK : Proteinase K
PrP : Prion Protein
PrP^{C} : Cellular Prion Protein
PrP^{Sc} : Scrapie Prion Protein
REMD : Replica Exchange Molecular Dynamics
sCJD : Sporadic Creutzfeldt-Jakob Disease
SOD : Superoxide Dismutase
vCJD : Variant Creutzfeldt-Jakob Disease
VPSPr : Variably Protease-Sensitive Prionopathy
WT : Wild Type
TSE : Transmissible Spongiform Encephalopathies

SYMBOLS

Ala/A **:** Alanine
Arg/R **:** Arginine
Asn/N **:** Asparagine
Asp/D **:** Aspartic acid
Cys/C **:** Cysteine
Gln/Q **:** Glutamine
Glu/E **:** Glutamic acid
Gly/G **:** Glycine
His/H **:** Histidine
Leu/L **:** Leucine
Lys/K **:** Lysine
Met/M **:** Methionine
Thr/T **:** Threonine
Tyr/Y **:** Tyrosine
Val/V **:** Valine
α **:** Alpha
β **:** Beta
ε **:** Epsilon
δ **:** Delta
Δ **:** Deletion
Cu **:** Copper
Zn **:** Zinc
H **:** Helix
B **:** Beta strand
pH **:** Potential of hydrogen
K **:** Kelvin
mM **:** Millimolar
NaCl **:** Sodium chloride
NaOAc **:** Sodium acetate

LIST OF TABLES

Page

Table 1.1 : Some milestones in Prion disease chronology **8**
Table 3.1 : Sequences of 3 different variants **27**

LIST OF FIGURES

Page

Figure 1.1 : H1 (green), H2 (red) and H3 (blue) with 2 two β-strands arw shown. H2 and H3 are linked with a disulfide bridge (SS). Different variations of the protein are also represented **3**
Figure 1.2 : Octarepeats region on N-terminal of PrP **5**
Figure 1.3 : Transportation and spreading of PrPSc via exosomes in proion disease on left and protective role of exosomal PrPC in Alzheimer Disease on right **5**
Figure 1.4 : Side chains of residues in cyan are tought to bind to protein X **9**
Figure 1.5 : Scheme of PrP packaging **10**
Figure 1.6 : Sequence of prion protein; very strongly protected, strongly protected, moderately protected, and weakly protected are shown as brown, red, blue, and green, respectively, in monomer and and in fibril forms. Half-green and half-red line represents conformational heterogeneity in the fibrils **11**
Figure 1.7 : SP; spontaneously formed amyloid fibrils, PMCA; fibrils formed by protein misfolding cyclic amplification buffer **12**
Figure 1.8 : (a) β-helix model, (b) β-spiral model, (c) parallel in-register β-sheet model **14**
Figure 1.9 : Definite and possible mutations **15**
Figure 1.10 : Different PrP gene mutation and their effect on the onset and duration of the disease **16**
Figure 3.1 : Cluster number (0-7) vs. time graphic of first ARQ simulation **28**
Figure 3.2 : Different clusters and interactions of ARQ simulation **29**
Figure 3.3 : Cluster number (0-8) vs. time graphic of second ARQ simulation **30**
Figure 3.4 : Different clusters and interactions of ARQ simulation 2 ..... **30**
Figure 3.5 : Cluster number (0-40) vs. time graphic of first VRQ simulation **31**
Figure 3.6 : Different clusters and interactions of VRQ simulation 1 ..... **32**
Figure 3.7 : Cluster number (0-16) vs. time graphic of second VRQ simulation **33**
Figure 3.8 : Different clusters and interactions of VRQ simulation 2 ..... **33**
Figure 3.9 : Cluster number (0-12) vs. time graphic of first ARR simulation **34**
Figure 3.10 : Different clusters and interactions of ARR simulation 1 ..... **35**
Figure 3.11 : Cluster number (0-6) vs. time graphic of second ARR simulation **36**
Figure 3.12 : Different clusters and interactions of ARR simulation 2 ..... **37**
Figure 3.13 : Cluster number (0-7) vs. time graphic of ARQ helix restrain simulation **38**
Figure 3.14 : Different clusters and interactions of ARQ-helix simulation **39**
Figure 3.15 : Cluster number (0-14) vs. time graphic of ARQ β-sheet restrain simulation **39**
Figure 3.16 : Different clusters and interactions of ARQ-beta simulation **40**
Figure 3.17 : Cluster number (0 and 1) vs. time graphic of VRQ helix restrain simulation **41**
Figure 3.18 : Cluster and interactions of VRQ-helix simulation **41**

Figure 3.19 : Cluster number (0-3) vs. time graphic of VRQ beta restrain simulation **42**
Figure 3.20 : Clusters and interactions of VRQ-beta simulation **42**
Figure 3.21 : Cluster number (0-2) vs. time graphic of ARR helix restrain simulation **43**
Figure 3.22 : Clusters and interactions of ARR-helix simulation **43**
Figure 3.23 : Cluster number (0-7) vs. time graphic of ARR beta restrain simulation **44**
Figure 3.24 : Cluster and interactions of ARR-beta simulation **45**
Figure 3.25 : Intramolecular salt bridges were preserved while intermolecular salt bridges were also formed **49**
Figure 3.26 : Intramolecular salt bridges were preserved while intermolecular salt bridges were also formed **49**
Figure 3.27 : V12-M157 hydrogen bond formation **50**
Figure 3.28 : Unwinding of H1 ..... **50**
Figure 3.29 : Unwinding of H1 was not related to N-terminal sequence **51**
Figure 3.30 : Protonation of D147 of H1 ..... **52**
Figure 3.31 : Protonation of D150 of H1 ..... **52**
Figure 3.32 : Protonation of E149 of H1 ..... **53**
Figure 3.33 : Protonation of E155 of H1 ..... **53**
Figure 3.34 : Unfolding oh H1 when all GLU and ASP residues protonated **53**
Figure 3.35 : Energy profile to unfold H1, when only D147 (pink) of H1 was protonated **55**
Figure 3.36 : Energy profile to unfold H1, when only D150 (pink) of H1 was protonated **55**
Figure 3.37 : Energy profile to unfold H1, when only E149 (pink) of H1 was protonated **56**
Figure 3.38 : Energy profile to unfold H1, when only E155 (pink) of H1 was protonated **56**
Figure 3.39 : Unfolded H1 and {H^{99}SQWNKPSKPKTNMK^{113}} in parallel manner **59**
Figure 3.40 : Unfolded H1 and {H^{99}SQWNKPSKPKTNMK^{113}} in anti-parallel manner **59**
Figure 3.41 : Unfolded H1 and {T^{193}TTTKGENFTETDIK^{207}} in parallel manner **60**
Figure 3.42 : Unfolded H1 and {T^{193}TTTKGENFTETDIK^{207}} in anti-parallel manner **60**
Figure 3.43 : Unfolded H1 and {K^{197}GENFTETDIKIMER^{211}} in parallel manner **61**
Figure 3.44 : Unfolded H1 and {K^{197}GENFTETDIKIMER^{211}} in anti-parallel manner **61**
Figure 3.45 : Starting structure determined the final conformation of H1 ..... **62**
Figure 3.46 : Loop structure could not unfold helical H1 ..... **62**
Figure 3.47 : Loop structures protected their beginning position **63**
Figure 3.48 : REMD result of H1 and H1B1 loop together. A) Helical structure that was dominant through the simulation, B) 4% of the simulation showed loop conformation with a helical part **64**
Figure 3.49 : REMD result of two H1 strands **65**
Figure 3.50 : REMD result of H1-{K^{197}GENFTETDIKIMER^{211}} **65**
Figure 3.51 : REMD result of H1-{H^{99}SQWNKPSKPKTNMK^{113}} **66**
Figure 3.52 : REMD result of two loop H1-{H^{99}SQWNKPSKPKTNMK^{113}} **67**

Figure 3.53 : REMD result of two loop H1-{H^{99}SQWNKPSKPKTNMK^{113}}, helix formation..... **68**
Figure 3.54 : Circle like structure (left), hairpin structure (right)..... **71**
Figure 3.55 : Increased β-sheet content when ETDIK, KIMER, VVEQM, ERVVE, MERVV, TKGEN, TTTKG, KQHTV residues restrained separately in different REMD simulations..... **71**
Figure 3.56 : Short β-sheet formation when VNITV, NITVK, HTVTT, TTTTK, TTKGE and GENFT residues restrained separately in different REMD simulations..... **73**
Figure 3.57 : Circle-like shape when QHTVT, HTVTT, TTKGE, FTETD residues restrained separately in different REMD simulations **75**
Figure 3.58 : Only restrained TTTTK, TVKQH and NFTET showed β-sheet structure when restrained separately in different REMD simulations, the rest was in helical shape formation..... **75**
Figure 3.59 : Dimerization potential of restrained KIMER and ETDIK **77**

A MOLECULAR DYNAMICS STUDY OF THE PRION PROTEIN

SUMMARY

Transmissible spongiform encephalopathies are caused by the conversion of the cellular prion protein PrP^{C} into a misfolded form, PrP^{Sc}. In sheep populations there is a polymorphism at positions 136 (alanine/valine), 154 (arginine/histidine) and 171 (arginine/glutamine). While the A136-R154-R171 (ARR) variant confers highest resistance to scrapie, the V136-R154-Q171 (VRQ) variant leads to highest scrapie susceptibility. The A136-R154-Q171 (ARQ) variant with intermediate resistance is considered as wild type. To identify important conformational rearrangements at the initial steps of misfolding, microseconds long restrained and unrestrained molecular dynamics simulations have been prefomed at neutral pH, at 310 K and 330 K on naturally existing prion variants. Also, unfolding potentials of all three helicas of prion protein structure were also conducted at differentiated temperatures with the help of replica exchange molecular dynamic simulations. Moreover, at differentiated pH conditions unfolding potential of helix 1 and interaction of helix 1 with some other sequences were also conducted.

Susceptibility of the disease might be related to hyrophobic side chain of the valine at position 136 which seemed to ease the unfolding process. While arginine at position 171 worked as a clamp to keep helix 2 and helix 3 of the cellular prion protein structure together. That might be the reason why VRQ is the most susceptable one where ARR is the most resistance. On the other hand, unfolding of helix 1 played the most critical role since it was the most stable helical structure in all conducted simulations. Inter- and/or intramolecular salt bridges of helix 1 were important to keep helix 1 stable in both helical structure and/or unfolded structure. Energy calculation showed that not high energy was needen to unwind helix 1. This helical structure of hydrophilic H1 might be broken by another hydrophilic sequence of the same prion protein, and its unwinding might be the key point to catalyze the complete unfolding of the protein.

PRION PROTEİNİN MOLEKÜLER DİNAMİK SİMÜLASYONLARI İLE ARAŞTIRILMASI

ÖZET

Transmissible spongiform encephalopathies (Bulaşıcı süngerimsi ensefalopatiler) hücresel prion proteini olan PrP^{C}'nin yanlış katlanmış, açılmış yapı olan PrP^{Sc}'ye dönüşmesi sonucu ortaya çıkar. Koyun populasyonunda; pozisyon 136 (alanin/valin), 154 (arjinin/histidin) ve 171 (arjinin/glutamin)'de olmak üzere üç faklı çeşitlilik söz konusudur. A136-R154-R171 (ARR) varyantı koyunlarda gözlenen deli dana hastalığına yüksek dayanıklılık gösterirken; V136-R154-Q171 (VRQ) varyantı bu hastalığa yüksek oranda yatkınlık göstermektedir. A136-R154-Q171 (ARQ) varyantı ise orta seviyede hastalığa dayanıklılık gösterir ve doğadaki vahşi tip olarak kabul edilir. Yanlış katlanmanın ilk aşamalarındaki önemli yapısal şekillenmeleri belirlemek adına, nötr pH'da 310 K ve 330 K sıcaklıklarında kısıtlama getirilen ve getirilmeyen şartlarda mikrosaniye uzunluğunda doğada var olan üç varyant incelenmiştir. Ayrıca, prion proteinin yapısında bulunan üç heliks replika değişim moleküler dinamik simulasyonları sayesinde farklı sıcaklıklarda incelenmiş ve açılma potensiyallerine bakılmıştır. Heliks 1'in farklı pH değerlerindeki açılma durumu ve heliks 1'in diğer amino asit dizilimleri ile olan etkileşimi de ayrıca çalışılmıştır.

Hastalığa yatkınlık VRQ varyantında 136. pozisyonda bulunan valinin geniş yan hidrofobik yan zincirinden kaynaklı olabilir. Alanin bulunduran diğer varyantlardan farklı olarak valinin varlığı bulunduğu ortamda hidrofobik alana geçmesiyle bir gerilim yaratmakta ve helix 1'in helix 2 ve 3'ten ayrılmasını kolaylaştırmaktadır. ARQ ve ARR varyantındaki alanin ise küçük yan zincirinden dolayı rahatlıkla hidrofilik ve hidrofobik alanlarda bulunabilmekte ve valin kadar ortamda bir gerilim yaratmadan farklı şekilde konumlanabilmektedir.

ARR varyantında bulunan ve 171. pozisyonda yer alan arjinin ise hücresel prion proteinin yapısını bir arada tutan bir klips misali heliks 2 ve heliks 3'ü bir arada tuttuğu gözlenmiştir. Bu görevin yapıyı sağlamlaştırdığı düşünülecek olunursa VRQ'nun hem valin'den dolayı gevşeyen yapısı hem de glutaminin yapıyı tutmaması nedeniyle hastalığa yatkın olması açıklanabilinir. Aynı şekilde ARR'nin hem 136. pozisyonda alanin hem de 171. pozisyonda arjinin içermesi ise en dayanıklı varyant olduğunu açıklamakla kalmayıp, ARQ'nun da ARR'den neden daha zayıf bir yapıya sahip olduğunu da bize göstermektedir.

Heliks 1'in tüm simulasyonlarımızda bu kadar sabit bir yapıda olduğunu görmek, helix 1'in yapısal değişimde kritik bir rol üstlendiğini bize düşündürdü. Helix 1'in moleküler içi ve moleküler arası oluşturduğu tuz köprüleri yapının stabilitesinde önemli rol oynamakta idi. Bu etkileşimlerin, heliks yapısını korumakta etkili olduğu gibi, heliks yapısının bozulması sonrası aynı zamanda da bozuk yapının korunmasında da etkili olduklarını gözlemledik.

Düşük pH'ın prion proteinin bozulmasını tetikleği bilinmekte olup; düşük pH'ın heliks 1'in üzerindeki etkisini incelemek üzere yapısında bulunan glutamik asit ve aspartik

asitlerin protone durumlarını birer birer veya hepsini aynı anda değiştirerek yapığımız gözlemlerde, heliks 1'deki tam açılma sadece tüm aspartik ve glutamik asitler protone olduğunda söz konusu olmuştur.

Heliks 1'in farklı sekanslarla dimer oluşturma potansiyeli de incelenmiştir. Buna bağlı olarak; 2 adet heliks 1 sekansının dimer oluşumu, bazı bazik sekanslar ile heliks 1'in etkileşimi, valin yapı birimlerin oluşan beta zinciri ile heliks 1'in dimer oluşumu, bazı iyonların heliks 1 üzerindeki etkisi ve heliks 1'in simulasyonlar kullanmadığımız hücre zarı ile etkileşime giren N-ucu ile olan dimer oluşturma kapasitesi de mercek altına alınmış olup; helix 1'in tamamen açılması için gerekli olan şartlar sağlanmaya çalışılmıştır.

Heliks 1'in tamamen açılması ve heliks yapısından uzaklaşması sağlayacak enerji miktarı da hesaplanarak gerekli olan enerjinin aslında hiç de yüksek olmadığı görülmüştür. Bu sonuca istinaden heliks 1 yapısı replika değişim moleküler dinamik simülasyonuna tabi tutulup, yapının açılması için gerekli olan enerji bariyerlerinin kolayca aşılması amaçlanmıştır.

Başlangıç geometrisi açılmış bir yapı olarak seçilen heliks 1 hem standart 310K moleküler dinamik simulasyonunda hem de replika değişim moleküler dinamik simulasyonunda, prion proteinin yapısında bulanan bazı yüklü sekanslar ile etkileşimi incelenmiştir. Pozitif yüklü sekansların heliks 1'i bozarak bu şekilde tutma kapasitesini olduğu anlaşılmıştır. Bu basamağın proteinin tamamen bozulması için gerekli en önemli adımlardan biri olduğu kanaatine varılmştır. Özellikle hidrofilik {H^{99}SQWNKPSKPKTNMK^{113}}sekansının heliks 1 yapısını bozulmuş bir şekilde tutma kapasitesi hem standart moleküler dinamik simulsyonu ile hem de replika değişim moleküler dinamik simulasyonu ile çift kontrol yapılarak gösterilmiş ve yapıyı bozuk tutmadaki en önemli aday sekans olarak öne çıkmıştır. Heliks 1'deki bu çözülme eyleminin ve bu şekilde açık olarak kalmasının tüm prion proteinin yapısındaki değişimi için önemli bir adım olduğuna inanılmaktadır.

Aynı şekilde heliks 2 ve heliks 3'ün de birlikte oluşturdukları kompleks yapılar replika değişim moleküler dinamik simulasyonları ile incelenmiştir. Yanlızca bu iki heliks yapının birlikte incelenmesindeki sebep; sadece iki bölgenin varlığında da hastalığın ortaya çıktığının bilinmesinden dolayıdır. Bu iki bölgenin incelenmesi sırasında sanki daha önceden yapıyı bozan bir prion proteinin varlığı kabul edilerek, heliks 2 ve heliks 3 üzerindeki beş yapı birimlik alan sabitlenerek beta ipliği oluşturacak şekilde simule edilmiştir. Bu beş birimlik bölgeler her bir simulasyon için farklı alanda oluşacak şekilde yapılmış ve toplam otuz adet sabitlenmiş bölge otuz adet farklı replika değişim moleküler dinamik simulasyonu ile incelenmiş ve bu iki heliks bölgesinin beta ipliği oluşturma potansiyeli gözlenmiştir. Yapılan simulasyonlar sonu bazı aday bölgeler elde edilmişse bile, bu yapıların dimerizasyonu çok fazla incelenmemiş; sadece aday olan iki bölge üzerinde durulmuştur.

Heliks 1 gibi, heliks 2 ve heliks 3'ün birlikte çalışıldığı simulasyonlardan elde edilen sonuçlar ile olası yapısal düzenleme çalışmaları yapılmalı, bu sonuçlar ile belirlenen aday bölgelerin prion proteinin kalan kısımları ile olan ilişkisine ve oluşturabileceği kompleks yapılara ayrıntılı bir şekilde bakılmalıdır. Her ne kadar tek başlarına heliks 2 ve heliks 3 hastalık yapıyor olsa bile, heliks 1'in varlığında da alacakları konformasyonel olası şekiller düşünülmeli ve birbirleri üzerine yapacakları katlanmaları göz önünde bulundurularak olası yanlış katlanmış prion protein yapıları oluşturulmalıdır.

Hâlâ hastalıklı yapının tam olarak şeklinin bilinmiyor olması ve hastalığa sadece belli başlı bölgelerin bile sebep olmasından dolayı, heliks 1, helik 2 ve heliks 3'ün bozulması ve açılması sonucu ile farklı konformasyonel yapıların oluşabileceği göz ardı edilmemelidir. Oluşabilecek tüm farklı yapılardaki ortak bir noktanın bulunması da hastalığın tüm alt tiplerinin tedavisi için ortak bir çözüm olacaktır.

1. INTRODUCTION

In many neurodegenerative disorders, some specific proteins misfold and aggregate as proteinaceous seeds that structurally corrupt native proteins, causing them to aggregate (Jucker and Walker, 2013). Protein misfolding and protein deposit formation is observed in as Alzheimer's disease, Parkinson's disease (Silveira et al., 2005), Huntington's disease, amyloid polyneuropathy (Colacino et.al., 2006).

This misfolding of endogenous proteins lead to protein aggregation such as amyloid fibril-rich deposits, like misfolding of the mammalian prion protein (Larda et al., 2013). Transmissible Spongiform Encephalopathies (TSE) are caused by the misfolding of prion proteins (De Simone et al., 2007), which is a glycoprotein (Wadsworth et al., 2003; Ribeiro and Alencastro, 2013). These aggregates may range from small oligomers to large masses of amyloid that functionally affects the nervous system by gaining a toxic function and/or lose their normal function, in the end causing death (Jucker and Walker, 2013). Term "prion" derived from proteinaceous and infectious and defined as proteinaceous infectious particles (Prusiner, 1998). However, the pathogenic "seed" is not well understood whether it is formed from one or more molecules (Frost and Diamond, 2010).

1.1 Structure of Prion Protein

Prion protein (PrP) is the cause of TSEs like Creutzfeldt−Jakob disease and bovine spongiform encephalopathy. The normal form of PrP (PrP^{C}) is monomeric and soluble, but pathogenic form (PrP^{Sc}) has a high β-structure content and can aggregate into amyloid fibrils (Vila-Viçosa et al., 2012). Prion diseases result from the misfolding of normal prion protein (PrP) from its cellular form (PrP^{C}) to a virulent scrapie form (PrP^{Sc}). This abnormal scrapie form catalyzes the conversion of PrP^{C} to itself (Prusiner, 1998).

The biological function of PrP is not yet fully understood, but it may have a role in signal transduction e.g., for olfactory signals, and the regulation of metal metabolism

(Van der Kamp and Daggett, 2009). Human PrP is a cell surface copper-binding (Prusiner, 1998) protein with 208 residue (23–230) and with up to two carbohydrate moieties (linked by N-glycosylation) and a glycosylphosphatidy-linositol (GPI)-anchor at C-terminus (Van der Kamp and Daggett, 2009).

Human PrP^{C} has a flexible N-terminal domain with no defined structure (aa 23−124) (Rossetti and Carloni, 2017), a globular domain (125–228) which consists of three helices and a short antiparallel β-sheet, and a short flexible C-terminal domain (229–230/231) (Van der Kamp and Daggett, 2009). Protein itself is associated largely with neuronal membranes, dominantly in alpha helical structure (Van der Kamp and Daggett, 2009). NMR structure of PrP^{C} shows that N-terminal part is unstructured but C-terminal globular domain is structured, having three α-helices and two short β-strands (Prusiner, 1998; Diaz-Espinoza and Soto, 2012), and a C-terminal glycosylphosphatidylinositol anchor at its C-terminal Ser231 which anchors it to outer surface of cell membrane (Prusiner, 1998; Van der Kamp and Daggett, 2011). It also includes a disulfide bond between C179 and C214 and is glycosylated at Asn181 and Asn197 (Stahl et al., 1993; Van der Kamp and Daggett, 2011) in un-, mono-, and diglycosylated forms (Singh and Udgaonkar, 2015a). In mammalians, PrP^{C} has 210 amino acids H1 (144–153), H2 (172–192), and H3 (200–225), and a double-stranded antiparallel β-sheet, S1 (129–130) and S2 (162–163) (De Simone et al., 2007). The human prion protein is a single gene PRNP product which is located on the short arm of chromosome 20 and the result is 253 amino acids long with signal sequences at both ends that are removed post-translationally. It also has five amino-terminal octapeptide repeats (Singh and Udgaonkar, 2015a; Mead, 2006).

The amino acid sequences of PrP^{C} and PrP^{Sc} are the same, so there are no chemical differences, but they differ in structural design. PrP^{C} is dominantly α-helical in structure (Prusiner, 1998; Stahl et al., 1993), but PrP^{Sc} has a high β-sheet structure (Requena and Wille, 2014). Moreover, replacement of some amino acids in prion protein catalayze its conformational transition from PrP^{C} to PrP^{Sc} (Van der Kamp and Daggett, 2011).

Mutations in the β2–α2 loop have effect on susceptibility like S170N and N174T can cause spontaneous TSE (Taguchi and Schätzl 2013), but in mouse Y169G, S170N, N174T show resistance to infection (Caldarulo et al., 2017).

It is believed that B1-H1-B2 is important for β-sheet seeding and it has been suggested that H1 is the primary interaction site for this conversion (Adrover et al., 2010), also the C terminus of H3 may be the recognition point for PrP^{Sc} also known as Protein-X (Prusiner, 1998). β-sheet core of amyloids is formed by H2, a major part of H3, and the loop between them and the rest of PrP does not contribute to oligomer formation efficiently (Adrover et al., 2010).

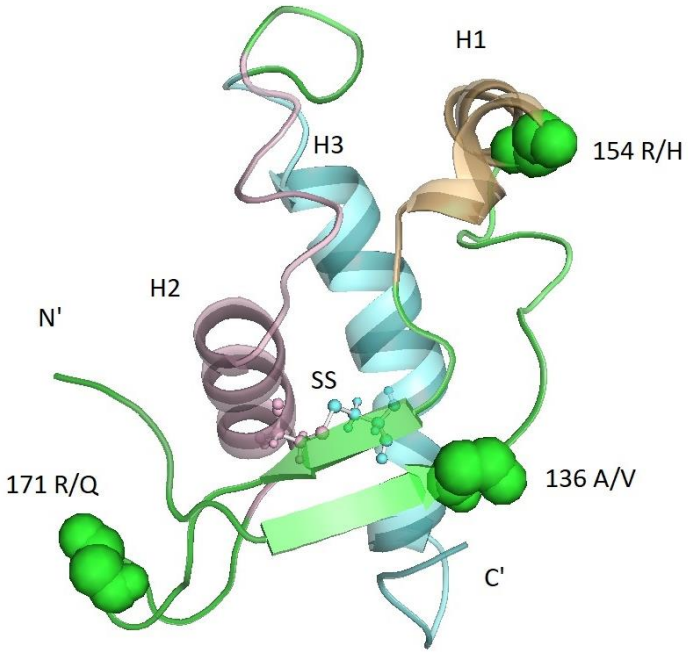

Figure 1.1: H1 (orange), H2 (pink) and H3 (blue) with 2 two β-strands are shown. H2 and H3 are linked with a disulfide bridge(SS). Different variations of the protein are also represented(Chen et al., 2011).

The polymorphism of ovine PrP gives some information about the scrapie susceptibility (Cosseddu et. Al., 2007). Polymorphisms of ovine PrP (ovPrP) are positioned at 136 (A/V), 154 (H/R), and 171 (Q/R) (Figure 1.1). The A136R154R171 (ARR) and A136H154Q171 (AHQ) alleles show resistance, whereas the V136R154Q171 (VRQ) and A136R154Q171 (ARQ) genotypes are related with susceptibility. The allele ARQ is the wild type with low resistancy. On the other hand, ARR shows the hight resistance, but VRQ has the highest susceptibility (Cosseddu et. Al., 2007).

PrP amyloid fibrils may be toxic and/or infective, and also evidence suggests that soluble misfolded oligomeric forms of PrP are toxic and/or infectious. Low pH environments, such as in the endocytic pathway, seem to favor misfolding and

aggregation of PrP. The oligomers that are formed after misfolding can disrupt lipid membranes. Conformational conversion of helix 2 and helix 3 into β structure in the oligomers defines the big step in oligomerization. The isolated helix 2 and 3 forms oligomers faster than full length PrP does, suggesting that interactions with helix 1 protect PrP from oligomerization (Singh and Udgaonkar, 2015a).

1.2 Function of Prion Protein

The function of PrP^C is not well known (Singh and Udgaonkar, 2015a). Normal prion protein (PrP^C) is a glycosylated, glycosylphosphatidylinositol-anchored cell surface glycoprotein of neuron cells (Sakudo et al., 2010). In the NMR structures the disordered N-terminal end of the prion protein (aa 51-91) consists of octapeptide repeats (Figure 1.2). That part may form a complex with copper ions (Prusiner, 1998; Linden, 2017; Rossetti and Carloni, 2017) or other metals (Singh and Udgaonkar, 2015a). Optical spectroscopy revealed that Cu^{2+} induces an α-helix formation in these peptides. It was observed that deletion of one octapeptide repeat is not associated with prion disease in humans (Wadsworth et al., 2003). PrP-deficient mice showed lower levels of Zn/Cu superoxide dismutase (SOD) activity which is important for copper metabolism (Prusiner, 1998). PrP^C is actually more dominant in the hippocampus, meaning it may have a function in memory, and it also has a protection role in neuroprotection. PrP^C appears to have a role in signal transduction, besides homeostasis of copper, it functions in cellular signaling, neuroprotection, cell adhesion and synaptogenesis. As functions of the prion protein (PrP), protection of neural cells against oxidative stress, hypoxia, ischemia, and hypoglycemia can be listed (Linden, 2017).

Prion protein may also function as a cell surface scaffold protein, and it may be related to immune response, energy metabolism, cancer, and stress conditions (Linden, 2017).

PrP^C is also found on exosomes which promotes spreading of PrP^{Sc} in prion disease but plays a protective role in Alzheimer disease (Figure 1.3) (Hartmann et al., 2017).

1.3 Prion Diseases

As part of neurodegenerative diseases, human transmissible spongiform encephalopathies (TSEs) are rare and show complex epidemiology and phenotypic

variability (Head and Ironside, 2012) and are fatal neurodegenerative disorders (Linden, 2017).

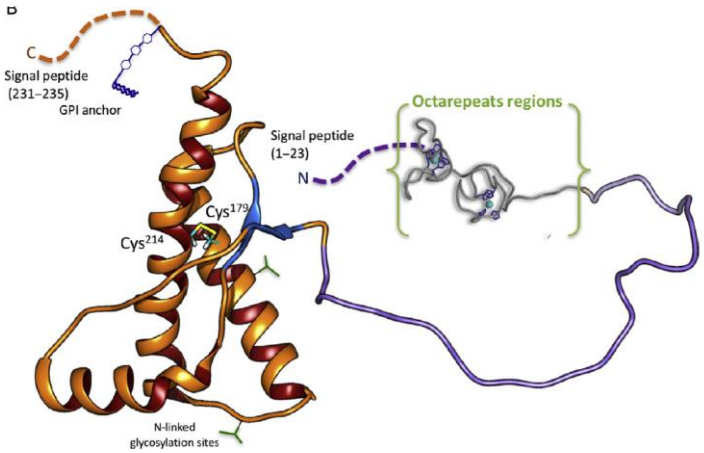

Figure 1.2: Octarepeats region on N-terminal of PrP (Rossetti and Carloni, 2017).

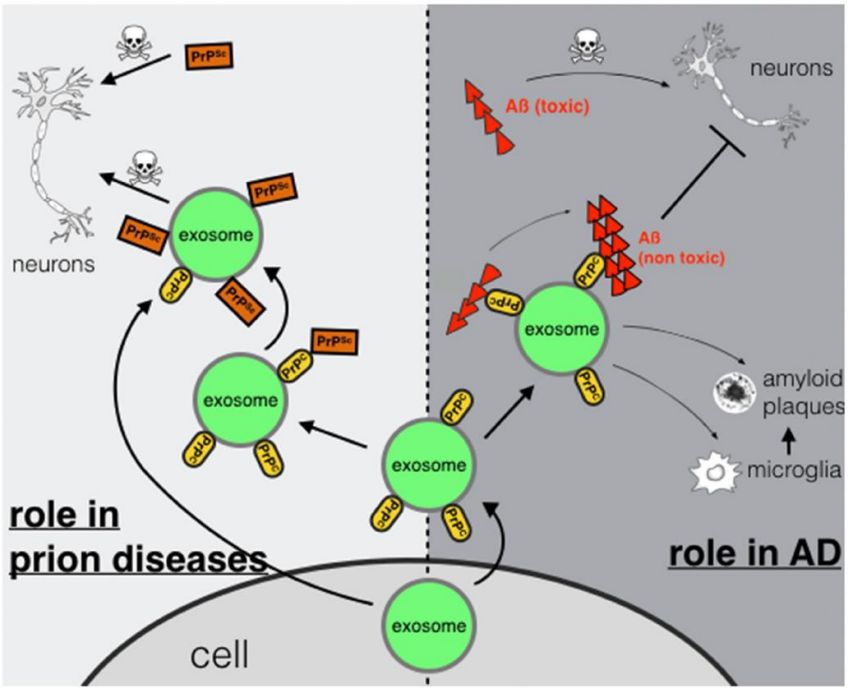

Figure 1.3: Transportation and spreading of PrP^{Sc} via exosomes in prion disease on left and protective role of exosomal PrP^{C} in Alzheimer Disease on right (Hartmann et al., 2017).

According to protein only hypothesis, there are two forms of this protein: benign PrP^{C} form and infectious scrapie form (PrP^{Sc}). β-sheet existence in PrP (121-231) may be considered as initiation of the transition from PrP^{C} to PrP^{Sc} (Riek et al. 1996).

The prion protein only hypothesis remarks that possible exposure to disease-associated isoform a virulent form, PrP^{Sc}, starts a conformational change from naturally existing PrP^{C} to PrP^{Sc} (Head and Ironside, 2012) which is insoluble and partially resistant to

proteases and form self-aggregates (Head and Ironside, 2012). So PrP^{Sc} binds to PrP^{C} templating autocayalytic conversion/transition of native protein to misfolded PrP^{Sc} conformation (Aguzzi, 2006).

Bacterially expressed recombinant murine PrP was generated and injected intracerebrally into mice, to prove once more that altered conformation of the prion protein indeed the reason of the disease (Wang et al., 2010).

PrP^{Sc} recruites and converts native PrP^{C} molecules, resulting in the formation of oligomers and larger aggregates. Prion protein aggregation may be formed both extracellularly and intracellularly (Ross and Poirier, 2004), deposited in neuronal plaques which are one of the hallmarks of prion disease (Head and Ironside, 2012), having a long silent incubation time. An autopsy study showed that 40% of cases were undiagnosed while they were alive (Mead, 2006).

Humans TSEs are mainly caused by transplantion of tissue or blood transfusions or consumption of infected beef products (Aguzzi, 2006; Zhang et al., 2015). PrP^{Sc} can exist in multiple conformations according to infection of different strains of TSE agent. Treatment of PrP^{Sc} with PK generates a C-terminal PK-resistant core (PrP 27-30). In addition, two novel PK-resistant fragments were identified recently in patients with sporadic CJD (cleavage at residues 154/156 and 162/167). Multiple factors such as gene polymorphism, glycosylation, and/or other cellular factors may contribute to conformational diversity of PrP^{Sc} (Bocharova et al., 2005).

Even tiny quantities of PrP^{Sc} exposure can trigger the autocatalytic conversion of host PrP^{C} to PrP^{Sc}. Small PrP^{Sc} aggregate acts as a nucleus to recruit monomeric PrP^{C} into the growing PrP^{Sc} polymer. For PrP^{Sc} to produce TSEs, sufficient number of agents are needed to trigger prion replication. Moreover, when prions enter the body by consumption of contaminated food, that protein should resist degradation in the digestive system and penetrate the intestinal barrier (Soto, 2012).

Even tough the mechanism of disease/transition is not well understood (Wadsworth et al., 2003; Ribeiro and Alencastro, 2013); it is known that the cellular form of prion (PrP^{C}), under physiological conditions, can change into the harmful abnormal scrapie form (PrP^{Sc}). PrP^{C} is highly riched in alpha-helical, on the other hand PrP^{Sc} is highly enriched in β-structure (Prusiner, 1998). This misfolded prion protein, PrP^{Sc}, accumulates inside the brain, forming amyloid plaques, resulting in neuronal cell loss,

vacuolation of brain tissue, cognitive loss, motor deficits, and death (Sepulveda et. al., 2016; Aguzzi, 2006; Hosszu et al.2010). These β-sheet-rich aggregates are also infectious (Diaz-Espinoza and Soto, 2012; Stöhr et al., 2008).

Prion disease can be classified as infectious, familial, and sporadic forms (Prusiner, 1998; Shamsir and Dalby, 2005; Jucker and Walker, 2013). The most common TSE is Creutzfeldt–Jakob disease in humans (CJD) (Prusiner, 1998; Aguzzi, 2006), and it was first discovered in 1920s (Aguzzi, 2006). It can be classified as sporadic (sCJD), familial (fCJD), iatrogenic (iCJD), and variant (vCJD). Sporadic form is the most frequent one (about 85% of cases of disease) (Wadsworth et al., 2003), but even that is rare (Aguzzi, 2006). CJD's occurance is one or two cases per million each year which are mostly idiopathic and so called sporadic CJD (sCJD) and it is characterized by shorter duration period affecting elders. Familial or genetic forms of the disease (fCJD or gCJD) include point mutations, insertions, and deletions in the prion protein gene, PRNP (Head and Ironside, 2012). Transmission of familial form is in autosomal dominant pattern (Aguzzi, 2006). Iatrogenic CJD (iCJD) occur as a result of transfer of growth hormone derived from the pituitary glands of contaminated human cadavers, dura mater grafting, surgical instruments, stereotactic EEG electrodes and corneal transplantation (Wadsworth et al., 2003; Mead,2006; Head and Ironside, 2012). Variant CJD (vCJD) pass through blood transfusion from asymptomatic infected people (Wadsworth et al., 2003). vCJD has an early age at onset showing behavioural or psychiatric signs, with long disease duration. Then, sensory abnormalities, ataxia, and dementia are observed (Head and Ironside, 2012). To sum up, prion disease may be sporadic, can occur with environmental transmission (from eating infected brain tissue or via infected surgical instruments) or with genetic mutations (Ross and Poirier, 2004). Most of the prion diseases arise sporadically or through inherited mutations (Frost and Diamond, 2010).

The pathology of a prionotic brain characterized by spongiform degeneration, loss of neurons, gliosis, and the accumulation of aggregated PrP forming amyloid (Jucker and Walker, 2013). Symptoms of CJD include neuronal loss, spongiform change, and amyloid plaques formation, and these plaques are the assets of the disease pathology (Head and Ironside, 2012). But these plaques observed not only in Creutzfeldt-Jakob disease, but in Alzheimer's, Parkinson's disease too (Diaz-Espinoza and Soto, 2012). Soluble peptides and proteins come together as soluble oligomeric structure and end

up in insoluble amyloid fibrils. How amyloid plaques are causing neurotoxicity is still not clear, but in Alzheimer's disease; it has been shown that β amyloid peptides form aggregates that cause ion-conducting pores in neuronal membranes, which lead to imbalance calcium ions across the membranes, causing cell death or trigger the signaling for apoptosis (Ding et al., 2012).

In nonhuman species; scrapie in sheep, bovine spongiform encephalopathy in cattle (mad cow diseases) (Prusiner, 1998; Stöhr et al., 2008; Hosszu et al.2010), chronic wasting disease in cervids (deer and elk) (Prusiner, 1998; Larda et al., 2013; Choi et al., 2016), transmissible mink encephalopathy can be observed (Jucker and Walker, 2013). On the other hand, rabbits, horses, and dogs do not affected by prions. Salt bridges, that are known, are absent in disease causing human mutants of the prion protein, but those salt bridges which are stable can be observed in species known to be resistant to prion disease like frog (Zhang et al.,2015).

Table 1.1: Some milestones in Prion disease chronology (Aguzzi, 2006).

Years	Discoveries
Mid 18th century	Earliest description of scrapie recorded.
1920	First possible cases of CJD described.
1939	Experimental transmission of scrapie reported.
1955–57	Kuru discovered among Fore people of Papua New Guinea.
1959	Similarities between Kuru and scrapie noted.
1961	Multiple strains of scrapie agent described.
1961	Scrapie transmitted to mice.
1963	Transmission of Kuru to chimpanzees reported.
1967	First statement of the protein-only hypothesis.
1980	Protease resistant, highly hydrophobic protein discovered in hamster brain fractions highly enriched for scrapie infectivity.
1989	Mutation in PrP linked to Gerstmann–Straussler syndrome. Importance of isologous PrP^{C}/PrP^{Sc} interactions established.
2003	Transgenic expression of soluble PrP inhibits prion replication.

Residues 180–205 seem to be the region responsible for interaction between PrP^{C} and PrP^{Sc}. Side chains of residues 168, 172, 215, and 219 are involved in binding of PrP^{C} to PrP^{Sc} (Prusiner, 1998). These are shown in cyan in Figure 1.4.

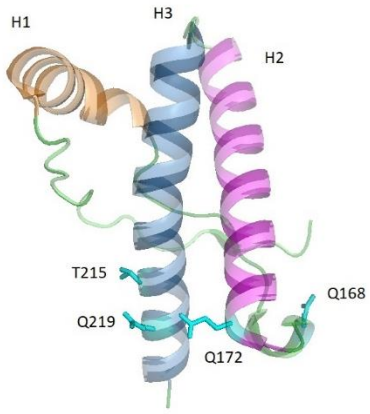

Figure 1.4: Side chains of residues in cyan are tought to bind to protein X (Prusiner, 1998).

Low-resolution technics showed a high β-sheet content. Proteinase K (PK) treatment is used to discriminate PrP^{Sc} from PrP^{C}. This treatment totally digests PrP^{C} but leaves about 60 to 70 N-terminal residues of PrP^{Sc} according to prion strains and keeping a protease-resistant part which is highly infectious (135 to 150 residues) (Munoz-Montesino et al., 2016).

Main feature of TSEs is the deposition of aggregated and structurally abnormal protein in the brain and lymphoreticular tissues. There is a long incubation time of prion disease, varying from several years to several decades. Some PRNP mutations cause octapeptide repeat expansion both in mouse and man. Besides from mutations, PRNP may also comprise polymorphisms that increase susceptibility to prion disease (Aguzzi, 2006). As genetic polymorphism, codon 129 codes for either methionine (M) or valine (V) (Wadsworth et al., 2003) but M is more dominant (Wadsworth et al., 2003, Head and Ironside, 2012). All cases of vCJD have the MET/MET, rather than the VAL/VAL or MET/VAL configuration at position 129. A LYS, rather than a GLU residue at position 219 is thought to be more protective against sCJD. There is no disease specific nucleic acid so that the 'protein-only' hypothesis is the only reasonable theory. Peptides derived from the PrP region 106–126 form aggregates and are toxic to cultured neuronal cells (Aguzzi, 2006). Scrapie agent entering from the oral route, transferred from the intestinal mucosa via the M cells (uptake of macromolecules from lumen) to the central nervous system (CNS) (Cosseddu et. Al., 2007). Nevertheless,

neither physico-chemical nature of the agent is known, nor the function of the normal prion protein (Aguzzi, 2006).

1.4 Prion Protein and Endosome Pathway

PrP^{Sc} is related with extracellular vesicles known as exosomes. The exact mechanism how prion disease is transmitted intercellularly is not yet fully identified but direct cell-cell contact, tunnelling nanotubes, and extracellular vesicles such as microvesicles and exosomes have been proposed as a mechanism to spread prions intercellularly. Exosomes are also capable of transmitting infectivity between heterologous cell types. Intraluminal vesicles (ILV) formation is known to be regulated by the endosomal sorting complexes required for transport machinery, although an alternative neutral sphingomyelinase pathway has been suggested to also regulate this process (Figure 1.5) (Guo et al., 2015).

Exosomes are involved in the propagation of the pathogenic PrP form, but also important for intercellular communication and transport of the non-pathogenic PrP molecule between cells (Guitart et al., 2016).

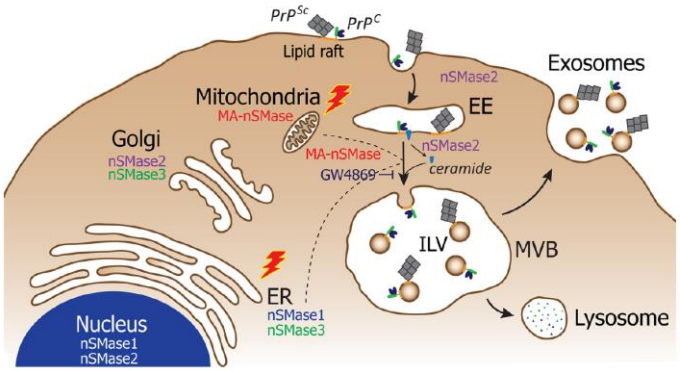

Figure 1.5: Scheme of PrP packaging (Guo et al., 2015).

1.5 Prion Protein Conversion and PrP^{Sc} Models

There are some models that tried to explain how the transition occurs; like the heterodimer model, the cooperative model (maybe an oligomeric enzyme), and the model of seeded polymerization. Experimently most supported model is seeded polymerization (Stöhr et al., 2008). Transition can be induced in vivo either by an infection with prions, by spontaneous conversion, or by mutations in the sequence of PrP (Stöhr et al., 2008).

As conversion model, a former model describes it as; a single particle of PrP^{C} interacts with PrP^{Sc} to form more PrP^{Sc}. Later, this prediction evolved into another model as; an oligomer or short polymer of PrP^{Sc}, instead of single PrP^{Sc} particle, interacts with PrP^{C} to form more PrP^{Sc} particles. There are some speculations about an additional chaperone protein (ex: protein X that mentioned above), while other models suggested that an imbalance in metal binding may be a key factor in the formation and propagation of PrP^{Sc} (Sakudo et al., 2010).

At physiological pH and in the presence of denaturants, PrP^{Sc} forms long straight, 8- to 10-nm-wide amyloid fibrils, but at low pH, it forms different types of β-rich oligomers (Singh and Udgaonkar, 2013). So, protonation of some residues destabilizes PrP^{C}, catalyzing PrP^{Sc} transition (Hosszu et al., 2010). Amyloid aggregates are cytotoxic that may affect membrane structure. The differences between monomer and the fibrils are (Figure 1.6) (Singh and Udgaonkar, 2013):

(1) "α1 is moderately protected in the monomer but weakly protected in the fibrils;

(2) α2 is weakly protected in the native monomer but strongly protected in the fibrils;

(3) α3 is strongly protected in both monomer and even more so in the fibrils;

(4) β-strand 2 is moderately protected in the monomer but strongly protected in the fibrils;

(5) the core of the fibrils, which are strongly protected are residues ~159–225 (Singh and Udgaonkar, 2013).

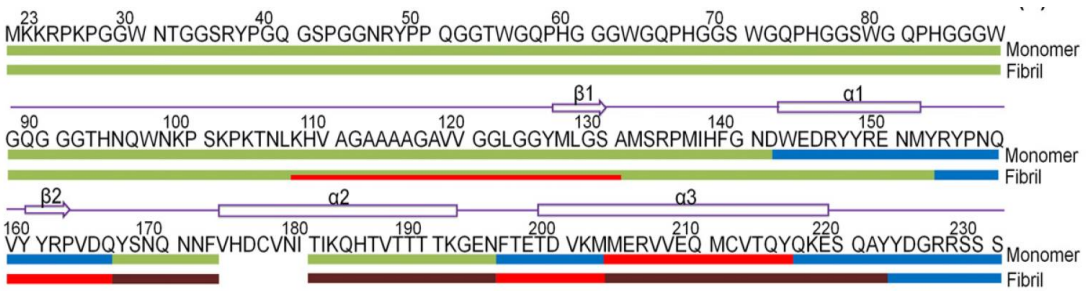

Figure 1.6: Sequence of prion protein; very strongly protected, strongly protected, moderately protected, and weakly protected are shown as brown, red, blue, and green, respectively, in monomer and and in fibril forms. Half green and half-red line represents conformational heterogeneity in the fibrils (Singh and Udgaonkar, 2013).

Syrian hamster prion protein was also studied with hydrogen/deuterium exchange and region ~163-223 region found to be the β-core structure. Residues up to 161 were unstructured, residues from 170 to 213 were highly protected where residues 161/162-168, 161-174/175 and 218-224 showed slightly lower level of protection (Smirnovas et al., 2009) (Figure 1.7).

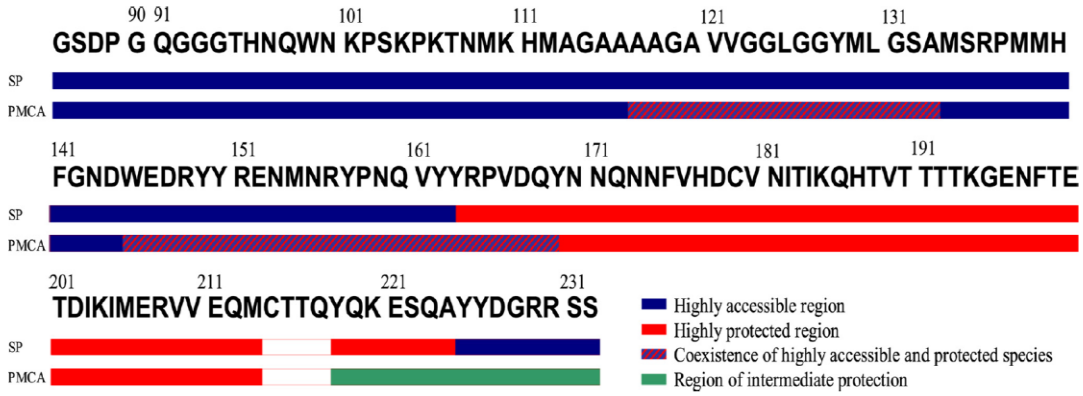

Figure 1.7: SP; spontaneously formed amyloid fibrils, PMCA; fibrils formed by protein misfolding cyclic amplification buffer (Smirnovas et al., 2009).

To seperate PrP^{C} from PrP^{Sc} and substypes of PrP^{Sc}, some biochemical and immunological assays have been conducted. These assays work according to Proteinase K (PK) resistance; in fibrillar PrP residues from 23 to ~90 is proteinase K-sensitive and solvent-accessible (Novitskaya et al., 2006). Proteinase K digests PrP^{C} completely but cleaves PrP^{Sc} specifically at residue 89 or 90 leaving the C terminus (amino acids 90–231) intact; this protease-resistant fragment is fully infectious (Stöhr et al., 2008). Scrapie form of the protein shows detergent insolubility, protease resistance and increased β-sheet content when compared to cellular form (Hosszu et al.2010). If PK and detergents are used, PrP 27–30 assembles into prion rods (Stöhr et al., 2008). Also, some antibodies were used to monitor transition from PrP^{C} to PrP^{Sc} (Novitskaya et al., 2006).

On the other hand, it is also believed that PrP^{C} is actually in equilibrium with a metastable intermediate, PrP* (Kuwata et al., 2002). PrP^{C} fluctuates between native state and a series of other conformations, one or more, that can self-associate in a form a stable PrP^{Sc} structure (Hosszu et al.2010). PrP*, interacts with a template PrP^{Sc} molecule so that the transition can occur. The structure of this intermediate may provide information on how mechanism of transition occurs as a post-translational process (Kuwata et al., 2002).

As suggested structural models for PrP^{Sc} are (Figure 1.8) (Diaz-Espinoza and Soto, 2012; Singh et al., 2012; Singh and Udgaonkar, 2015a; Yang et al., 2015);

1-β-helix model: The most popular one. N-terminal residues of PrP27-30 (~90–175) forming left-handed β-helices that are horizontally stacked and include a long unstructured loop encompassing residues 145–163; keeping α-helices 2 and 3 mainly preserved.

2-The β-spiral model: spiraling core of extended sheets, comprising from 2 original β-strands and two new β-strands (116−119 and 135−140). Natively unfolded N-terminal region can be observed, and most of the C-terminal remains intact, preserving the three original α-helices of PrP^{C}.

3-The (extended) parallel in-register β-sheet model: a stack of parallel β-sheets. PrP^{Sc} consists of β-strands and relatively short turns and/or loops, with no α-helices present at C-terminal, α-helices 2 and 3 turn into β-sheet, together with the unfolding of β-strand 1 and α-helix 1.

In β-helical model; helix 1 loses its α-helix structure and involves in the formation of one left handed β-helix. Even though two models that fail to explain several biophysical properties of PrP^{Sc}, the parallel in-register β-sheet model for fibrillar PrP^{Sc} has strong experimental support (Singh and Udgaonkar, 2015a). In both the β-helical and the β-spiral models, the C-terminal domain keeps its structure upon misfolding, whereas in the extended in-register β-sheet model, the entire protein refolds into a mainly β-sheet conformation (Figure 1.8). In-register β-sheet model may be the model that proves misfolded aggregates having the ability to self-propagate (Diaz-Espinoza and Soto, 2012).

Also, Cobb et al. proposed a fibril model in which seven new β-strands formed in sequence 159−219 (helix 2 and 3) which are stacked in a parallel, in-registered manner (Yang et al., 2015).

Parallel in-register β-sheet model is consistent with the observation that only α-helices 2 and 3 of PrP^{C} can oligomerize and form straight fibrils (Singh et al., 2012); since it has been shown that the H2-H3 core is also highly fibrillogenic by itself (Adrover et al., 2010; Garrec, 2013).

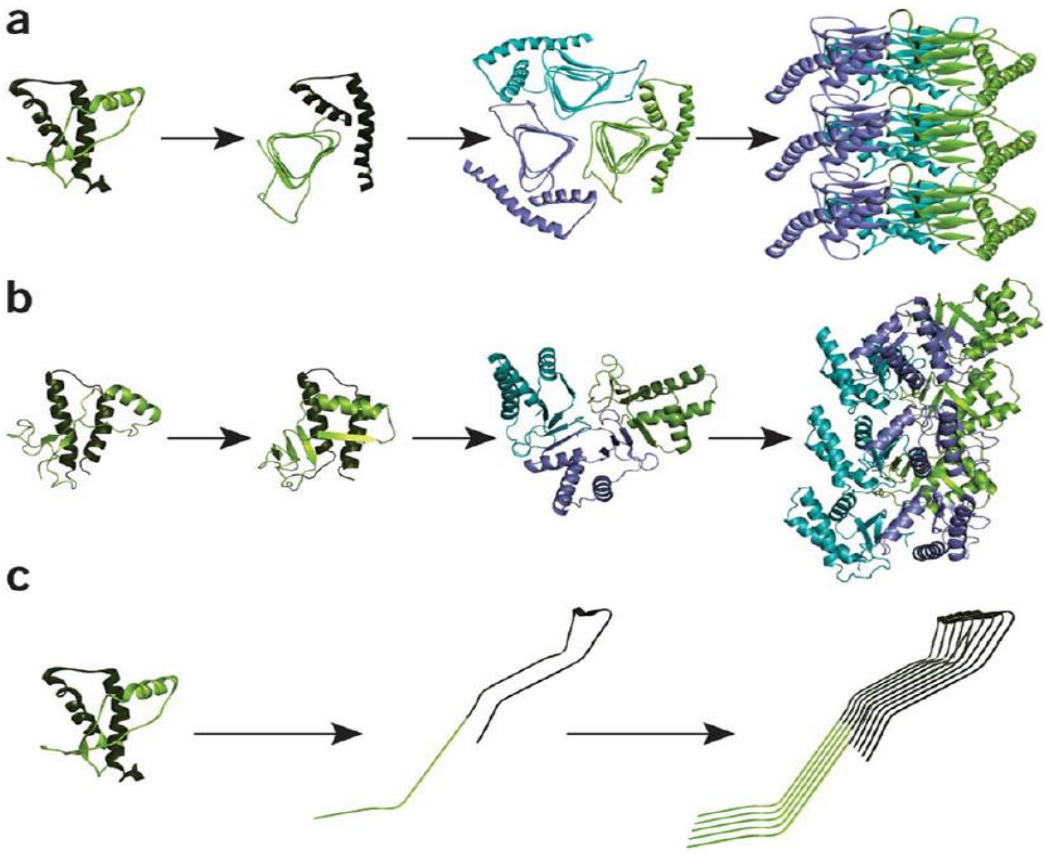

Figure 1.8: (a) β-helix model, (b) β-spiral model, (c) parallel in register β-sheet model (Singh and Udgaonkar, 2015a).

1.6 Prion Protein Gene (PRNP) and Mutations

Most common single amino acid mutations are D202N, E211Q, and Q217R (Guo et.al., 2012). Experimental studies show that the H2–H3 region is enough to form fibrils and to reproduce the oligomerization pathway. When Cys179–Cys214 disulfide bridge of H2 and H3 breaks, the misfolding propensity of the protein is increased. However, the stability of the disulfide bond is under debate; because it is not clear whether the bond remains intact or is dissappeared and then reformed during the $PrP^{C} \rightarrow PrP^{Sc}$ conversion.

Disease can be triggered by mutations in the human prion protein gene (PRNP), especially autosomal dominant mutations, infection/dietary exposure with tissue containing PrP^{Sc} or by rare sporadic events (Wadsworth et al., 2003). It can be classified as inherited, sporadic (unknown cause) and acquired forms (Mead, 2006). More than 30 PRNP mutations have been characterized within the PrP gene PRNP that may result in prion disease. However, when these mutant forms expressed, as

recombinant proteins, they do not misfold the normal cellular form; meaning that PrP^{C} instability does not appear to be the major factor (Hosszu et al.2010), but instead a conformational change of PrP^{C} to PrP^{Sc} is more necessary than covalent modification (Wadsworth et al., 2003).

FFI and CJD are two clinicopathologically different diseases, but the same mutation (GAC-to-AAC) of PRNP at codon 178 causes a substitution of aspartic acid with asparagine (D178N). Also, methionine–valine polymorphism at codon 129 affects the susceptibility and phenotype of the disease. Cleavage site in the two diseases by protease result in 21 kDa in CJD and 19 kDa in FFI (Shamsir and Dalby,2005).

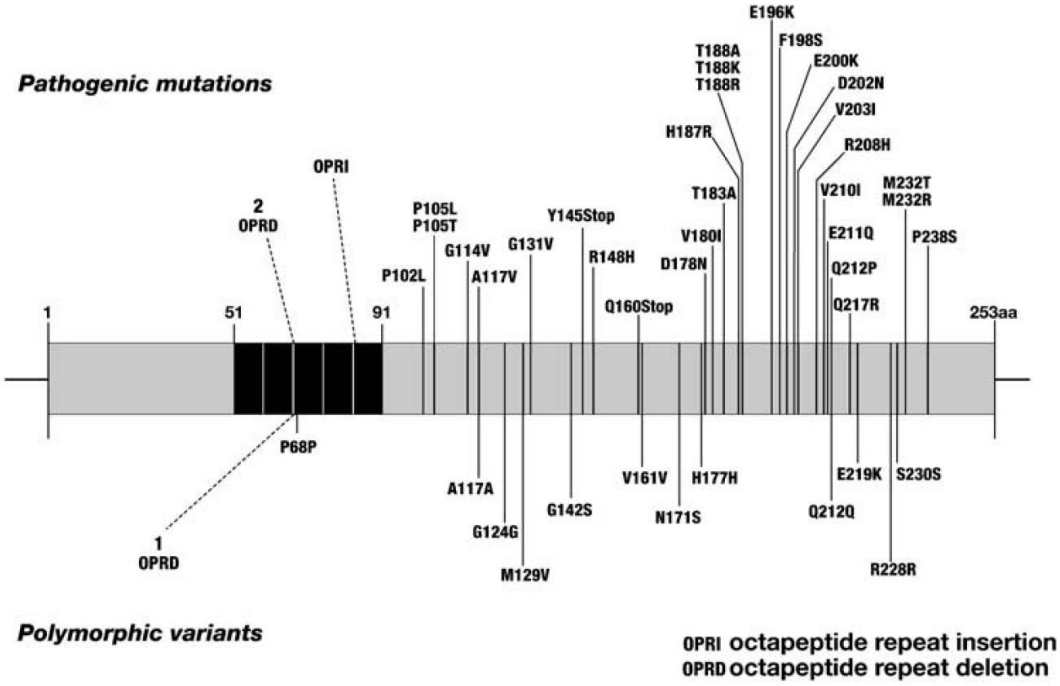

Figure 1.9: Definite and possible mutations (Mead. 2006).

All Creutzfeldt–Jakob diseased patients have an identical genotype at polymorphic codon 129 of PRNP (Mead. 2006). Different PRNP mutations have been identified affecting the stability, processing and/or cellular interactions (Van der Kamp and Daggett, 2009) as shown on Figure 1.9. Most common worldwide PRNP mutations are E200K, D178N, P102L, and insertion of additional octapeptide repeats. Remaining mutations are also shown in Figure 1.9 (Mead, 2006). In the 1950s, kuru patients in the South Fore with both methionine (129M) and valine (129V) homozygous individuals had early onset of disease, whereas heterozygous individuals had a delayed

onset. Besides, the P102L mutation was first reported in Finnish families with a CJD-like illness (Figure 1.10).

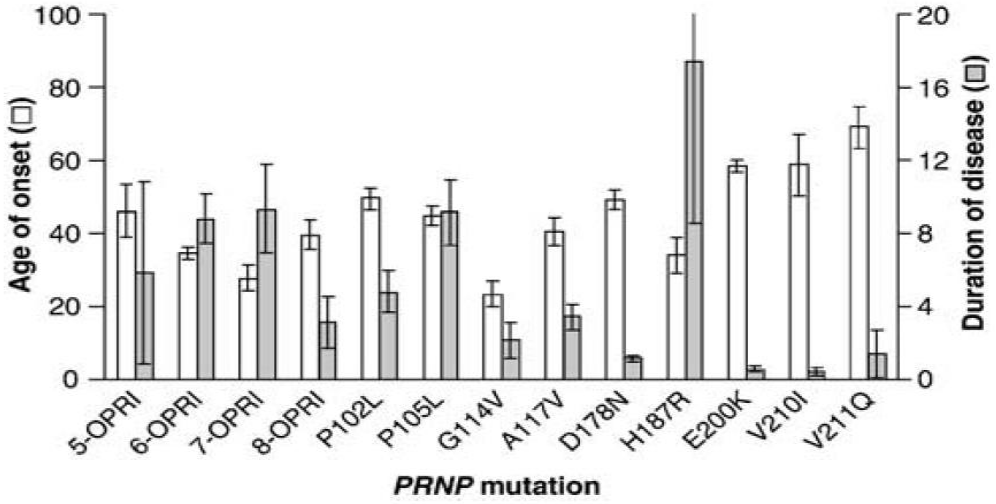

Figure 1.10: Different PrP gene mutation and their effect on the onset and duration of the disease (Mead, 2006).

Protease resistant fragments of 21kDa and 19kDa are observed for gCJD (D178N-129V), gCJD E200K-129M and FFI (D178N-129M) respectively. Also, different prion diseases show different glycosylation ratios (Head and Ironside, 2012).

CJD is genetically more observed among Libyan Jews and the mutation related to those families was found at the first position of codon 200 causing a single nucleotide to change from G to A; which is resulted in a change from glutamate to lysine. Other mutations were found to be leucine substitution at codon 102 which is linked to GSS disease mostly and valine substitution at codon 117, also 6 tandem repeat insertion at codon 53 are seen in familial CJD patients (Hsiao et al., 1991).

M129V, N171S, E219K, P102L(129M), meaning P102L with M at the position 129, P105L with 129V, Y145STOP with 129M, D178N with 129M, D178N with 129V, V180I, V180I with M232R, E200K, V203I, R208H, V210I, E211Q, M232R, E211K are all observed mutations in different prion related diseases (Sakudo et al., 2010).

Mutations related to GSS in the flexible N-terminus of human PrP are P102L, P105L/S/T, G114V and A117V. Truncated PrP was formed because of two stop mutations Y145stop and Q160stop. R148H, D178N, E196K, E200K, R208H and E211Q affect salt-bridge interactions in the globular PrP domain. Both E200K and D178N mutation significantly affect the protein stability. T183A causes abnormal glycosylation. V180I, F198S and V210I may also cause abnormal glycosylation.

H187R results in accumulation of the protein inside lysosomes instead of reaching to the cell surface. T188R and T188K cause increased proteinase K resistance and detergent insolubility causing a higher degree of aggregation. D202N PrP accumulates inside the endoplasmic reticulum without having a mature conformation. Q212P PrP accumulates and forms aggresomes in the cytosol because of proteasomal inhibition. Q217R PrP lacks a GPI-anchor. G131V recPrP (90–231) indicated the extension of the S1/S2 β-sheet but does not affect the overall stability. F198S leaves a gap in the hydrophobic core. M232R and M232T cause PrP to be bound to the membrane in a different orientation (Van der Kamp and Daggett, 2009).

1.7 Computational Studies About Prion Protein

Molecular dynamics simulations (MD) have been used to investigate the misfolding pattern of the prion protein caused by some mutations. Some mutations that are mentioned above like D202N, E211Q and Q217R of human PrP were studied by using MD simulations. Results indicated that mutations caused no obvious structural changes, but these mutations made the residues 174–184 and 200–215 more flexible compared to wild type (WT) PrP. However, these mutations changed the overall electrostatic potential distributions which in return might influence the intermolecular interactions during the aggregation process and they also affected the thermodynamic stabilities of PrP. Compared to Q217R mutant, D202N and E211Q mutants were more hydrophobic and might be more prone to undergo self-assembly than WT PrP (Guo et.al, 2012).

Mutation at codon 178 (D178N) and the polymorphism at codon 129 (M or V) of human PrP were also analyzed by MD simulations at normal and high temperature. The existence of methionine causes a higher stability than valine. Valine demonstrated elongation of existing β-sheets and formation of new β-sheets. So, it was concluded that mutation caused an increasement in β-sheet content (Shamsir and Dalby, 2005). Another MD study showed that same mutation (D178N) disturbed the interactions with both strands of the native β-sheet, affecting its stability, by increasing instability in S2. V180I, F198S, V203I, and V210I significantly reduced stability (van der Kamp and Daggett, 2011). Moreover, Asp178 at helix 2 makes a salt bridge with Arg164 in β-strand 2, so mutation of it affects the protein stability making that hydrogen bond between the side chain carbonyl of Asn178 and the guanidine side group of Arg164

disappear. MD simulations of prion with Asp178Asn mutation at 300 and 500K were undertaken. At 300K, there was a breakdown in helix 1 and changes in helix 3 as β sheet elongation, a small 3_{10}-helix at the end of helix 1 (154–156); a split in helix 3 (between residues 216–219), movement of the N-terminal region (124–135) and movement of the loop just before helix 2 (164-172) were observed. At 500K helix 3 became longer and straighter (El-Bastawissy et al., 2001).

Simulation of the 109–219 fragment of hamster PrP with D147N mutation showed an increase conversion efficiency; as a 20-ns MD simulation at strongly acidic pH resulted in a three-stranded sheet (formed by extension of the native sheet) and an isolated strand in residues 135–140 of S1-H1 loop (Kamp and Daggett, 2011).

Mutation of either Asp-144 and Asp-147 to asparagine increased the efficiency of conversion from PrP^{C} to PrP^{Sc} 2- to 3-fold. At low pH, D147N mutant formed extended secondary structure and the core of the β-structure was a three-stranded sheet, E1–E3, and an isolated strand, E4 (DeMarco and Daggett, 2004).

When mutations T193I and R148H are associated with fCJD were undertaken with MD simulations, it was found that both mutated forms were conformationally steadier than the native prion protein. R148H caused depletion of native β-sheet content, H1 became less fluctuating, two new turn regions formed (around residues 180 and 200 located in H2 and H3 helices) and conversion of a 3_{10} region to coil form occurred. T193I forms a steady H1 helix, also native β-sheet content decreases and a new 3_{10} region in H2 forms (Borgohain et al., 2016).

Since rabbit PrP^{C} had NMR and X-ray structures, it was also used as a model for MD studies to observe soluble PrP^{C} to insoluble PrP^{Sc} conversion. Mainly surface electrostatic charge distributions of MD trajectories of wild type, I214V mutant, and S173N mutant were analysed. At low pH three helices of wild type were unfolded, where three helices of mutant ones were all unfolded under neutral and low-pH conditions. I214V had more β-sheet structure at low-pH at the C-terminus; so that residue at position 214 might be important for the conversion of rabbit PrP^{C} to PrP^{Sc}. S173N mutation changed the electrostatic potential in β2–α2 loop. It was found that surface electrostatic charge distributions should be important for the structural stability of rabbit PrP^{C} but not the only reason for the PrP^{C} stability. Unfolding of the mutants (S173N and I214V) were not just related to electrostatic potential; but it might be

important for the wild type because of the surface positive electrostatic charge distributions (Zhang et al.,2015).

It is known that the oligomeric form states are transient, characterization of atomic structure has failed so far. Monomer and dimer forms of PrP125-228 and its CJD-causing T183A variant, which prevents glycosylation of Asn181, were analyzed by coarse-grained protein molecular dynamics simulations for 1.5 microsecond at various temperatures. T183A caused a decrease in the thermodynamic stability of PrP monomer, so that H2-H3 have much higher propensity for intra- and inter-β-sheets formation. T183A mutation accelerated the conversion of the helix H2 to β-sheet in the monomer and dimer too, but not at low temperatures (Chebaro and Derreumaux, 2009).

Combination of the well-tempered ensemble, parallel tempering schemes and metadynamics were used to characterize the conformational free-energy surface of mouse PrP^{C} (121–231) that includes the β2–α2 loop (167–170), which shows a susceptibility to prion disease, and PrP^{C} with Y169A mutation showed no conformational transitions. 16 replicas temperature ranging from 300 K to 550 K were conducted with some restraints on the secondary and tertiary structural elements to avoid undesired unfolding keeping the structure folded at the higher temperatures. The calculations revealed that the exchange rate between the 3_{10}-helix turn, and the type I β-turn conformations were orders of magnitude faster in PrP^{C} with Y169A than in mPrP (121–231) (Caldarulo et al., 2017).

Explicit solvent simulations as a part of MD simulations were also used to investigate the human PrP protein; from residues 125 to 229 was chosen to analyze the stabilization energy of the PrP protein at 310K for 50 ns at either pH 7 or pH 2, by varying the protonation state of acidic and basic groups, to trigger the PrP^{C} to PrP^{Sc} conversion at low pH. Then the final structures of these two simulations were used as starting structures for two more simulations at 350K for 20 ns at pH 7 and 2. After 20ns the temperature was raised to 450K for 20 more nanoseconds to promote the unfolding and investigate possible pathways for infectious species formation. Main purpose of the study was to investigate the roles of structural motifs and residues in stabilization/destabilization and possible role in unfolded intermediates. Energy distributions were observed where in native conditions, the stabilization energy is

concentrated in the helices H1 and H3, whereas under misfolding conditions it was spread out over H2 (Colacino et al., 2006).

MD studies might show some conflicting results like as one of them suggested that helix 2 (α2) and helix 3 (α3) have gone extreme structural changes to form metastable monomeric state PrP^{C}. Another molecular dynamics simulation at low pH suggested that rearrangements in the N-terminal of α2 and α3 keeping their native conformations and α1 keeping its native structure either partially or completely to result in conformational change. But with the help of hydrogen–deuterium exchange and mass spectrometry amyloid fibril formation by recombinant mouse prion protein at pH 7 was analysed to clarify those kinds of conflicts, where monomer was directly added on to the fibril template. First helices 2 and 3 transformed into more stable β-sheet and secondly helix 1 unfolding occurred to result in the conformational conversion. Conformational change initiated in segment 159–225 which correlated with studies of some anti-prion drugs which bind to this segment, to stabilize PrP^{C} (Singh and Udgaonkar, 2013).

Different pH levels were also conducted using MD simulations. Baillod et al. (2012), investigated the conformational change of C-terminus of mouse prion from residues 124-226 at pH4, conducting replica exchange molecular dynamics (REMD) simulation for 2.8 μs total time. As a result, increased level of β-structure was observed (Baillod et al., 2012). Loss of helical structure and gain of β-structures at the same time were observed with pH decrease. The effects of a change in pH to 7 were also studied to see the reversibility of PrP misfolding. Simulations showed that even at pH as low as 1.7, it was possible to revert the misfolding process, but when pH value is 1.0, it was not possible to revert (Vila-Viçosa et al., 2012). According to MD simulations of mouse PrP at pH 4.5, like observed inside endosome, protonated imidazole ring of H187 caused an electrostatic repulsion toward guanidinium group of R136, so sidechains of either H187 or R136 moved away from their native cavities. It was found that there are two possible routes of misfolding; when 187out=136in route unravels H2 (Cter) alone, but when 187in=136out, this unravels H2 (Cter) with simultaneous elongation of S1, S2 (Garrec, 2013).

To investigate aggregation of β-rich H2H3 domain of the ovine prion protein (H2H3-$OvPrP^{Sc}$), which declared as the part having the oligomerization activity, was analyzed via MD simulations. As starting structure β-rich H2H3-Ov PrP^{Sc} with a disulphide

bond between Cys182 and Cy217 with double β-hairpin structure was used which had obtained before at pH = 4 with REMD investigation. Then study carried out with the MD simulations at pH = 7 with a system running multiple replicas of a box composed of 18 β-rich H2H3-Ov PrP^{Sc} (miniPrP). The loss of secondary structure elements mainly happened from Thr191 to Asp205 where mostly the water molecules are located. At the same time, the miniPrP`s region kept the extended β-strand arrangement throughout the simulation. From Thr191 to Thr196 formed a β-bulge that the β-bulges were considered as initiator of dimerization and aggregation. Firstly, the formation of a base, composed of 5‑8 miniPrP units are neccessary to act as a nucleation complex and secondly other miniPrPs should attach for further growth (Collu et al., 2018).

Bovine PrP^{C}, which is similar to other mammalian species, was used to investigate the pH-induced misfolding, via MD simulations at pH 7, 5 and 4, respectively. Five 50 ns simulations were performed for each pH. In both mid- and low pH simulations, the flexible N-terminus formed non-native β-strands by interacting with the S1 strand. For the formation of this non-native β-strands; at low pH, hydrophobic contacts with M129 acted as a nucleation point; at mid-pH, polar contacts involving Q168 and D178 catalyzed the formation of a hairpin at the flexible N-terminus (Cheng and Daggett, 2014).

The conformational free energy surface of globular domain of sheep PrP which includes H1-H3, and β-sheet were also analyzed using REMD simulations which helped to characterize the partially unfolded states of the PrP. As a result, full detachment of helix H1 from H2–H3 core was observed as an intermediate which may be a good candidate for PrP aggregation (De Simone et al., 2007).

REMD simulations of the human prion protein globular domain at neutral pH showed a stable core (H2 and H3), while H1, although stable, showed an increased plasticity. In addition, MD simulations at low pH showed some loss of helical content, where H1 being mostly unstable. Probably H1 refolds for the PrP^{Sc} formation. The structural change starts after the detachment of H1 from H3. MD simulations of a peptide which contained H1 sequence showed the unfolding kinetics were related to the dielectric constant of the solvent and unfolding in water was faster than less polar solvents. MD and Monte Carlo/Molecular Dynamics (MC/MD) simulations both confirmed a stable β-sheet at S1 and S2. Because of the faster sampling: mixed MC/MD were used to

simulate the human prion protein D178N mutant. As a result, MC/MD simulations crossed a free energy barrier that resulted in the unfolding of helix H1. This change occurred after the loss of a specific hydrogen bond between H1 and H3, residues Tyr149 and Asp202, which did not occur in any MD simulations (Ribeiro and Alencastro, 2013).

Unfolding and refolding steps were also analysed by MD simulations using ovine prion protein. Separation of the H1 helix from H2H3 domain, and formation of stable β-sheets between H2 and H3 residues were observed (Chakroun et al., 2013).

Recent MD simulations suggested that PrP^{Sc} unit is considered to be a hexamer and it is the minimum infectious unit. PrP^{C} attaches to the PrP^{Sc} oligomer template, which is converted to the PrP^{Sc} trimer. "The resultant rod-like PrP^{Sc} is broken and acts as template for the conversion" (Sakudo et al., 2010).

Hydrophobicity patterns of H2 suggest that the PrP^{C} to PrP^{C}* (aggregation prone state) transition must be accompanied by alterations in the second half of H2. On the other hand, the stability of H1 eliminates its part in this transition. MD simulations of H2 and H3 togehter showed that the C-terminal end of H2 (residues 184–194) and residues 200–204 and 215–223 of H3 change from α-helical conformation to β and/or random coil state that these parts were involved in the transition to PrP^{C}* (Dima and Thirumalai, 2004).

How some species show resistance have also been taken into consideration. For example, buffalo has low susceptibility to TSEs like rabbits, horses, and dogs. To understand this resistance, molecular structure, and structural dynamics of buffalo PrP^{C} were studied. There are five hydrogen bonds at Asn143 of buffalo PrP^{C} where bovine/cattle do not have. Also, MD studies also revealed there is a strong salt bridge between ASP178–ARG164 (O–N), keeping the β2–α2 loop linked, maintains the stability in buffalo like in rabbits, dogs, or horses. Hydrogen bond SER170–TYR218 links this loop with the C-terminal end of H3 and salt brigde HIS187–ARG156 (N–O) (linking α-helices H2 and H1) contribute to this stability (Zhang et al., 2016).

Osborne et al., (2013) found that aggregation of hydrophilic GNNQQNY sequence of the N-terminal domain of the yeast protein is mainly controlled by H-bond formation which leads to formation of β-sheets at the beginning of the assembly. Groveman et al. (2014) formed an octameric structure which consisted of linear fibrils. This study

showed that residues 160-231 at C-terminus remained well packed and conserved β-sheet structure. Also, Ile and Phe maintained more tightly packing than the Leu residues.

1.8 Aim of the Study

Misfolded prion protein cannot be observed clearly because it easily aggregates and precipitates which limits use of any high-resolution viewing techniques. These limitations make computational methods more useful to investigate the conformational transitions (Vila-Viçosa et al., 2012).

Since we still don't know the X-ray crystallography and NMR structure of PrP^{Sc} (Silva et al., 2015), we aim to use ovine prion protein as model to investigate the initiation point of the misfolding and perhaps the possible misfolding pathways.

For this purpose, we decided to use molecular dynamics simulations, but since "explicit-solvent molecular dynamics simulations need high computational demands whereas implicit-solvent simulations are less computationally demanding and enable longer simulation times" (Lin and Pande, 2012); we continued our study with implicit solvent simulations, even though we are aware of that implicit-solvent simulations are lack of fully describing the water-peptide interactions.

During our study, we decided to use different varients of C-terminal globular ovine prion protein to better understand how these differences lead to misfolding and how they affect the disease susceptibility.

By analyzing misfolding pathways, we may encounter with an intermediate form which may act as the protein that catalyzes the unfolding of α-helices in PrP^{C} and refolding them into β-sheets or as Colacino et al. (2006) mentioned, we may observe the particular role of single residues that might be important for (de)stabilization. Adrover et al. (2010) showed that only the H2 and H3 part of PrP can maintain the fibrillization and give a stable hairpin structure to form amyloid fibers. Moreover, recombinant PrP without helix I (residues 23-88 and 141-176) keeps the ability to support PrP^{Sc} formation, forming β-sheet-rich aggregates (Hosszu et al., 2010). From these results, besides the globular part of the prion protein, we would simulate only H2 and H3 with the disulfide bond to test whether only H2-H3 structure can actually form a β-sheet core of PrP^{Sc} or not by REMD.

2. MATERIAL AND METHODS

Implicit-solvent molecular dynamics simulations were performed using Amber 11, 14 and 16 program packages with the ff10 force field. We used three ovine PrP variants which were taken from Protein Data Bank (PDB) having codes as 1TQB [V136, R154, Q171 (VRQ)], 1TQC [(A136, R154, R171 (ARR)] and 1TPX [A136, R154, Q171 (ARQ)]. Water molecules and antibodies were removed, and disulfide bond was formed between cysteines at positions 182 and 217. The N-terminal part of the proteins are discarded since it has no known effect on the formation of PrP^{Sc}. The C-terminal parts (G127-P223) of monomers of all three variants were used for the simulations.

Protonation states of histidines at neutral pH (pH = 7) had been decided using PropKa server as H143 as δ-protonated (HID), H180 as ε-protonated (HIE) and H190 as HIE form too.

Implicit solvent with a salt concentration of 0,1 molar were conducted. Electrostatic and van der Waals interactions between atoms were set to ignore more than 30Å. For minimization of all three structures, root mean square gradient 0.01 kcal/mol.Å was used. Minimization started with the steepest descent algorithm step number as 500 and continued with conjugate gradient algorithm with a maximum step number 90.000.

For the simulation period, the SHAKE algorithm was used allowing a time step of 2 fs. Initial temperature was 10K for every simulation and raised to 310K or to 330K by using a Langevin thermostat. The structures were saved to file every 2500 steps.

All simulations carried out for ~2μs and each variant was simulated separately for twice.

For restrained simulations, distance restraints of 2.1 Å between M132-Y166, and Q220- E224 were used to keep β-sheet and alpha helical structures, respectively.

Even though VRR is not observed widely in nature, we decided to simulate this one too under the same conditions (pH=7, 310K) to compare alanine-valine differences and arginine-glutamine differences at the same time.

Replica Exchange Molecular Dynamics (REMD) runs multiple MDs at the same time, so called replicas, of the system at different temperatures exchanging periodically. High temperatures maintain the crossing of the energy barriers, whereas low temperatures allow the efficient exploration of stable structures (De Simone et al.,2007). After a specified number of time steps, replicas at closed temperatures can be exchanged. High-energy structures are accepted to migrate to the replicas at lower temperatures when exchanged with each other. With the help of multiple temperatures, all energy traps overcome easily (Osborne et al., 2013). During REMD simulations a single high temperature can be used to generate an ensemble of structures to form reservoir (Roitberg et al., 2007), and we chose this temperature as 470K. The temperatures of the replicas can range from low values like 280 or 300 K up to high values such as 600 K (Okur et al., 2007). We decided to use 12 replicas ranging from 298K to 460K (298K, 310K, 322K, 335K, 349K, 363K, 377K, 392K, 408K, 425K, 442K, 460K). We restrained 5 amino acid long sequences between C182 and C217 to mimic PrP^{Sc}'s effect.

Also, since the endosomal compartment seems to be important in transition into PrP^{Sc}, to change and lower the pH in the system, we changed the protonation states of ionizable amino acid side chains of glutamate, and aspartate. These residues changed to GLU, and ASH, respectively. The temperature also kept as 310K and same force field was used.

REMD simulations of H1 to unfold were performed at temperatures 294, 310, 327, 344, 363, 382, 402, 423, 445, 468, 495 and 520 K. In order to prevent H1 and the other sequences moving infinitely away from each other, Y153A-Y153B, Y153-E203 and Y153-S106 distances were restrained at 20 Å.

3. RESULTS&DISCUSSION

3.1 MD Simulations Result

All three variants of the prion protein ARQ, ARR and VRQ were simulated for 2000ns at 310K and 1000ns at 330K. All variants at 310K were simulated for twice to see whether the results overlapped with each other or not. The sequences that were simulated, respectively, were:

Table 3.1: Sequences of 3 different variants.

127 136 154 171 228 GLGGYMLGSAMSRPLIHFGNDYEDRYYRENMYRYPNQVYYRPVDQYSNQNNFVHDCVNITVKQHTVTTTTKGENFTETDIKIMERVVEQMCITQYQRESQAY
127 136 154 171 228 GLGGYMLGSAMSRPLIHFGNDYEDRYYRENMYRYPNQVYYRPVDRYSNQNNFVHDCVNITVkQHTVTTTTKGENFTETDIKIMERVVEQMCITQYQRESQAY
127 136 154 171 228 GLGGYMLGSVMSRPLIHFGNDYEDRYYRENMYRYPNQVYYRPVDQYSNQNNFVHDCVNITVKQHTVTTTTKGENFTETDIKIMERVVEQMCITQYQRESQAY

The results below were the clusters of these simulations using distance between frames calculated by distance-Root Mean Square Deviation (RMSD) using C-alpha atoms of residues 177,191,142,207,136,224,146 and 160.

3.1.1 ARQ simulation-1 at 310K

One of the ARQ simulations displayed 5 conformations with populations higher than 5% (Figure 3.1). ARQ1_1 was similar to the crystallographic conformation with A136 partially buried between T219, Q229 and R223 of H3. R159 and Y160 interact with D205, connecting the C-terminus of H1 to the N-terminus of H3. The rest of the interactions between H1 and H3 were limited to the hydrophobic contacts between F144, Y153, Y160, I208 and V212 in addition to E149-R211 salt bridge. H1 was bent at the last turn and its N-terminus was relatively close to H3 (hereafter referred as close conformation). R139 of the B1-H1 loop made hydrogen bonds with the backbone oxygens of M157 and Y160. No unwinding was observed on any helix. Native β-sheet was formed between M132-Y166 and G134-V164. S135, A136, M137 form a long bulge, yielding a short β-sheet.

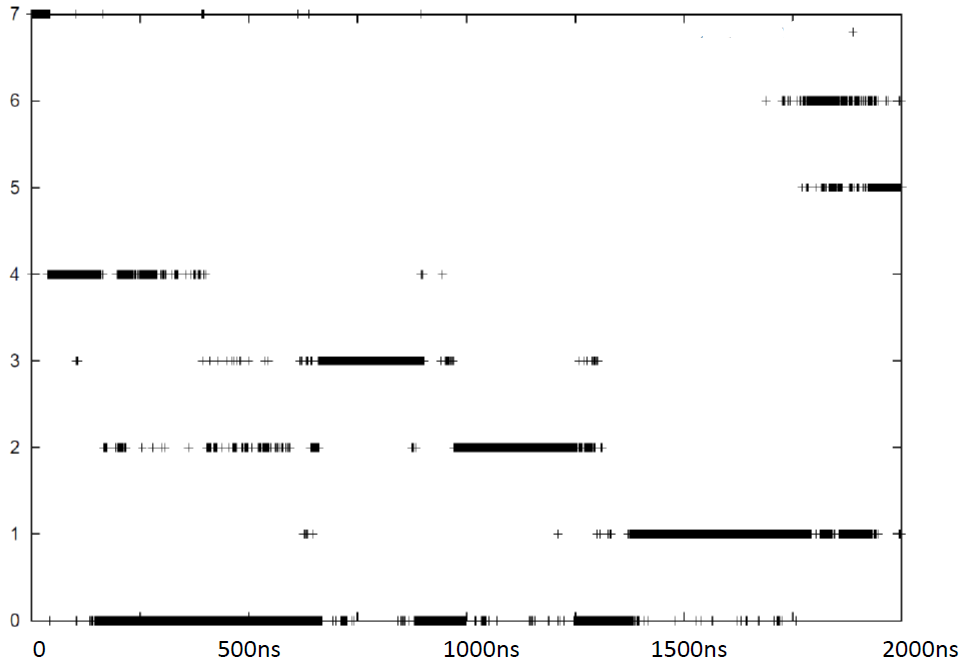

Figure 3.1: Cluster number (0-7) vs. time graphic of first ARQ simulation.

During the first half of the simulation, ARQ1_1 (cluster 4) was in equilibrium with ARQ1_2 (cluster 0), ARQ1_3 (cluster 2) and ARQ1_4 (cluster 3). In these conformations, residues 188-191 unwound to divide H2 into two shorter helices (in ARQ1_4 the whole C-terminal half of H2 unwinds). R139 of the B1-H1 loop made a salt bridge with E199 of the H2-H3 loop, restricting the fluctuations of the unwound region. Most of the H1-H3 interactions in ARQ1_1 were conserved in ARQ1_2 and ARQ1_3. An exception was the F144-I218 hydrophobic contact observed in ARQ1_3 pulling B1-H1 toward the middle of H3. On the other hand, in ARQ1_4, P140, I142, Y160, V212 hydrophobic interactions replaced F144, Y153, Y160, I208 hydrophobic interactions, E149-R211 salt bridge and Y160-D205 hydrogen bond. R159-D205 was conserved in all these structures. The native β-sheet shifted by one residue such that Y131-Y166 hydrogen bonds formed. Nevertheless, this shift did not affect the position of A136. Major differences between ARQ1_2, ARQ1_3 and ARQ1_4 were the positions of B1-H1 loop and H2-H3 loop. In addition, ARQ1_4 displayed a more open H1 conformation due to the lack of interactions with H3 at the N-terminal part of H1. Hence, these three conformations could be considered as one conformation exhibiting large fluctuations of H1, B1-H1 loop and H2-H3 loop.

During the remaining part of the simulation, mostly ARQ1_5 (cluster 1) was observed (in addition to a low population of ARQ1_2, ARQ1_3 and ARQ1_4). In this structure,

the native β-sheet shifted back to take its initial position. On the other hand, the C-terminal half of H2 remained in an unwound conformation. In addition, residues 206-209 of H3 were unwound. Nevertheless, R139-E199, E149-R211, R159-D205 salt bridges along with the P140, Y160, V212 hydrophobic cluster still maintained the stability in this region. All those interactions were shown below in Figure 3.2.

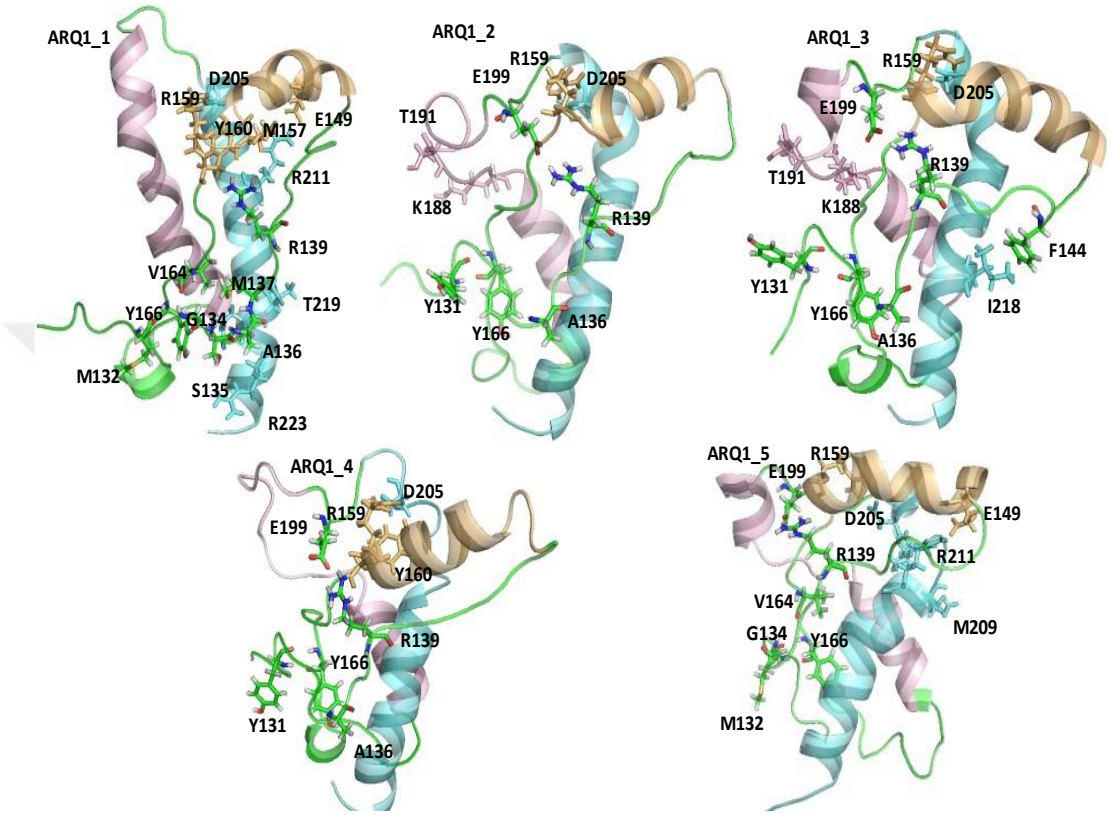

Figure 3.2: Different clusters and interactions of ARQ simulation 1.

3.1.2 ARQ simulation-2 at 310K

In the first 1.25 μs of the second unrestrained ARQ simulation (Figure 3.3), ARQ2_1, a structure similar to ARQ1_1 (cluster 4), was observed. The major differences between ARQ1_1 and ARQ2_1 were the lack of Y160-D205 and E149-R211 salt bridges and presence of R159-E199 salt bridge in ARQ2_1 (Figure 3.4). In addition, the hydrophobic cluster was composed of P140, I142, Y153, Y160, I208, M209, V212 and V213, leading to a more open H1 conformation. ARQ2_1 was in equilibrium with ARQ2_2 (cluster 0) and ARQ2_3 (cluster 1). These latter conformations corresponded to intermediates of the opening of the original β-sheet, eventually leading to ARQ2_4 (cluster 2) where B1 detached from B2 and folded into an alpha-helix (Figure 3.4). Meanwhile, a helix formed between L141 and N146. A136 was solvent exposed. H2 acquired a bent structure.

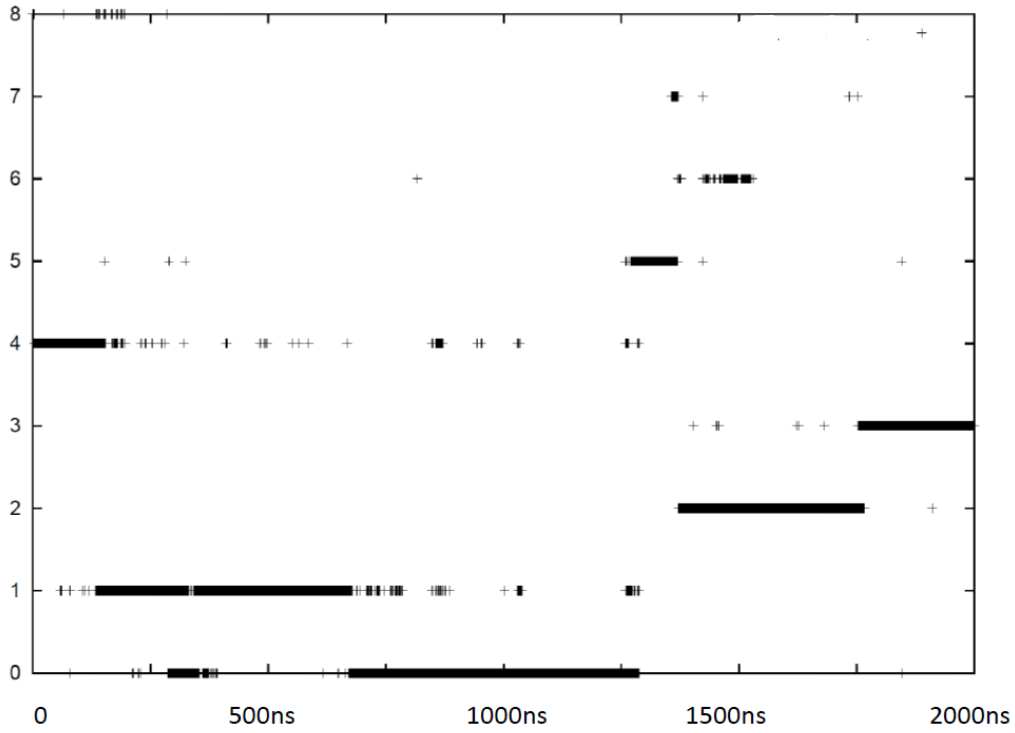

Figure 3.3: Cluster number (0-8) vs. time graphic of second ARQ simulation.

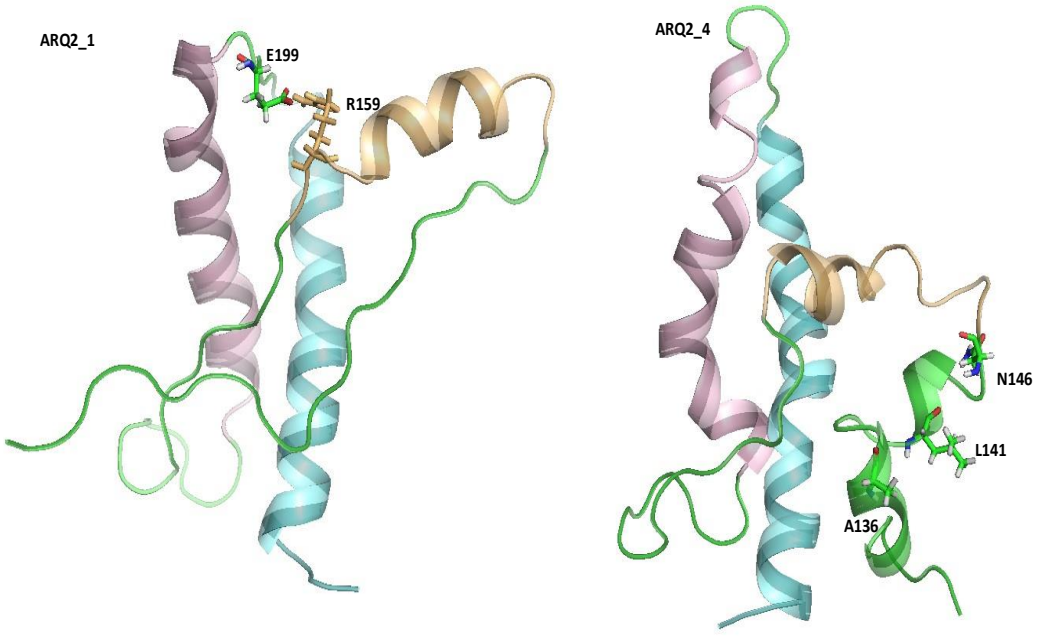

Figure 3.4: Different clusters and interactions of ARQ simulation 2.

In ARQ2_5 (cluster 3), observed in the last 0.25 μs, hydrogen bonds between Y131(CO)-Y166(NH), M137(CO)-V164(NH) and R139(NH)-N162(CO) formed, suggesting reformation of the β-sheet. A136 was partially buried between M137 and V164.

3.1.3 VRQ simulation-1 at 310K

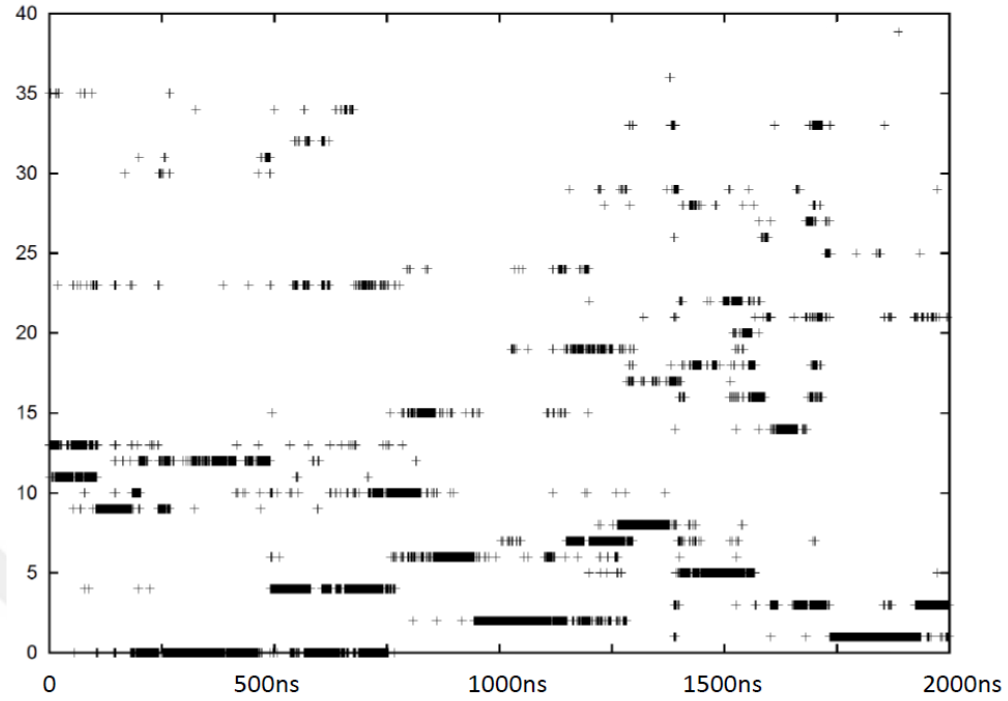

Figure 3.5: Cluster number (0-40) vs. time graphic of first VRQ simulation.

On Figure 3.5, in the first 0.25 μs, VRQ1_1 (cluster 13) and VRQ1_2 (cluster 11) were in equilibrium with each other. They both displayed stable native β-sheet, H2 and H3 helices. The bulge at S135-V136 was observed and V136 was solvent exposed as in the crystals. VRQ1_1 had a bent H1 structure compared to VRQ1_2. VRQ1_3 (cluster 9), VRQ1_4 (cluster 23) and VRQ1_5 (cluster 4) seemed to be the intermediates leading to VRQ1_6 (cluster 0). In VRQ1_3 the distance between H1 and B1-H1 increased, allowing R139 to change its position to interact with D150. In the other intermediates, VRQ1_4 and VRQ1_5, V136 was buried between M216-Q220 and the last turn of H1 was unwound. It seemed that valine with its side chain more hydrophobic than alanine preferred to stay buried in hydrophobic regions but unlike alanine, the bulkier valine side chain could not be accommodated between H1 and H3. This fact destabilized the structure. In VRQ1_6 the last turn of H1 (starting from M157) unwound and became a part of the H1-B2 loop. Though the R159-D205 salt bridge still persisted, unwinding the last turn of H1 caused a flexibility that allowed H1 and B1-H1 loop to slide on H3 toward its C-terminus. As a result, M137 was buried between T219-R223. The R139-D150 salt bridge pulled the N-terminus of H1 away from H3, leading to a wide open H1 conformation. The R139-D150 interaction was also observed in our helix restrained ARQ simulations but it did not make such an

impact on ARQ, because alanine with smaller size did not cause the destabilization of H1-H3 interaction. Thus, R139-D150 alone was not enough to largely disturb H1-H3 interactions but contributed to the destabilization of this interaction. VRQ1_7 (cluster 5) and VRQ1_8 (cluster 3) represented intermediates in which B1 separated from B2 and the T-rich region of H2 unwound. Then, B1 folded into an alpha-helix (from G129 to S138) in VRQ1_9 (cluster 8). Finally, loss of the β-sheet caused H2 to unwind completely in VRQ1_10 (cluster 1). Nevertheless, the R159-D205 interaction kept H1 and H3 in contact. All these clusters' respresentatives are shown on Figure 3.6.

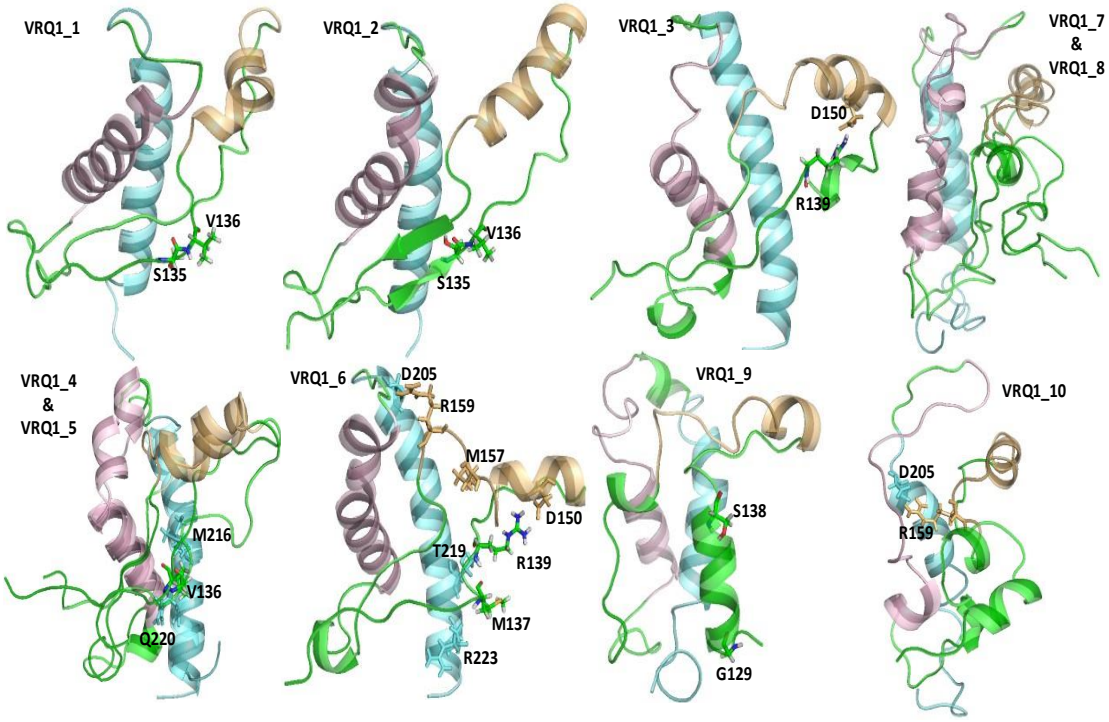

Figure 3.6: Different clusters and interactions of VRQ simulation 1.

3.1.4 VRQ simulation-2 at 310K

Even though V136 was solvent exposed at the beginning of the second VRQ simulation which started with the crystallographic structure, it moved immediately toward the C-terminus of H3, becoming buried in a hydrophobic pocket formed by M216, T219 and Q220. This structure (VRQ2_1, cluster 0) remained stable for 1.25μs (Figure 3.7).

The native β-sheet and R159-D205 salt bridge also remained intact. After 1.25 μs, because of the difficulty in keeping the bulky V136 in a buried position, the structure evolved into a more deformed conformation in a stepwise manner. First, V136 moved further toward the C-terminus into the pocket formed by T219, Y221 and Q222.

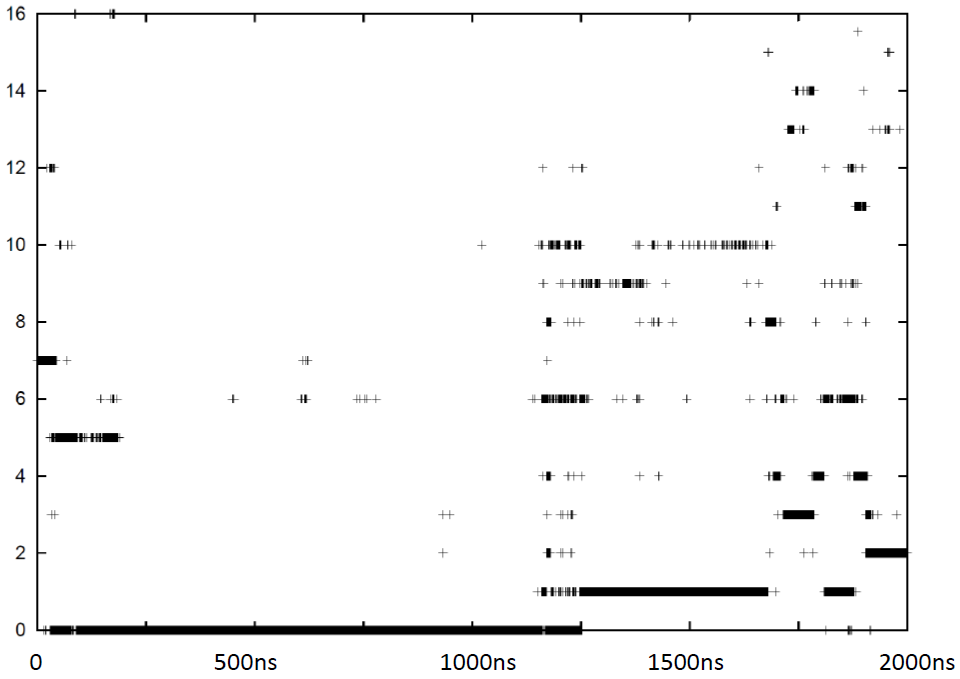

Figure 3.7: Cluster number (0-16) vs. time graphic of second VRQ simulation.

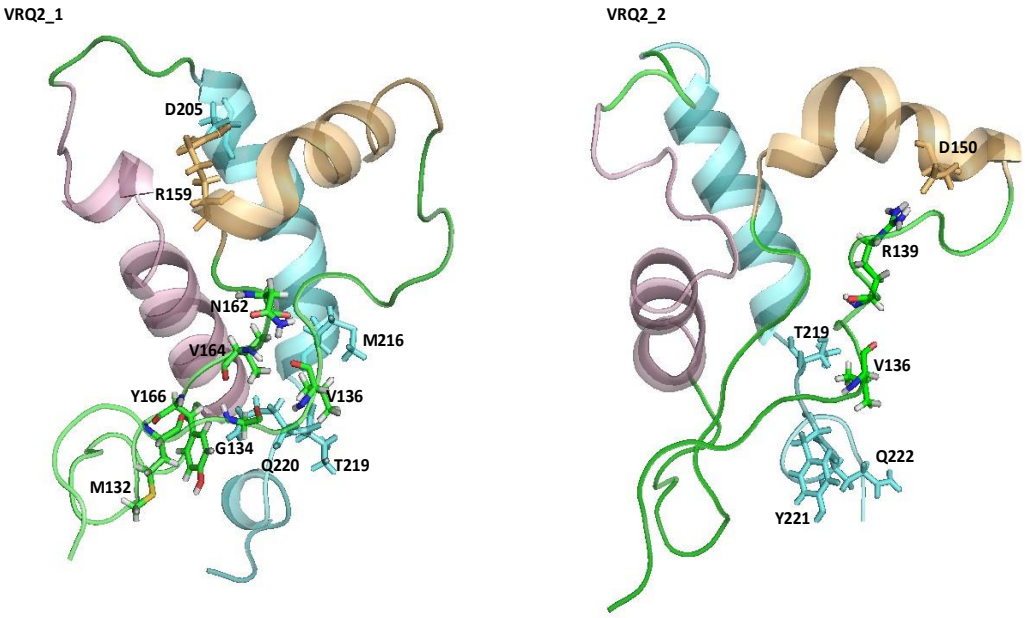

Figure 3.8: Different clusters and interactions of VRQ simulation 2.

Meanwhile, R139 formed a salt bridge with D150, pulling the N-terminus of H1 away from H3, leading to a highly open structure of H1 (VRQ2_2, cluster 1). The H1-H3 hydrophobic interactions were limited to only M157, Y160 and V212 interactions. The T-rich region of H2 was deformed. There were also a series of short-lived conformations in equilibrium with VRQ2_2 which differed from each other by the extent of deformation of H2 and the conformation of B1-H1 loop (Figure 3.8).

3.1.5 ARR simulation-1 at 310K

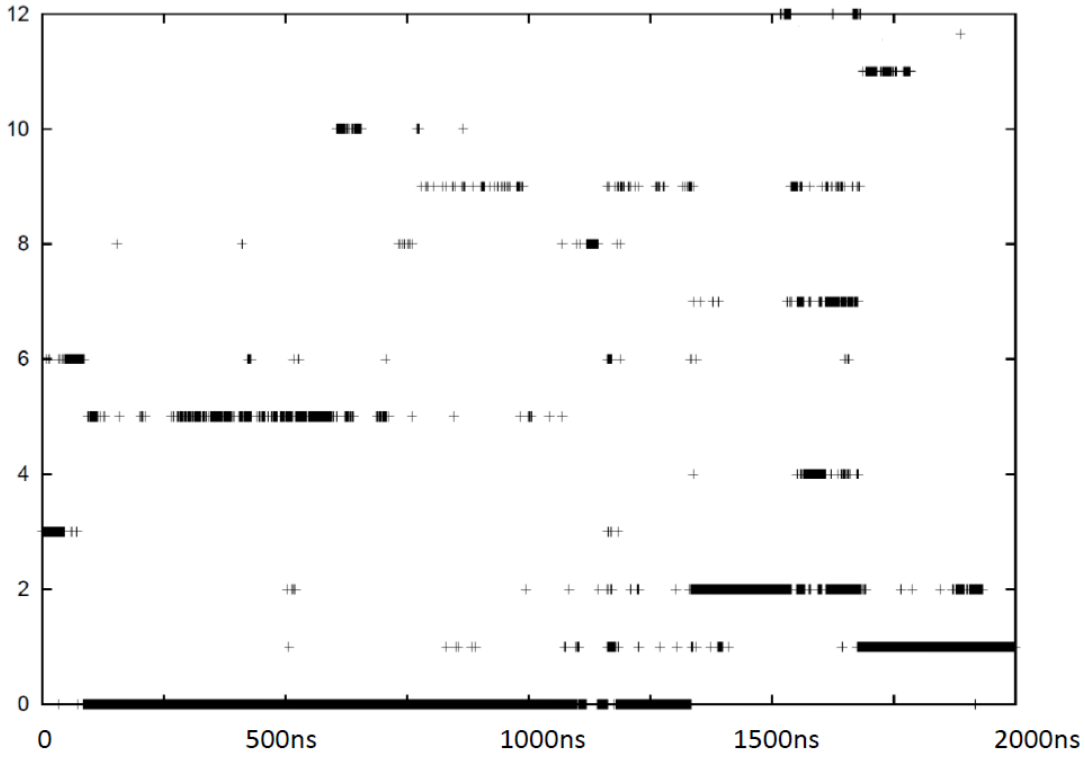

Figure 3.9: Cluster number (0-12) vs. time graphic of first ARR simulation.

A136 explored 3 major conformations in addition to 10 short-lived structures. In the most abundant one (ARR1_1, cluster 0) that covered almost 1.25 μs, it was completely buried between M216, T219 and Q220 of H3. Its NH group made a hydrogen bond with the CO group of N162 leading to an extended regular β-strand without a bulge. Because of its small side chain, it could easily accommodate at this positon without destabilizing the interactions between H1, B1-H1 and H3. This contrasted with the observations in VRQ simulations where V136 at the same position led to some dramatic effects like wide opening of B1-H1 loop and H1 from H3. This structure was in equilibrium with one where A136 was fully solvent exposed as in the crystallographic structure (ARR1_2, cluster 1) and another one (ARR1_3, cluster 5) where A136 was adjacent to T219 and Q220 though it was mostly solvent exposed unlike ARQ1_1. In both structures, B1 comprised only M132 and G134 followed by a wide bulge (Figure 3.10).

In all three structures, a 3_{10}-helix formed between L141 and F144. At the same time, the R139-D150 interaction was observed. As a result, the N-terminus of H1 opened to make H1 located away from H3.

In all structures, including the short-lived ones, the C-terminus of H3 unwound and oscillated. In one of the short-lived conformations (ARR1_4), the C-terminus even interacted with B1 to form a three-stranded β-sheet (cluster 2).

In ARR1_2 and ARR1_4 the region between P168 and N174 formed an α-helix. This region was part of the B2-H2 loop in other structures. In ARR1_2, R171 of this helix made a salt bridge with E224. In ARQ and VRQ, the asparagine at this position could not form such an interaction.

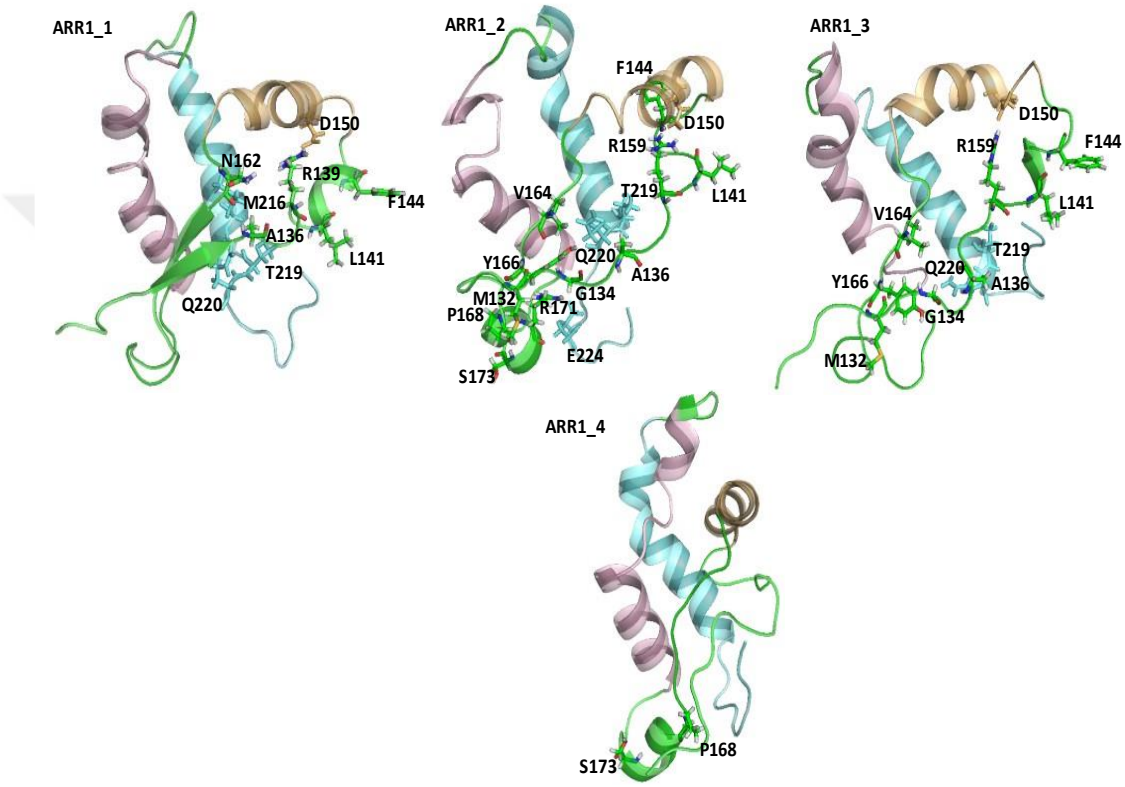

Figure 3.10: Different clusters and interactions of ARR simulation 1.

3.1.6 ARR simulation-2 at 310K

Shortly after starting the simulation from the crystallographic structure, the native β-sheet shifted by one residue leading to the L133-Y166 and S135-V164 hydrogen bonds instead of M132-Y166 and G134-V164 (ARR2_1, cluster 1 on Figure 3.11). H1 was in a closed conformation with respect to H3. H2 was unwound starting from Q189. A136 was close to T219 and Q220 but completely solvent exposed as in ARR1_3.

In ARR2_2 (cluster 2), the C-terminus of H3 interacted with B1 through M137-Q222 and R139-T219 backbone hydrogen bonds. A136 was solvent exposed while M137 NH group was incorporated into the native β-sheet.

In ARR2_3 (cluster 0) the native β-sheet was restored. In addition, M137-Q222 and R139-R223 hydrogen bonds were observed between the C-terminus and H1-B1 loop. Starting from V183, H2 was disordered.

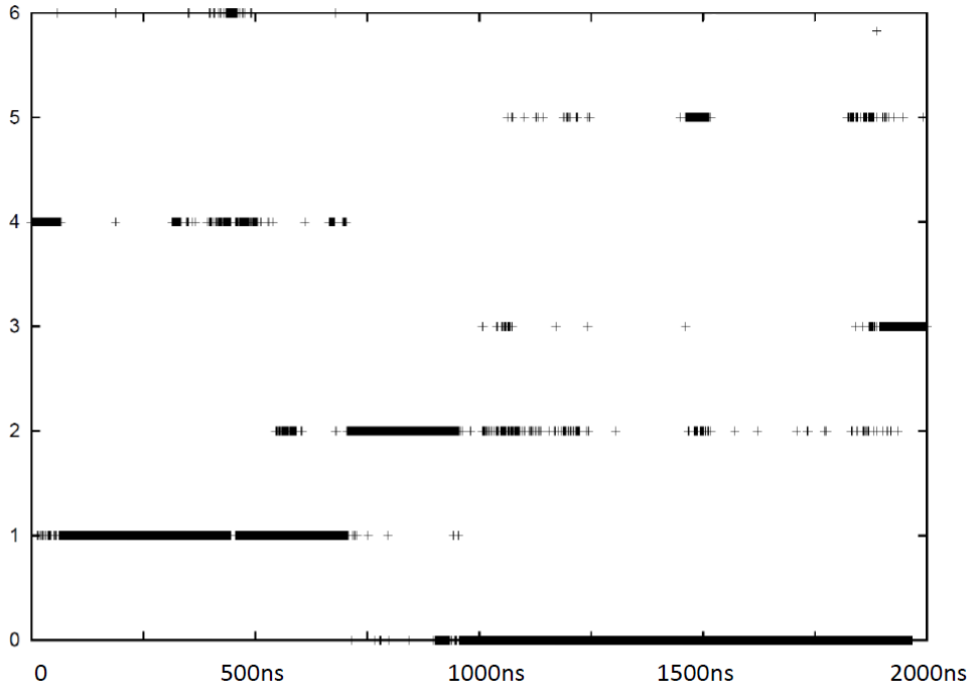

Figure 3.11: Cluster number (0-6) vs. time graphic of second ARR simulation.

In ARR2_4 (cluster 3), B1 and B2 were completely separated. M137-Q222 and R139-R223 hydrogen bonds still persisted while the C-terminus was held in place by the R171-Y228 salt bridge. These interactions might prevent further separation of B1. Meanwhile, Y165-V187, Q163-Q189 hydrogen bonds formed a short β-sheet between B2 and the C-terminal part of H2. Thus, the native β-sheet was replaced by two β-sheets, one with B1 and C-terminus of H3, another one between B2 and C-terminus of H2. At the first glance, this increase in the β-sheet content at the expense of C-terminal parts of H2 and H3 could be interpreted as the initial step of misfolding into a scrapie conformation. However, since ARR2_4 was in equilibrium with ARR2_2 and ARR2_3, it was also possible that these new β-sheets might prevent further unfolding by stabilizing a PrP* type structure. Nevertheless, it had also to be noted that R171-Y228 salt bridge would not be possible in a GPI-anchored protein (see Figure 3.12).

3.2 Restrained Simulations

During these simulations of different variants, mentioned above, at 310K, we had observed an excessive opening of N-terminus of the truncated prion. In physiological

conditions, prion has a very long N-terminal which functions in binding of ions and interacts with cell membrane surface (Singh et al., 2017). Also, N-terminal amino acids from 90 to 124 was found to be not flexible as known from NMR analysis (Kaimann et al., 2008).

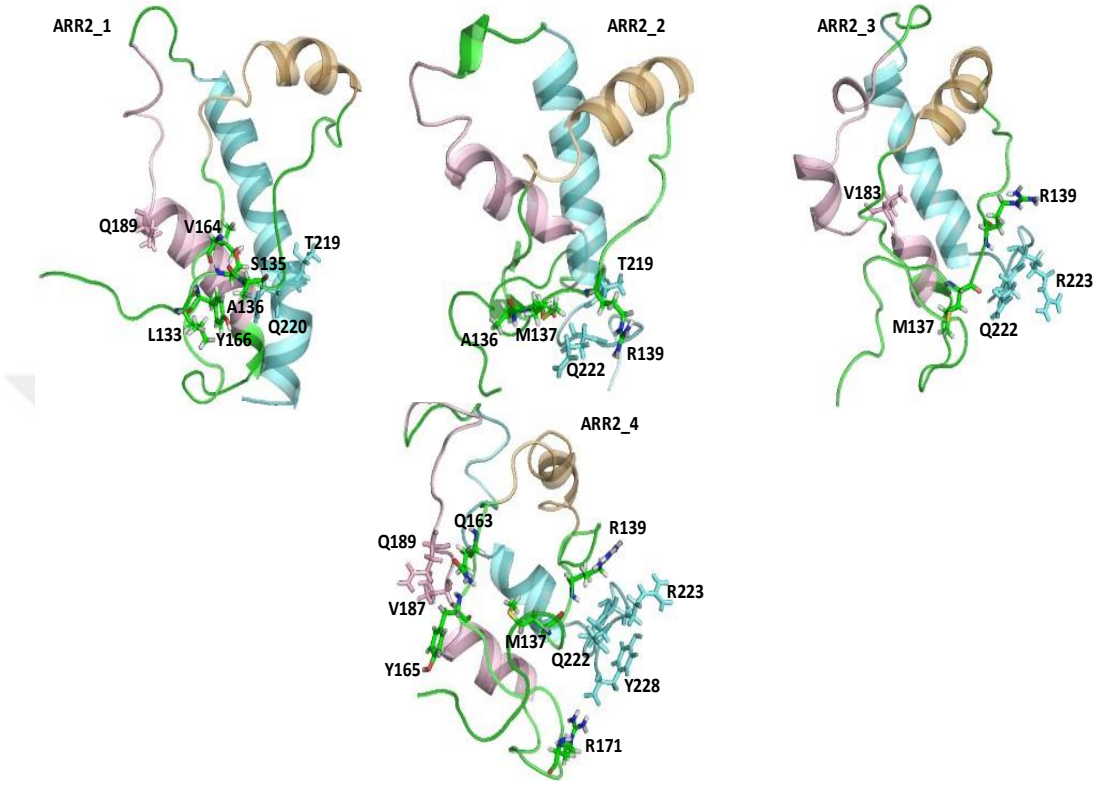

Figure 3.12: Different clusters and interactions of ARR simulation 2.

So, what we had observed about N-terminal movement during these simulations was overcome by putting distance restraint between M132 and Y166 to stabilize N-terminus as in cellular conditions. The same scenario was also seen for the C-terminus of the protein. Normally, C-terminal is GPI-anchored to cell membrane so it should not be as flexible as what we had observed in our simulations. To avoid C-terminal movement we had put restraint to the last turn of C-terminus of H3. These restrained simulations were also conducted for 2000ns at temperatures of 310 and 330K.

3.2.1 TPX-ARQ helix restrain

During the entire simulation 4 conformations were in equilibrium with each other (Figure 3.13). In ARQ3_1 (cluster 0) and ARQ3_2 (cluster 1) the β-sheet shifted by one residue such that L133-Y166, S135-V164 and M137-N162 hydrogen bonds were formed. This removed the bulge and created a continuous β-sheet.

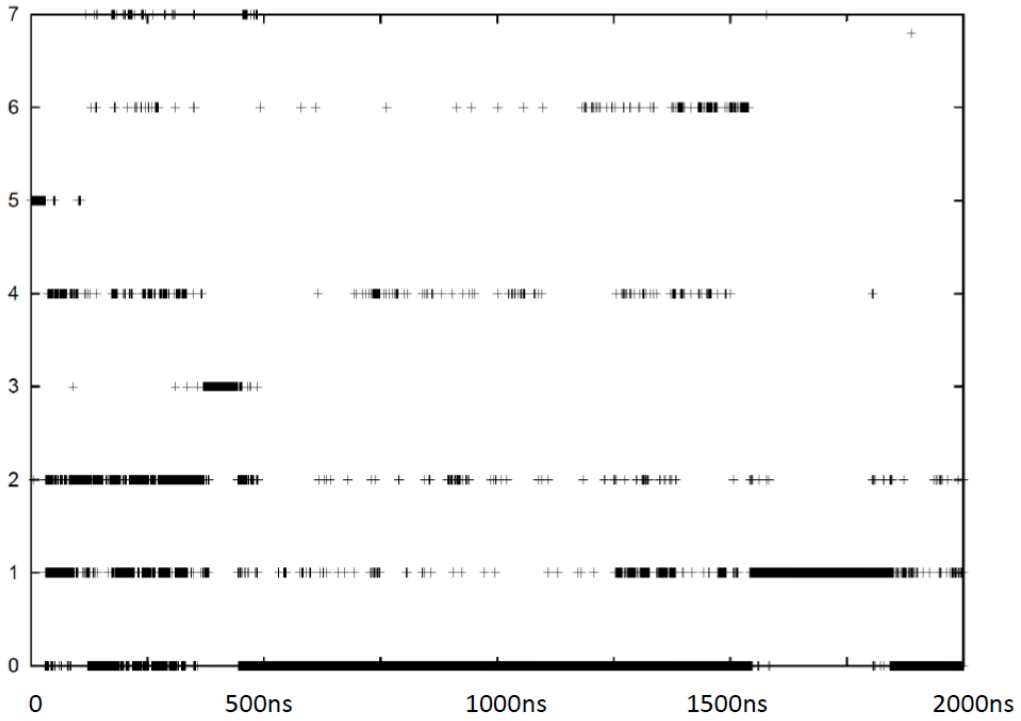

Figure 3.13: Cluster number (0-7) vs. time graphic of ARQ helix restrain simulation.

On the other hand, in ARQ3_3 (cluster 2) and ARQ3_4 (cluster 4), the native β-sheet seen in the crystals was observed. Thus, although ARQ3_1 and ARQ3_2 displayed a longer and continuous β-sheet, this should not be considered as the beginning of the misfolding toward a β-sheet rich structure as this type of β-sheet was in equilibrium with the shorter β-sheet seen in ARQ3_3 and ARQ3_4. In both cases, M137 interacted with M216 and T219. Thus, the β sheet faced a different turn of H3 compared to the previous simulation (one turn closer to the N-terminus of H3). A136 was totally solvent exposed in all structures. ARQ3_1 and ARQ3_2 differed in the orientation of the 6 N-terminal residues. ARQ3_3 and ARQ3_4 differed in the structure of the B1-H1 and B2-H2 loops. In all structures, the C-terminal T-rich half of H2 was unwound, while R159-Y160-D205 interactions attached the C-terminus of H1 to the N-terminus of H3. The fluctuations in the T-rich region and H2-H3 loop were further restricted by E199-R159 and T196-R159 interactions in ARQ3_2 and ARQ3_4. On the other hand, R139 interacted with D150, favouring an open H1 conformation (see Figure 3.14).

3.2.2 TPX-ARQ β-sheet restrain

Throughout the whole simulation 10 conformations were observed (Figure 3.15) to be in equilibrium with each other. The most abundant structure ARQ4_1 (cluster 0) had a H1 conformation similar to ARQ1_1. The β-sheet displayed the bulge at S135-A136

as in ARQ1_4, but M137 made a hydrogen bond with N162. Thus, the bulge was not as wide as in ARQ1_4. The side chain of M137 was located between M216-T219 as in ARQ3_1. A136 was solvent-exposed.

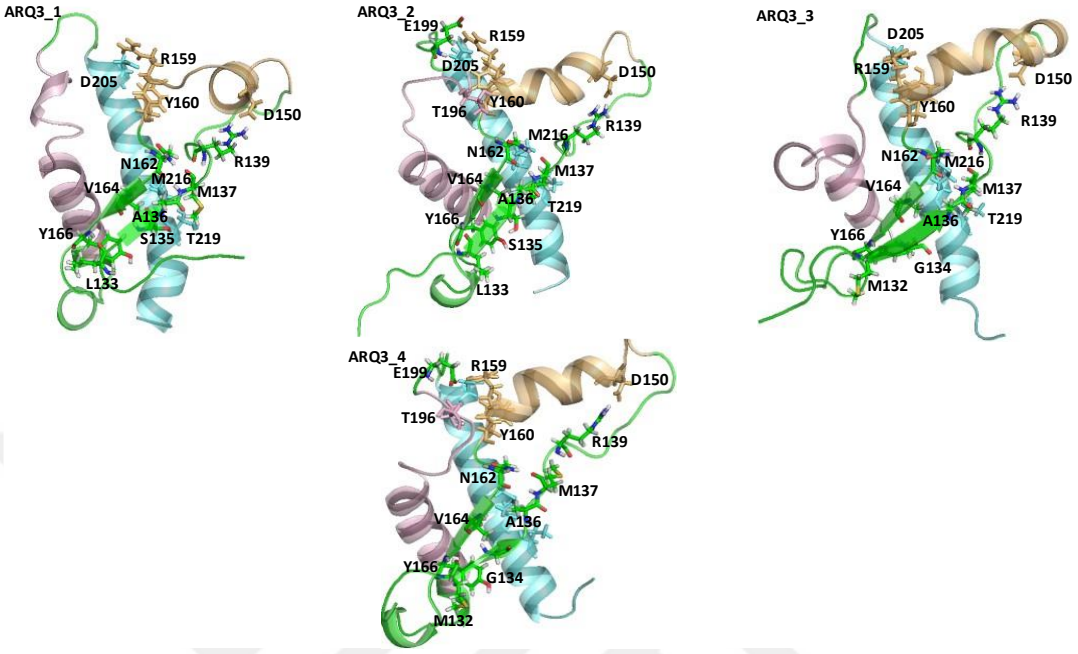

Figure 3.14: Different clusters and interactions of ARQ-helix simulation.

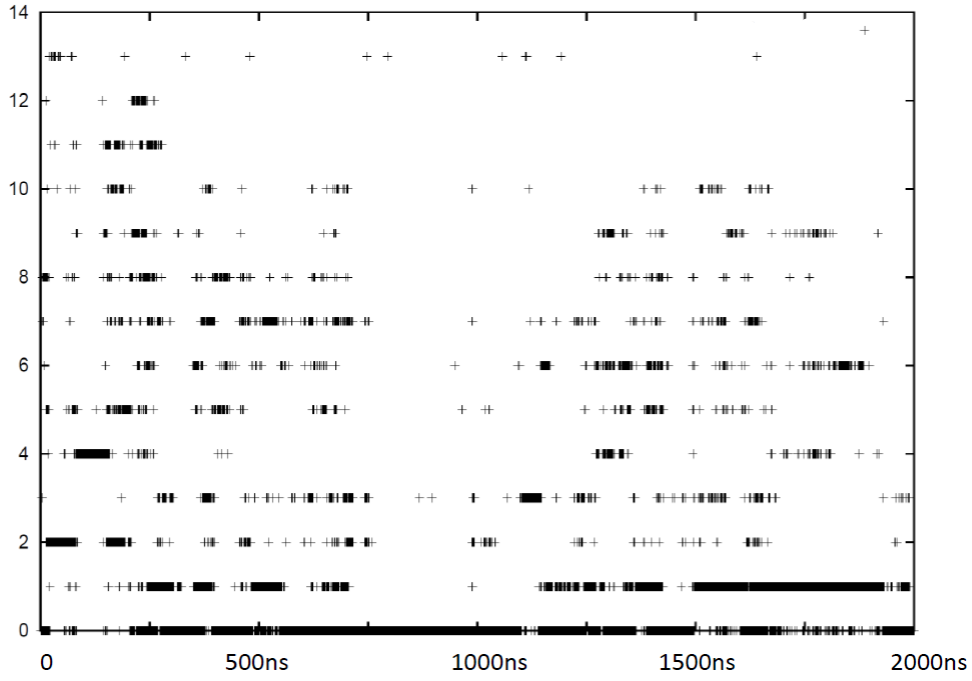

Figure 3.15: Cluster number (0-14) vs. time graphic of ARQ β-sheet restrain simulation.

The T-rich region of H2 was unwound. R159-Y160-D205 interactions kept H1 close to the N-terminus of H3. In ARQ4_2 (cluster 1), the A136-M137 peptide bond was

oriented in an opposite direction with respect to ARQ4_1, partially burying A136 between M216-T219. The T-rich region of H2 adopted a different (but still unwound) conformation. The rest of the structure was similar to ARQ4_1. ARQ4_3 (cluster 2) differed from ARQ4_1 in that no part of H2 was unwound. The remaining conformations differed from ARQ4_1 or ARQ4_2 in the geometry of the T-rich region of H2 and H2-H3 loop. Thus, all the structures in this simulation belonged to the same basin on the potential energy surface, the C-terminal part of H2, H2-H3 loop and S135-A136-M137 displaying fluctuations. Clearly, restraining the β-sheet largely reduced the conformational flexibility of PrP^C.

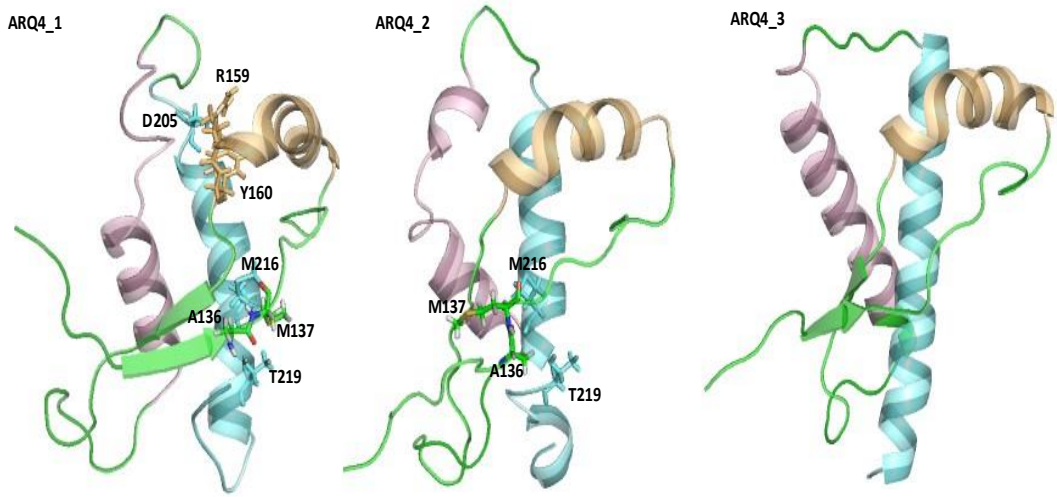

Figure 3.16: Different clusters and interactions of ARQ-beta simulation.

3.2.3 TQB-VRQ helix restrain

The simulation was dominated by one major conformation (VRQ3_1, cluster 0, Figure 3.17). Even though we had not restrained the native β-sheet here, it remained very stable throughout the whole simulation. A 3_{10}-helix was observed between S135 and R139 (Figure 3.18), keeping V136 constantly in a completely solvent exposed conformation. In addition, an α-helix formed between L141 and G145 on B1-H1 loop. The C-terminus of H2 was partially unwound, the T-rich region forming a one-turn helix.

3.2.4 TQB-VRQ β-sheet restrain

Three conformations in equilibrium with each other were observed (Figure 3.19). They were similar to VRQ2_2 with the exception of R139-D150 salt bridge absent in this simulation. They differed from each other by the orientation of H1 (Figure 3.20). This

simulation thus further confirmed that a buried V136 conformation made H1 more mobile.

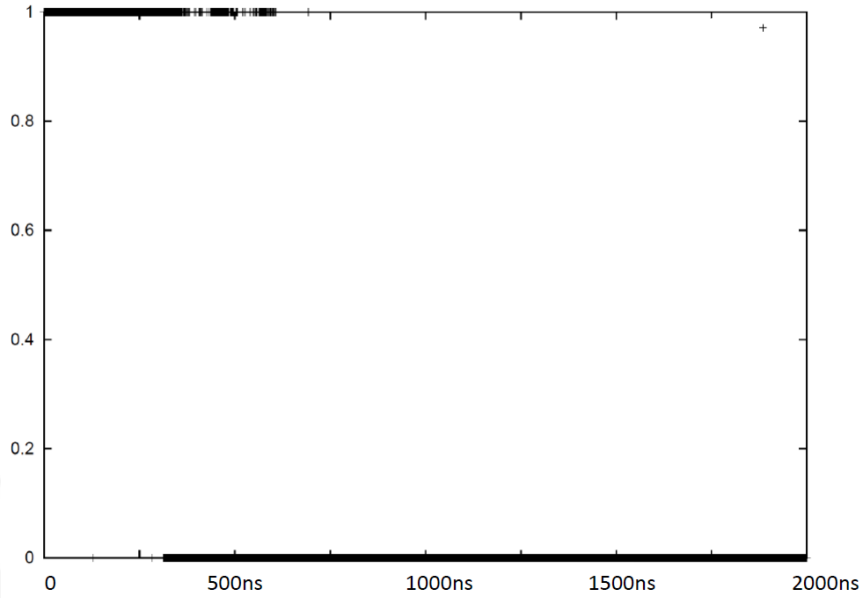

Figure 3.17: Cluster number (0 and 1) vs. time graphic of VRQ helix restrain simulation.

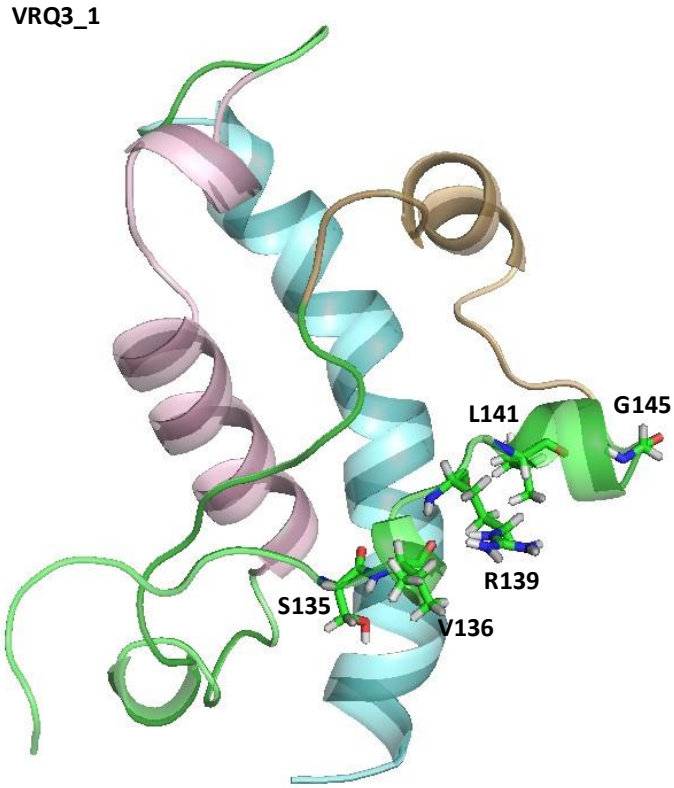

Figure 3.18: Cluster and interactions of VRQ-helix simulation.

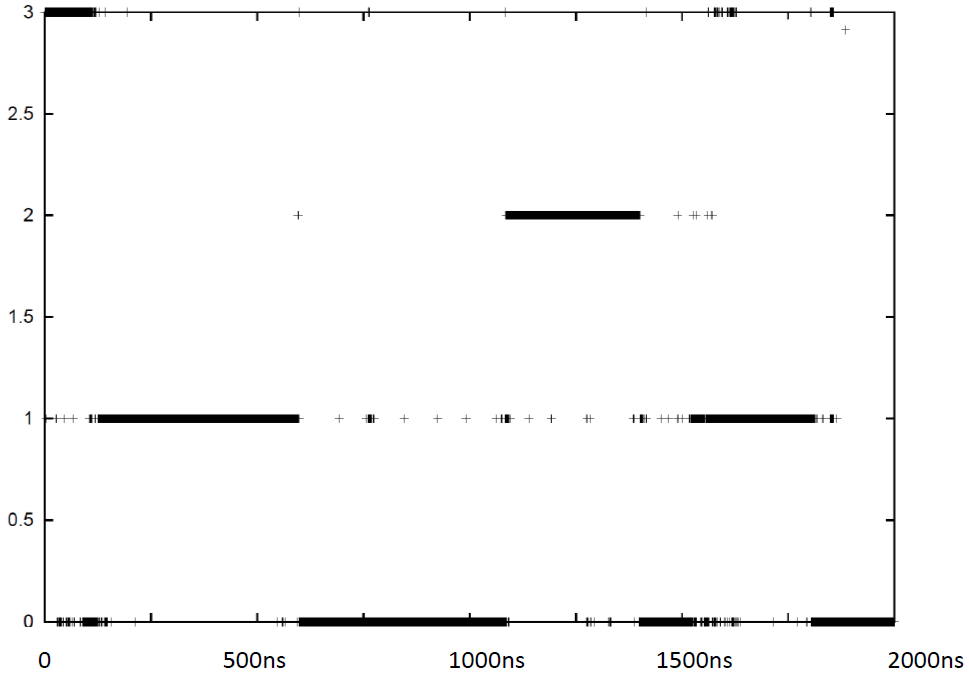

Figure 3.19: Cluster number (0-3) vs. time graphic of VRQ beta restrain simulation.

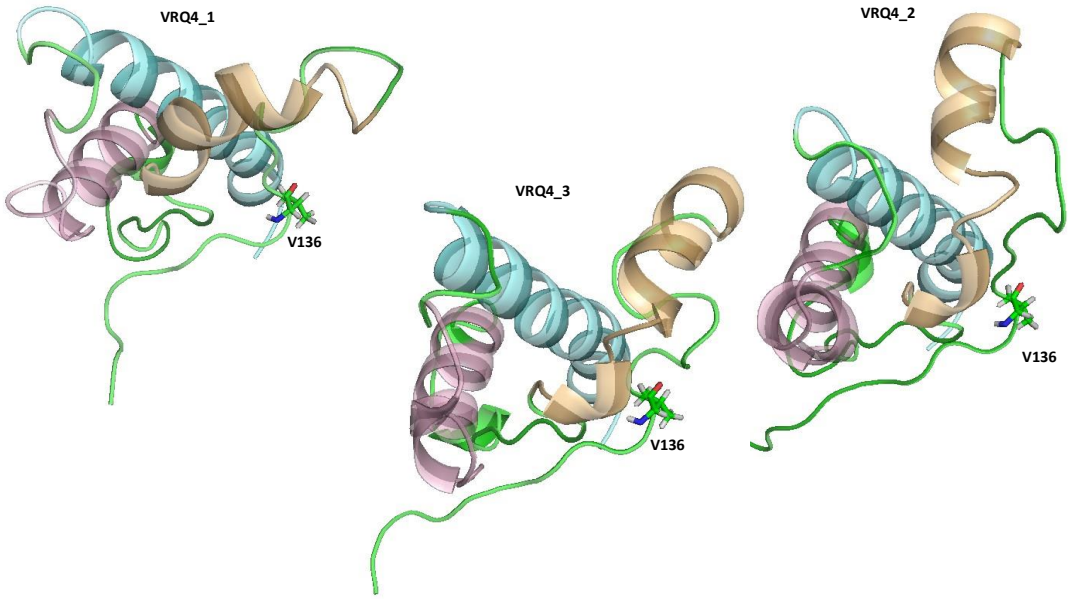

Figure 3.20: Clusters and interactions of VRQ-beta simulation.

3.2.5 TQC-ARR helix restrain

The ARR helix simulation was dominated mainly by ARR3_1 (cluster 0) (Figure 3.21) which was mostly similar to the crystal structure except that A136 was partially buried between T219-Q220 and R223. This structure was in equilibrium with ARR3_2 where H1 was in an open conformation with respect to H3. In both structures, R171 made salt bridges with E224 and Y228. Thus, when the movement of the C-terminus was

restricted, mimicking a GPI-anchored PrP, the interaction between R171 and the C-terminus significantly reduced the conformational movements (Figure 3.22).

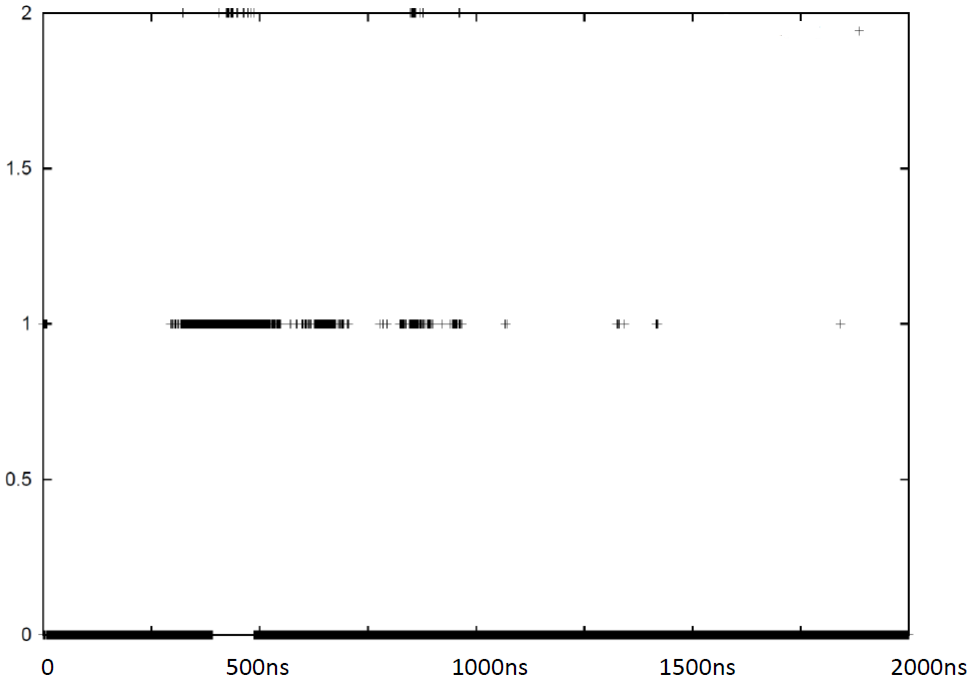

Figure 3.21: Cluster number (0-2) vs. time graphic of ARR helix restrain simulation.

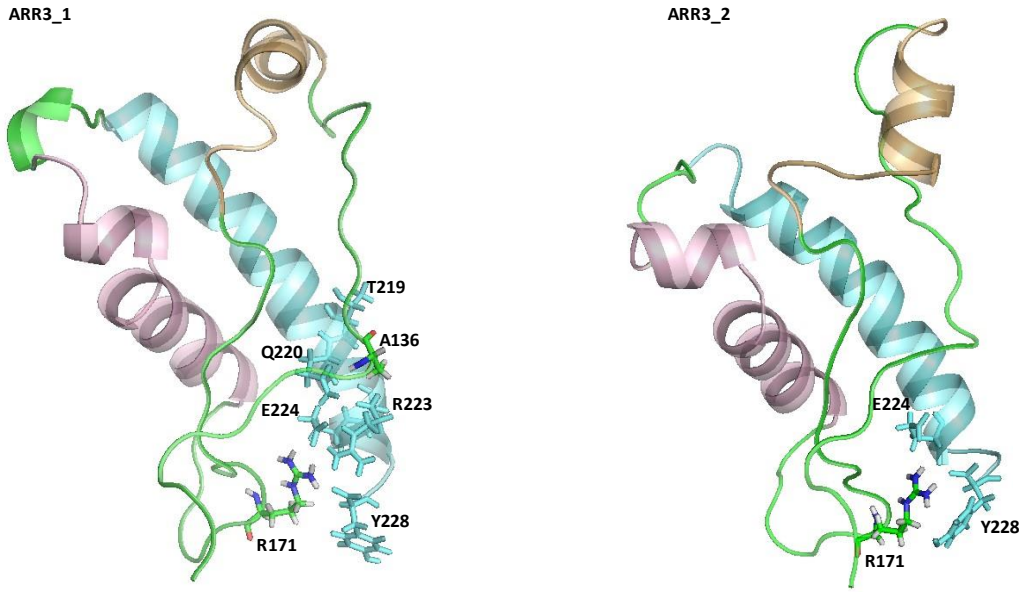

Figure 3.22: Clusters and interactions of ARR-helix simulation.

3.2.6 TQC-ARR β-sheet restrain

The conformation ARR4_1 (cluster 0) covered approximately 90% of the simulation (Figure 3.23). A helix between L141 and N146 (of normally B1-H1 loop) stabilized by the R139-D150 salt bridge was observed. H2-H3 loop folded into a helix and

becomes part of H3. The T-rich region of H2 was disordered. A136 became part of the β-sheet while its side chain was buried between B1-H1 loop and H3, making a hydrophobic interaction with M216. The last 2 turns of H3 unfolded, allowing S225 and A227 making hydrogen bonds with L133 and S135 of B1, respectively, adding a short strand to the β-sheet (Figure 3.24). However, such a structure could not be formed in a GPI-anchored protein. H1 was in a closed conformation relative to H3, and its C-terminus was attached to H3 by R159, Y160, D205 interactions. R171 did not interact with H3.

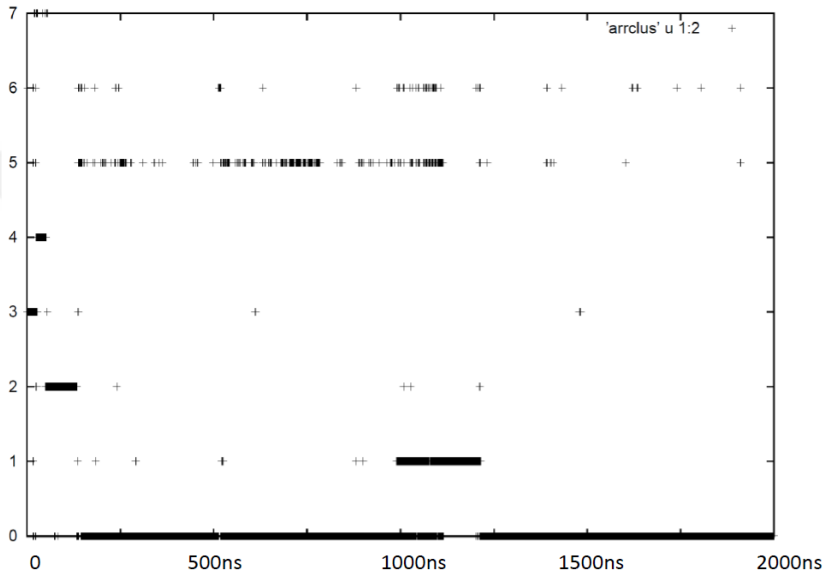

Figure 3.23: Cluster number (0-7) vs. time graphic of ARR beta restrain simulation.

The remaining 10% of the simulation was populated by several structures which differed from ARR4_1 by an open conformation of H1, by the absence of L141-N146 helix and by the conformation of the H2-H3 loop. In one of these structures, ARR4_2 (cluster 5), the T-rich region of H2 made backbone and side chain hydrogen bonds with the H1-B2 loop. In another one, ARR4_3 (cluster 1), R171 formed a salt bridge with E224. Although this interaction was not observed only in ARR4_3, in the other structures the presence of hydrogen bonds between B1 and C-terminus kept H3 and H2 close to each other, reducing conformational flexibility.

3.3 ARQ, VRQ and ARR Simulations at 330K

330K simulations were undertaken twice, to ease the unfolding of the protein; so that the main dislocation and misfolding pathways of the protein could be observed in a short period of time. Also restrained 330K simulations were also conducted.

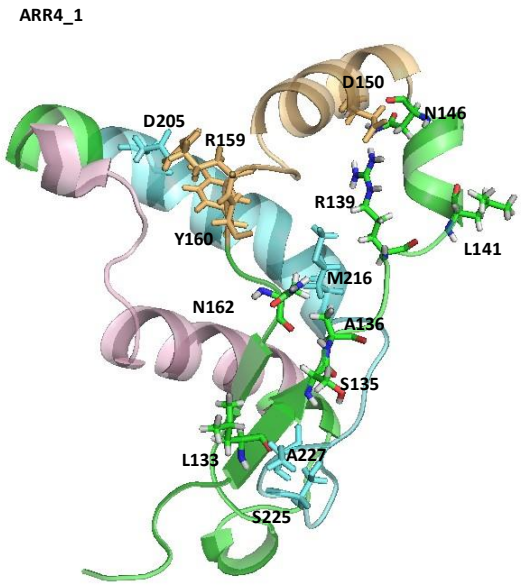

Figure 3.24: Cluster and interactions of ARR-beta simulation.

In the first ARQ simulation at 330K, R159-D205 salt bridge was taken over by R159-E199 to keep H1 close to H2 and H3. At 330K even salt bridge formation between R159 and E203 was observed that we had not seen at 310K simulations (529ns). As a result of 330K, B1 separated from B2 easily but reformed the β-sheet again. This time Y131 interacted with V164 (784ns). Also, Y165 of B2 made hydrogen bond with K188 of H2 when unfolding of B1 from B2 occurred. When simulated the second time, we observed the separation of B1 from B2 and refolded again by making interaction between G134 and Y166 for approximately 90% of the 1000ns simulation.

During VRQ simulation at 330K, B1 separated from B2. B1 came back to its original position but this time Y131 and M132 interacted with N162 and G134-Y160 interaction occurred (433ns). R159-D205 salt bridge was still protected but B1-H1 loop moved toward the C-terminus of H3 while N-terminus of B1 located at H2-H3 loop. Total separation of B1 from B2 gave a chance to form a small β sheet between B2 and H2 through the residues of V164-N184 and Q163-T186/V187 (819ns). B1-B2 interactions seemed to be important for the helical structure of H2, when B1 opened up B2 interacted with H2 to form small β sheet by unwinding H2. In the second simulation of the same conditions, when B1 moved away from B2, H2-B2 interactions became dominant. Q163, Y160 and Y158 made hydrogen bond with T186, K188 and H190 respectively. These interactions unwound H2, so that new β-sheet formation between H2 and B2 prevented ‘banana peeling’ of H1.

In the first simulation of ARR at 330K, H2 was unfolded, so that H2-B2 β-sheet formation was observed; even though the native β-sheet was preserved. While M132-Y166 and G134-V164 were protected, R167-D181, Y165-V183 and Q163-I185 hydrogen bonds were formed between B2 and H2 (520ns). These interactions were seen even when the R159-D205 salt bridge was broken. When ARR simulated at the same conditions, B1 separation from B2 promoted the B2-H2 β-sheet formation and then the addition of B1 formed a triple β-sheet. B1-B2 interactions were maintained by M137 and Y166, while B2-H2 interactions were between Y165-N184, R167-C182.

When native β-sheet of ARQ at 330K was protected with a restraint, unwinding of H2 was not observed. The salt bridge between R159-D205 was not seen in the majority of the simulation, so as a result H1 moved away from H2 and H3, but still H2 and H3 did not form a β-sheet. It seemed that for the unwinding of H2, B2 was the key strand to unfold H2. So that, B1 separation was an important step for the unwinding process of H2. On the other hand, when only the last turn of the C-terminus of H3 was restrained, B1 separated from B2 again causing the formation of a small β-sheet between B2 and H2 through hydrogen bonds of Y165-T186, Q163-K188 and R167-N184.

When the native β-sheet of ARR at 330K was protected, unwinding of H2 did not observed. The salt bridge between R159-D205 was protected throughout the simulation. In addition, when the last turn of helix at H3 was restrained, salt bridge formation between R159 and E203 was observed. B1 interaction with B2 was seen with some differentiations from original β-sheet but even these interactions of Y166-S135 or Y166-M137 kept B1 and B2 together so that the unfolding H2 did not occur. In the last 350ns of 2000ns B1 separated from B2 but B2-H2 β-sheet formation was not observed.

In β-sheet restrained VRQ simulation at 330K, the salt bridge between R159-D205 was broken so that H1 moved away from H2-H3 for a while but R159-E203 salt bridge was reformed to keep the structure together. 330K temperature unfolded H2, so that H2-B2 β-sheet formation was observed; even though the native β-sheet was preserved. P161-Q189, Q163-V187, Y165-I185 were keeping H2 and B2 together. But when H2 gained its helical content back these interactions were lost. In helix restrained simulation at 330K, B1 moved away from B2, so R167-C182, Y165-N184, N162/Q163-I185/T186 form H2-B2 β-sheet. Salt bridge formation between R159 and E206 was dominant throughout the simulation.

The overall results were of 330K simulations:

1. 330K simulations of ARR, ARQ and VRQ show the importance of R159-D205 salt bridge. Even at 330K this interaction is maintained to keep H1 and H3 together.
2. On the other hand, separation of B1 from B2 and opening of H1 from H3 occur more quickly and excessively at 330K.
3. Furthermore, even at 330K when native β-sheet is protected with a restraint, R171 of ARR at B2-H2 loop moves toward C-terminus of H3, which in return keeps the structure undeformed. On the other hand, Q171 of ARQ and VRQ at 330K cannot make this interaction constantly to maintain the stability.

Nevertheless, by restraining 330K simulations too, we have created the cellular conditions for N- and C-terminal so that only the unfolding of helices and β-sheet can be focused on.

3.4 VRR Simulation at 310K

VRR is a rare variant in nature and its resistancy or susceptibility to disease has not been known. To emphasize the importance of alanine-valine differences, we simulated VRR at neutral pH and 310K. Simulation of VRR showed that V136 tried to disturb the overall stability by separating B1 from B2, while R171 formed a salt bridge with Y228 to keep H2 and H3 in contact. Besides, salt bridge between R139 and E199 took place of R159-D205 salt bridge to kept H1 and H3 together. Nevertheless, V136 overcame these protection roles of R139-E199 and R171-Y228 salt bridges to loosen up the native β-sheet and reformed it in a shifted manner as V136 made a hydrogen bond with V164, while G134 formed a hydrogen bond with Y166. Also, H1 was now in widely open position with respect to H3.

3.5 Unfolding of H1

H1 is made of hydrophilic residues and is the most soluble helix in Protein Data Bank. In addition, H1 does not make any salt bridge interactions with rest of the PrP^{C} (Morrissey and Shakhnovich, 1999).

H1 was very stable during our simulations even at 330K. According to the experiments in the literature, we know that H1 should unfold to participate in PrP^{Sc} formation. Thus,

we modeled various conditions that may favor the unfolding of H1. PrP^{C} conversion into PrP^{Sc} occurs at low pH and in literature this transition process suggested to happen in endosome. To mimic that environment, we changed the protonation states of the aspartates and glutamates of H1 to unfold. Also, we neglected the effect of 126 amino acid residues at N-terminus when we simulated globular protein as ARQ, ARR and VRQ because this part of the protein is known to be unstructured in PrP^{C} and at least the first 90 residues do not form β-sheets in PrP^{Sc}. To understand whether N-terminal region could affect H1 stability or not inside endosome at low pH, simulation of H1 with the N-terminal, 56 amino acids was also conducted.

Besides, H1-H1 dimer formation and unfolding of H1 by using a polyvaline peptide as template were also analyzed to investigate whether H1 would unfold or not. In addition, H1 and N-terminal polybasic sequence dimer formation was also observed. Importance of polyanion existance for PrP^{C} to PrP^{Sc} transition, even in the absence of preexisting prion, was also shown (Deleault et al., 2007); so H1-ion interaction (like Cl- and K+ that are found in high concentration inside the physiological conditions) were also simulated.

3.5.1 H1-H1 dimer formation

Intramolecular salt bridges seem to be important for the stability of H1 as mentioned in the literature. We would like to test whether H1 is going to unfold when it interacts with another H1 to convert intramolecular salt bridges to intermolecular ones and form a dimer or not. We put a distance restrain of 30Å between E155 of first H1 strand and E155 of second H1 strand. With such a restraint, monomers move around each other freely to explore various dimer configurations whereas they cannot completely move apart. As a result of 1000ns simulation unfortunately no deformation or unwinding of helical structures were observed (Figure 3.25). Even C-terminal of H1, which had been very flexible in our globular domain simulations, was stable.

3.5.2 H1-Polybasic dimer formation

Even though hydrophobic or polar interactions do not play a role in binding, positively charged amino acids may play an important role for the interaction between the peptides and PrP^{Sc}. In peptide–PrP^{Sc} interaction, amino acid composition seems to be important for binding activity. Cationic domains of PrP^{C} and a specific domain of PrP^{Sc} seem to be important for the transition of PrP^{C} to PrP^{Sc} (Lau et al., 2007).

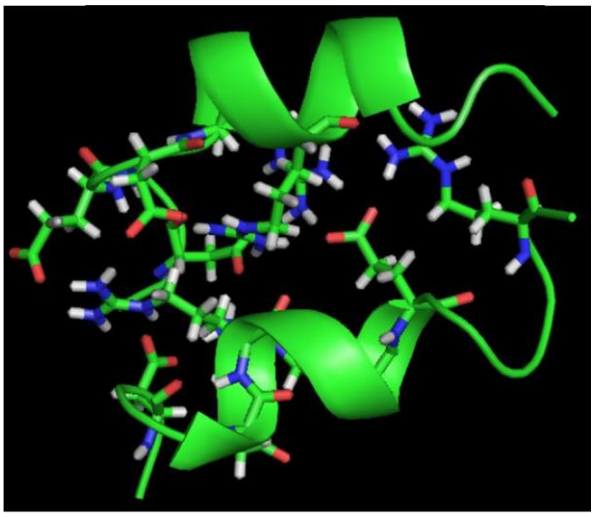

Figure 3.25: Intramolecular salt bridges were preserved while intermolecular salt bridges were also formed.

A positively charge sequence like KKRPK of N-terminal, that we did not consider during our ARQ, VRQ and ARR simulations, was used to unfold H1 by affecting intramolecular salt bridges. N156 of H1 and K2 of polybasic sequence had distance restrained as 30Å to keep two strands together. Only temporary interactions observed with the Arginine of the KKRPK sequence interacting with any one of the acidic residues (Figure 3.26). Merely the C-terminal YRY sequence of H1 unfolded for a while. But we know from our previous results that YRY was the most flexible part and had high potential to unwind, hence the movement observed in this region cannot be attributed to the effect of the polybasic sequence. Also, from literature survey we know that polybasic region of PrP^{C} is important to recognize and bind PrP^{Sc} (Turnbaugh et al., 2012), but polybasic sequence of PrP^{Sc} cannot recognize and bind to any region of PrP^{C}.

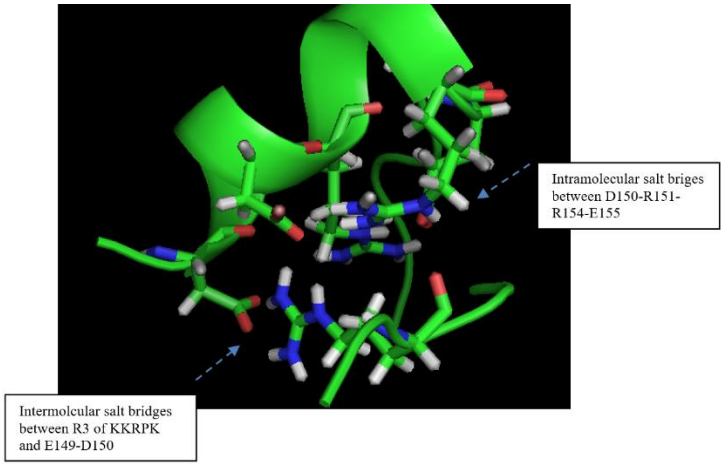

Figure 3.26: Intramolecular salt bridges were preserved while intermolecular salt bridges were also formed.

3.5.3 H1-Polyvaline dimer formation

To unfold H1, we tried a sequence made of 15 valine residues, which has high propensity to form β-strand, to unwind and form β-sheet with H1. We put distance restrain between V13-Y158, V14-R159, V15-Y160. Stable β-sheet formation was not observed. Only V12-M157 hydrogen bond was formed as an extra interaction except from our distance restraints (Figure 3.27).

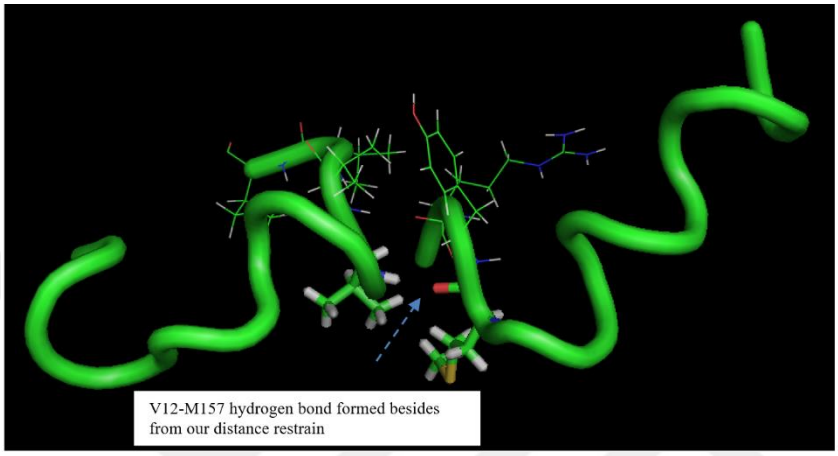

Figure 3.27: V12-M157 hydrogen bond formation.

On the other hand when we changed the protonation states of all aspartic acids and glutamic acids of H1, unwinding of H1 and short β-sheet formation was observed (Figure 3.28).

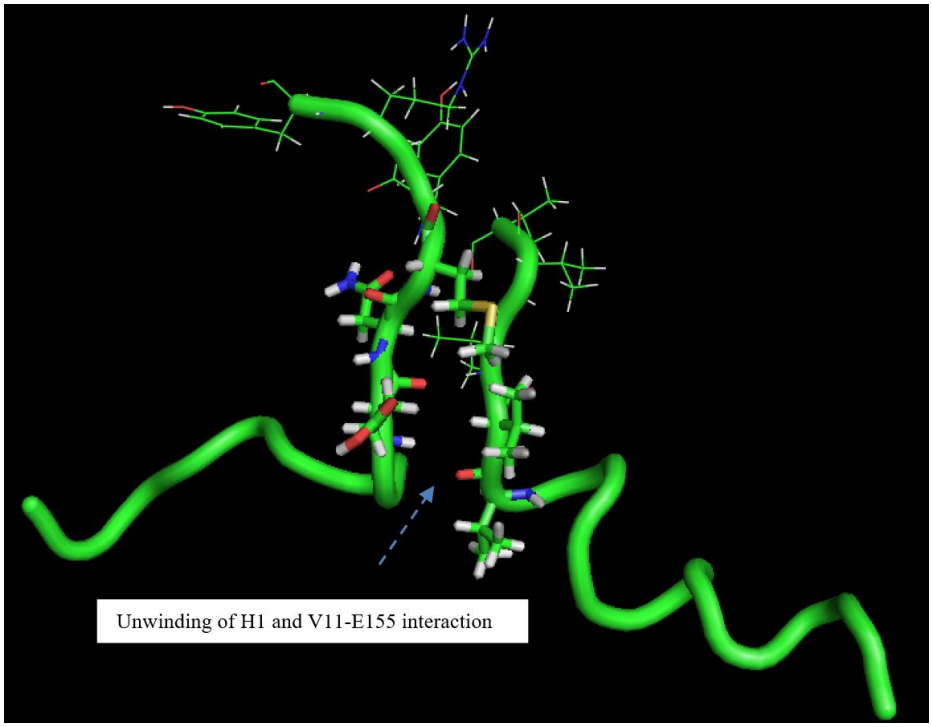

Figure 3.28: Unwinding of H1.

3.5.4 N-terminal-H1 intramolecular complex formation

Endosomal compartments seem to be an important step in the conversion of PrP^{C} to PrP^{Sc}. When cellular PrP is taken into those vesicles long N-terminal part would also enter inside those vesicles. To see how N-terminal sequence will affect H1 stability we created a low pH environment by changing protonation states of histidine, aspartic acid, and glutamic acid. Approximately 90 amino acid residues do not fold into β sheet structure of PrP^{Sc} and that's why we discarded first 90 residue and used the remaining 56 amino acids of N-terminus and B1 with H1 and B2 sequence. From our previous simulations that included H2-H3 only, we know that H2 and H3 can unwind. To observe whether N-terminus-B1-H1 and B2 parts are going to unfold or not, we simulated this 79 amino acids long sequence for about 1600ns. Unwinding of H1 did occur but N-terminal did not interact with H1 to form a stable β-sheet (Figure 3.29).

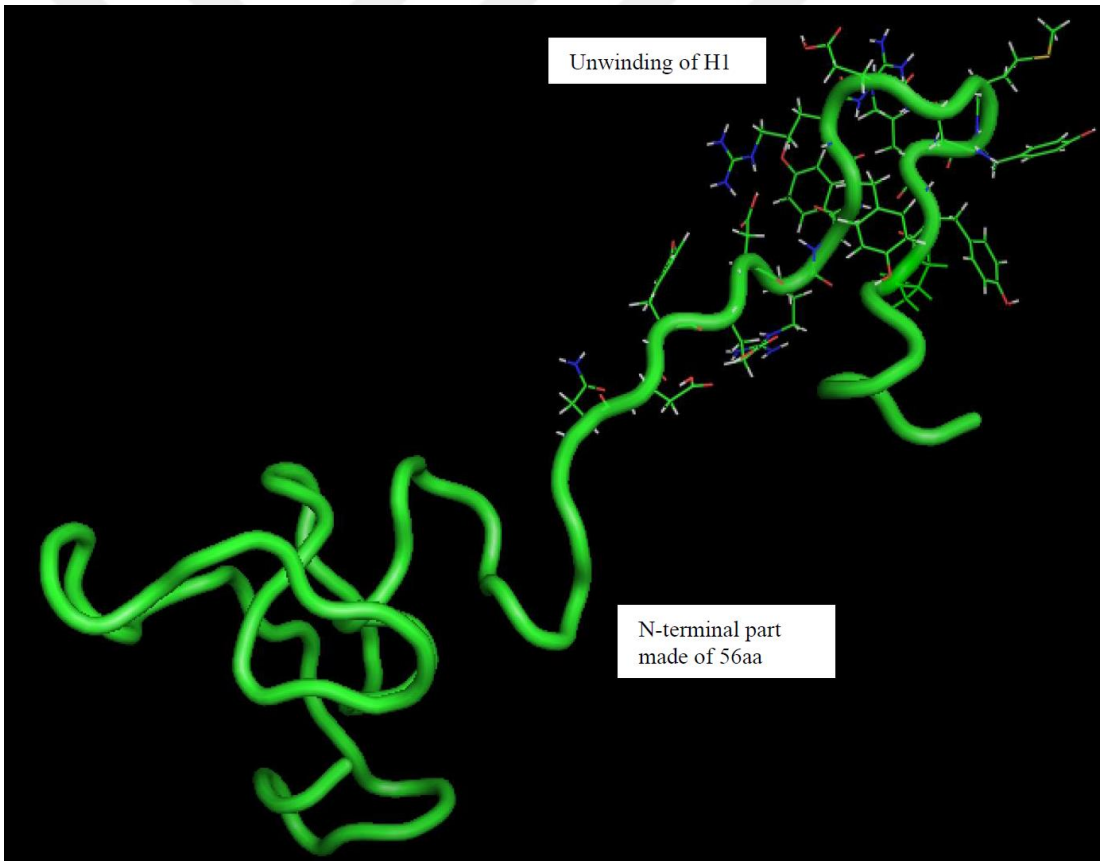

Figure 3.29: Unwinding of H1 was not related to N-terminal sequence.

3.5.5 H1-Cl^{-} and H1-K^{+} interaction

Even though implicit solvent simulations are not the best choice for monatomic ion simulations, we would like to make a preliminary study to see the effect of ions on H1

stability. Unfortunately, neither Cl^- nor K^+ had caused the unwinding of H1. They even failed to make stable ion pairs with the charged amino acids on H1 (data not shown).

3.5.6 Different protonation states of H1

To break down intramolecular interactions of H1 and maintain the unfolding; we decided to change protonation states of GLU and ASP found in H1 sequence. Each time we only protonated one residue. pH of lysosome is about 4-4.5, so it is unlikely that all glutamic and aspartic acids, which have very low pKa levels, would protonate at the same time inside lysosome. Although we have protonated all histidine, glutamic acid and aspartic acid residues when we were simulating N-terminal-H1, we planned to unfold the structure so that N-terminus and H1 can interact easily.

Even though unfolding of H1 occurred, it was temporary and besides, during this unfolding there were still some salt bridges to keep the structure together. Only arginine, glutamic acid and aspartic acid residues are shown below to see the intramolecular salt bridges. The first figures are the beginning positions, and the second ones are the most important deformations we observed during simulations for a short period of time (Figure 3.30 - Figure 3.33).

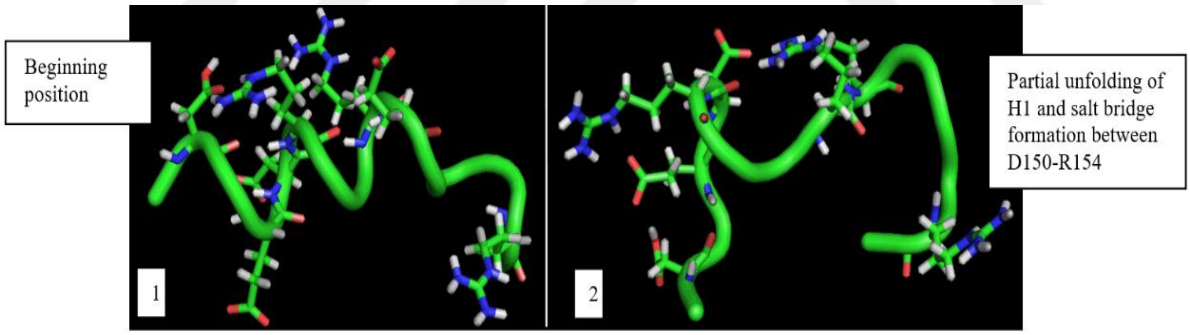

Figure 3.30: Protonation of D147 of H1.

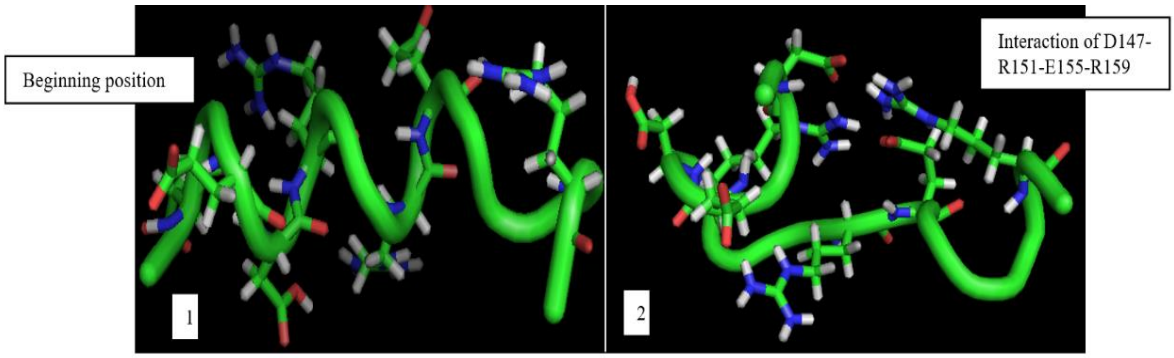

Figure 3.31: Protonation of D150 of H1.

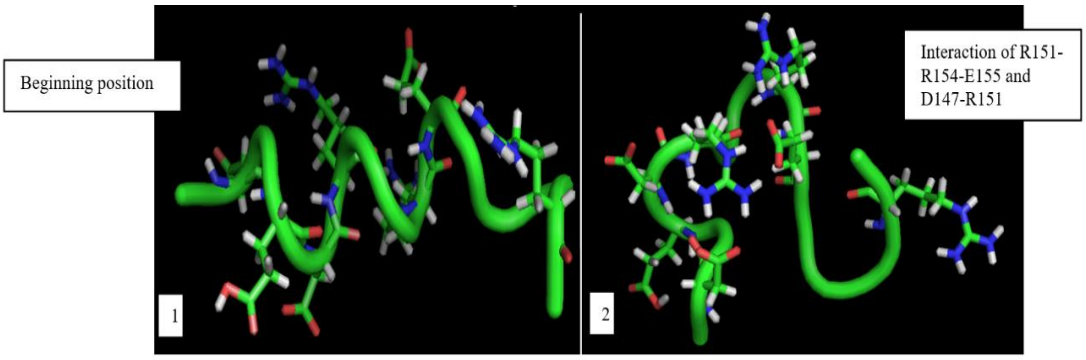

Figure 3.32: Protonation of E149 of H1.

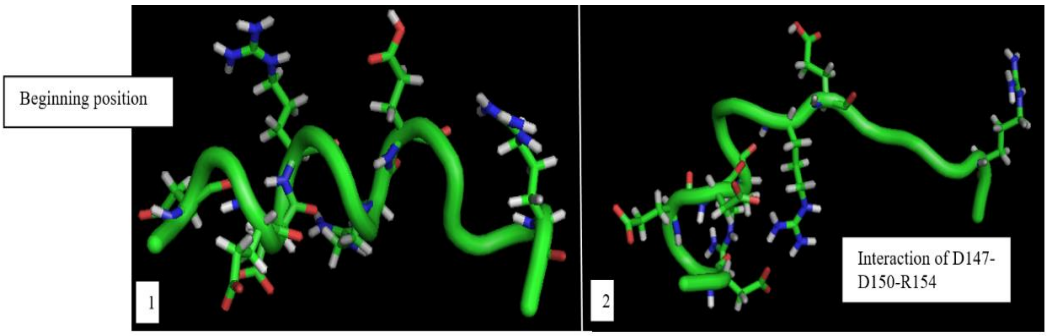

Figure 3.33: Protonation of E155 of H1.

When we protonated all GLU and ASP residues of H1, unfolding of H1 did occur as shown in Figure 3.34 but it was again temporary that helical structure reformed during the simulation.

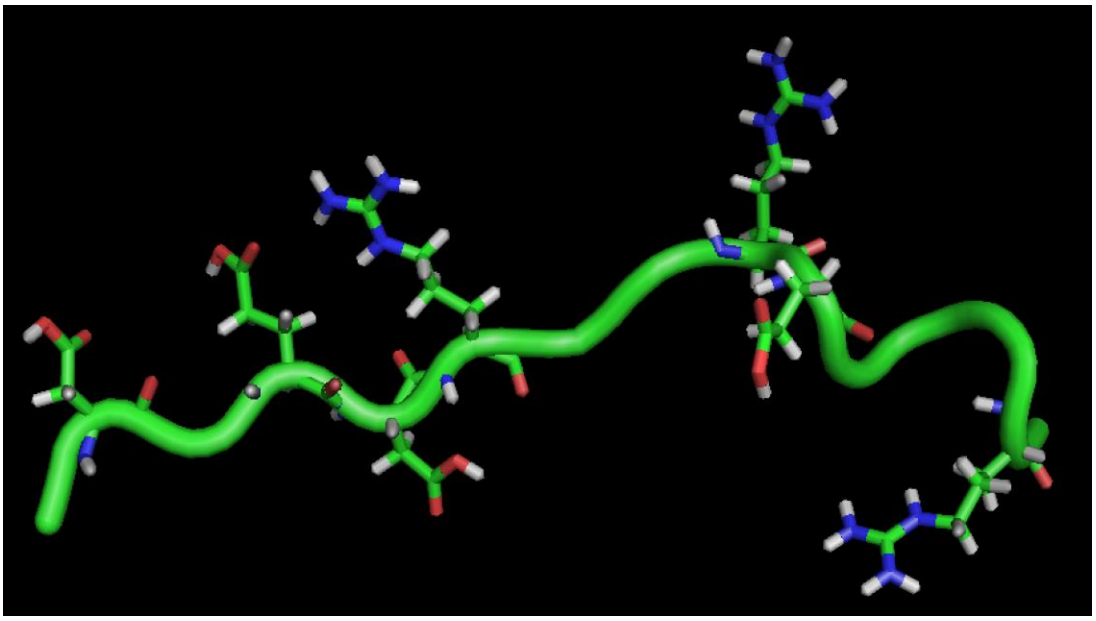

Figure 3.34: Unfolding of H1 when all GLU and ASP residues protonated.

At 310K and neutral pH unwinding of H1 seems unlikely. We tried a polybasic sequence to break down intramolecular salt bridges. Also, another H1 sequence and

some ions were used to break those intramolecular salt bridges. Unfortunately, we couldn't succeed in breaking those intramolecular interactions to increase the instability. If we look at it from the perspective of entropy, it is possible that monomers like another H1, a polyvaline or a polybasic sequence can interact easily with H1, but they couldn't unfold H1.

Fully protonated H1 was very flexible that it unfolds, so any chance it encounters with another monomer they may form a β-sheet. Enthalpy contribution to activation energy would be less in that situation. However, it is unlikely to protonate all glutamic and aspartic acids inside endosomal compartments, even though these compartments have low pH. So, protonation of these residues would be so rare entropic event, even for prion disease.

It seems that during our simulations, high enthalpy barrier contributes to the activation energy, so unfolding could not be observed. To prove this argument a potential mean force with umbrella sampling was used.

3.5.7 Potential Mean Force Energy calculations to unfold H1

H1 was very stable during our simulations even at 330K, and our MD simulations to unfold H1 by forming complexes with other sequences did not succeed, but we know from previous studies in literature, that H1 should unfold to participate in PrPSc formation (Colacino et.al., 2006). PrPC conversion into PrPSc is favored at low pH and in literature this transition process is suggested to happen in endosome. To mimic that enviroment we changed the protonation states of the aspartates and glutamates of H1 to make H1 stay unfolded. Each time we only protonated one residue. pH of lysosome is about 4-4.5, so it is unlikely that all glutamic and aspartic acids, which have very low pKa levels, would protonate at the same time inside lysosome. Following standard MD simulations, we decided to use potential mean force calculations of these protonated sequences to see the energy that is needed to unwind H1 and break intramolecular salt bridges.

The protonation states of Aspartates and Glutamates of H1 changed one by one to mimic the lysosome pH and to ease the unfolding, to calculate the energy that is needed to unfod H1.

The distance between two termini of H1 was raised to 40Å to unwind by potential mean force calculation where in each step 0.5Å were used to unfold the structure.

Besides, shortening of the same structure was also calculated with 0.5Å intervals again. As a result, distance of C- and N-terminus of H1 ranging from 5Å to 40Å was calculated. The energy that was needed for these processes are shown from Figure 3.35 to 3.38. with the final conformations [when distance between two termini is 5Å (left) and 40Å (right)].

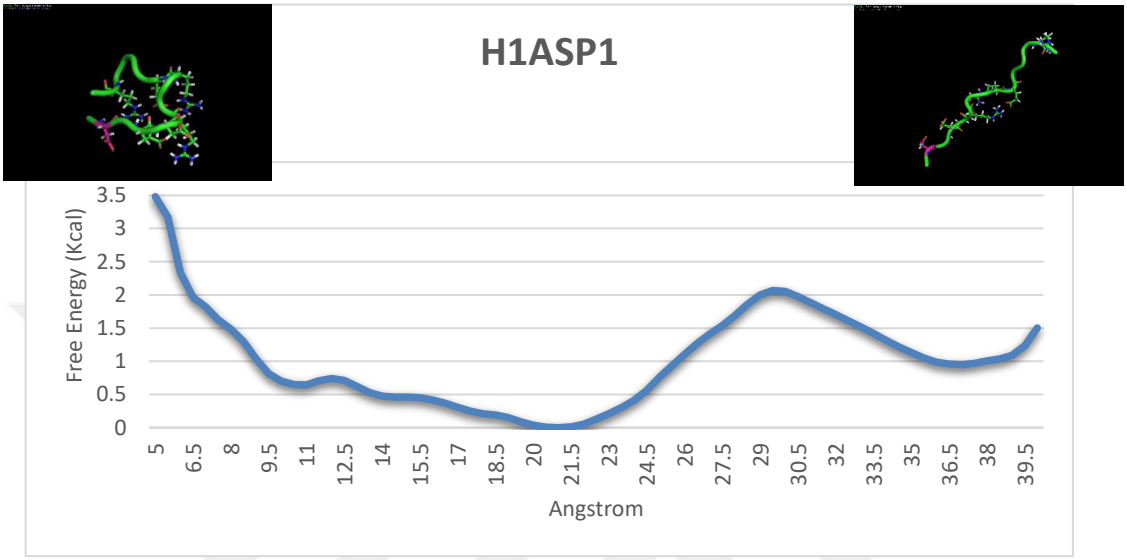

Figure 3.35: Energy profile to unfold H1, when only D147 (pink) of H1 was protonated.

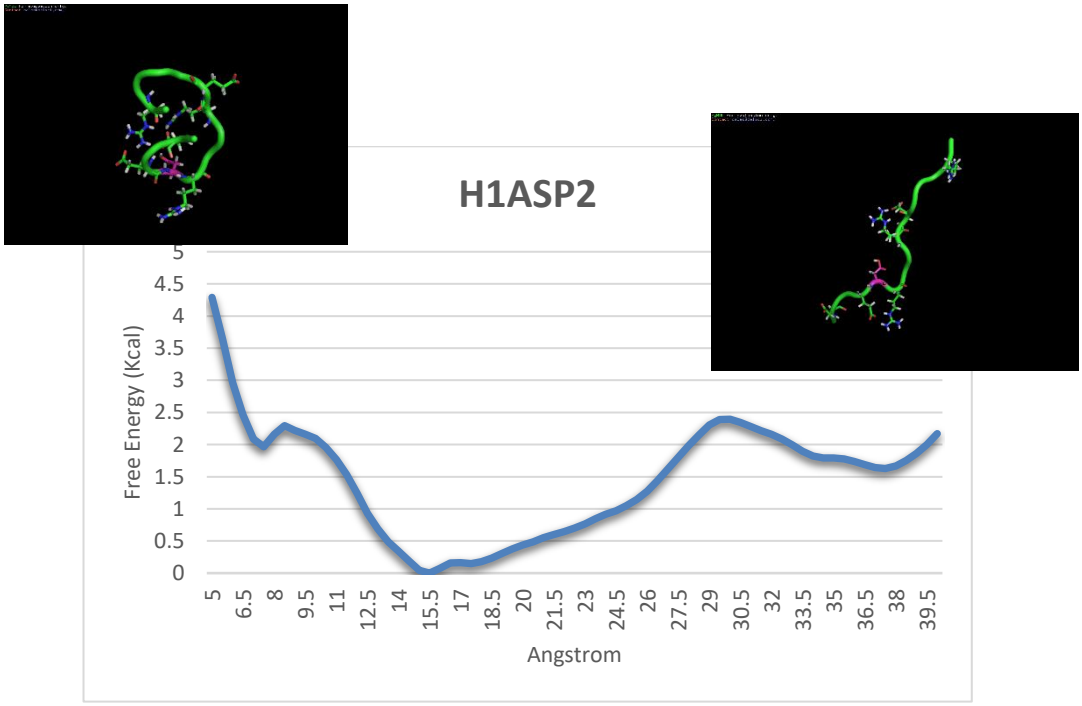

Figure 3.36: Energy profile to unfold H1, when only D150 (pink) of H1 was protonated.

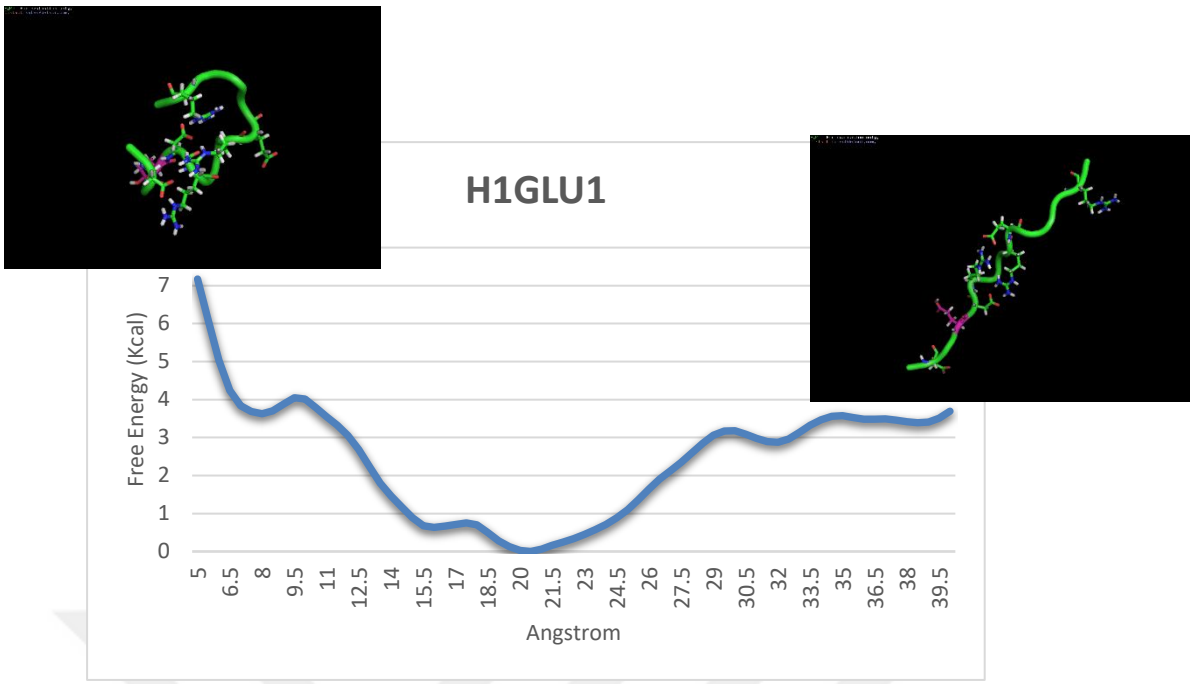

Figure 3.37: Energy profile to unfold H1, when only E149 (pink) of H1 was protonated.

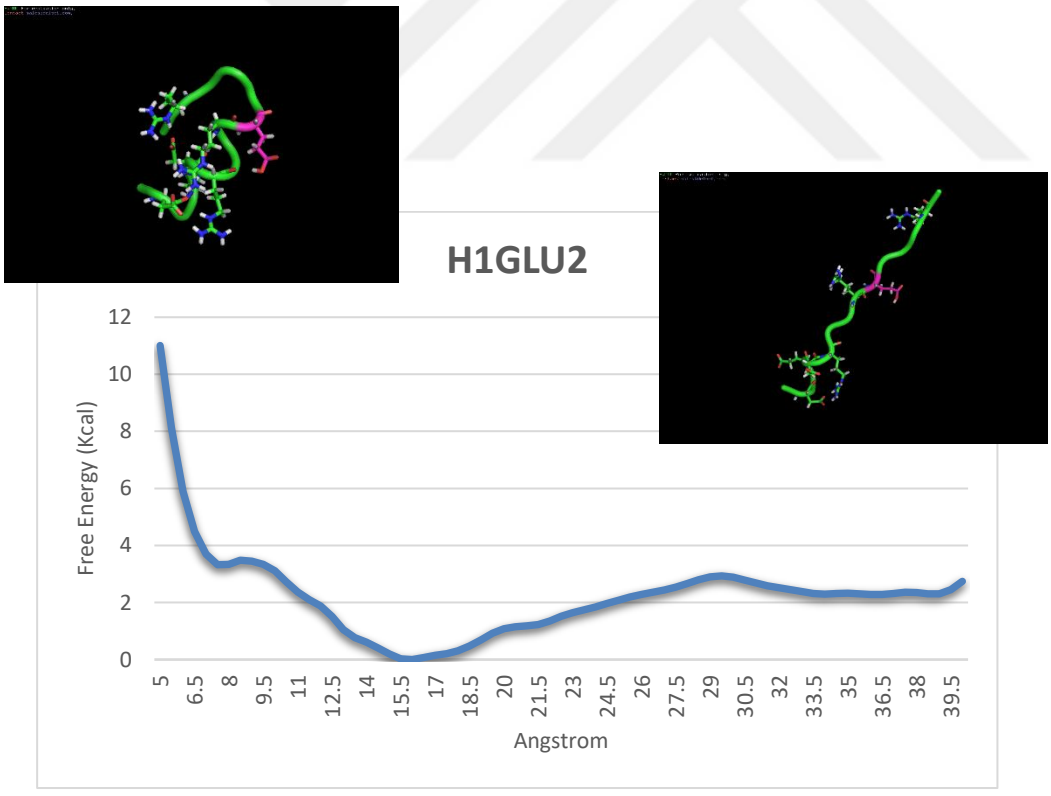

Figure 3.38: Energy profile to unfold H1, when only E155 (pink) of H1 was protonated.

As overall results of these potential mean force calculations;

-Energy that is needed to unwind the helix 1 is not high so it should be unfolded easily.

-Maybe it is not important to break all intramolecular salt bridges to unfold since some salt bridges are still protected even in 40Å open structure. Breaking only one salt bridge by the protonation of just one aspartic acid or glutamic acid is enough to make the free energy profile shallow and the structure very flexible.

-Though the barrier to unfold is low, still the free energy minimum corresponds to the helical structure. Thus, adjacent sequences should stabilize the unfolded structure.

-Except H1ASP2, compact structures retain significant helical character.

Unfolding barrier energy was found to be more than 20kcal/mol for the truncated prion protein (Singh et al.,2017), but less than 4 kcal was enough to unfold H1 in each case.

From that point of view, we decided to do replica exchange molecular dynamics to H1 and/or H1-B1 loop for better sampling. Also unfolded H1 and different sequences were used to form dimers. Main purpose of these simulations was to keep H1 unfolded by forming intermolcular salt bridges or beta sheets.

3.5.8 H1 and adjacent sequences

H1 alone and H1 with B1 to form helix or loop was analyzed seperately. Also, the effect of the rest of the protein on H1 structure was also analyzed. This effect should not be backbone-backbone interaction, since studies with H/D exchange and proteinase enzyme showed that this region is not protected (Singh and Udgaonkar, 2013) and, also this means it is not a buried region surrounded by the rest of the protein. On the other hand, side chain interaction may be a way of interaction between H1 and the rest of the protein. In addition, keeping C- and N-terminus of H1 at a constant distance may also be an important effect of the rest of the protein. So, we studied the interaction between charged sequences with a high potential to make side chain interactions with H1.

On the other hand, in Gerstmann-Sträussler-Scheinker (GSS) syndrome variant, which does not contain the part after H1 (Choi et al., 2016), H1 forms short helical structure where probably H1 of the two monomers contact each other. This is the reason why we examined H1 alone, two helical H1 together, H1 and neighbouring sequence H1-

B1 loop, charged sequences like {H^{99}SQWNKPSKPKTNMK^{113}}, {T^{193}TTTKGENFTETDIK^{207}}, {K^{197}GENFTETDIKIMER^{211}} and H1 seperately, whether these interactions are going to protect helical structure or unwind H1 to form a loop.

3.5.8.1 Standard MD Simulations:

Unwound H1 was used as starting structure of MD simulations and the ability of some sequences to keep H1 unfolded were investigated. These sequences were;

-Positively charged sequence from N-terminal of the globular protein: {H^{99}SQWNKPSKPKTNMK^{113}}

-H2-H3 loop sequence of a second prion protein that may interact with H1 to unfold: {T^{193}TTTKGENFTETDIK^{207}}

-H2-H3 loop and N-terminus of H3 sequence of a second prion protein that may interact with H1 to unfold: {K^{197}GENFTETDIKIMER^{211}}

All these sequences simulated in parallel and anti-parallel manner with unwound H1 (shown blue). A distance restrain of 10Å was used to prevent monomers moving away from each other. The results of each simulation after 2000ns can be found from Figures 3.39-3.44. (P: parallel, A: Anti-parallel).

During these simulations only anti-parallel HSQWNKPSKPKTNMK sequence and H1 simulation showed some promising results in which H1 kept its unfolded structure, probably by keeping the distance constant between C- and N-terminus of H1 at 7-8Å, whereas in the others H1 gained back its helical content.

For the unwinding of H1, we know that it should be separated from H2 and H3. We still don’t know whether it starts unfolding because of a metal ion, protonation, or dimer formation, but to keep H1 unfolded in scrapie form is another challenge. It may not participate in beta sheet structure, but it has to lose its helical structure, and N-terminus of globular prion protein may provide the interaction to keep H1 unwind.

Importance of the starting structure was also observed when we simulated H1 alone (Figure 3.45). When native helix structure of H1 simulated at 310K for 2000ns, salt bridges between arginine and aspartic acid residues protected the helical form throughout the whole simulation (Figure 3.45, left). But when the loop structure of H1 that was formed in H1-HSQWNKPSKPKTNMK simulation was simulated alone at

310K and for 1500ns, this time, salt bridges between arginine and glutamic acid residues kept the structure in loop shape even in the absence of the HSQWNKPSKPKTNMK sequence (Figure 3.45, right).

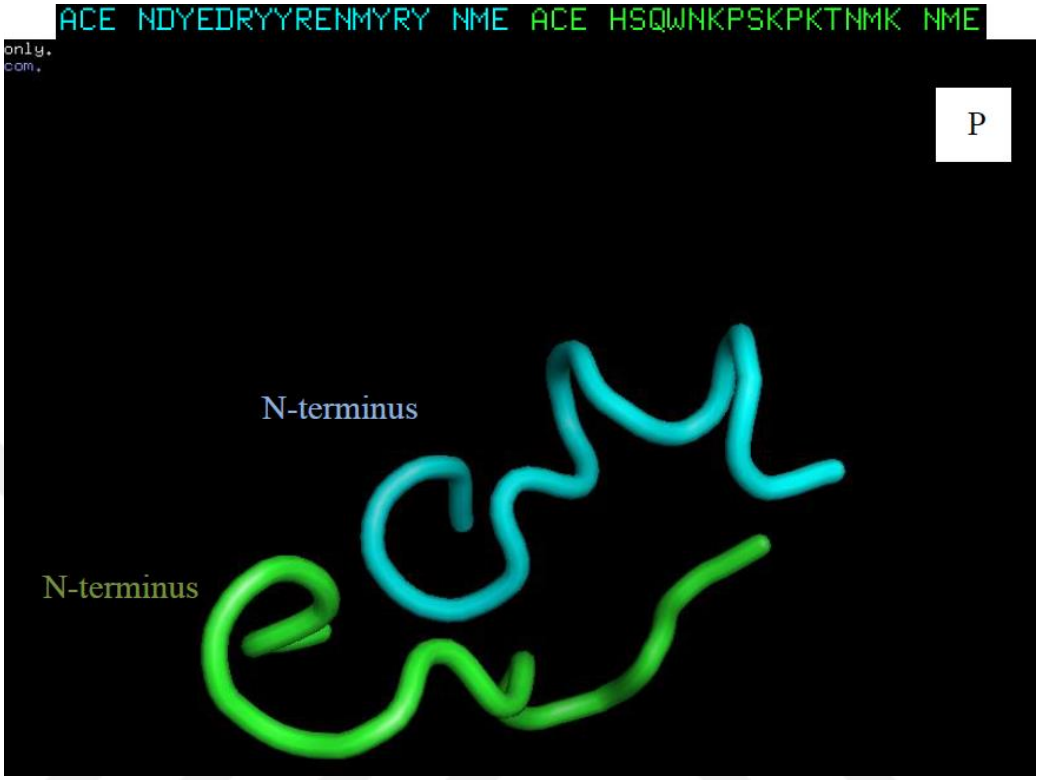

Figure 3.39: Unfolded H1 and {H^{99}SQWNKPSKPKTNMK^{113}} in parallel manner.

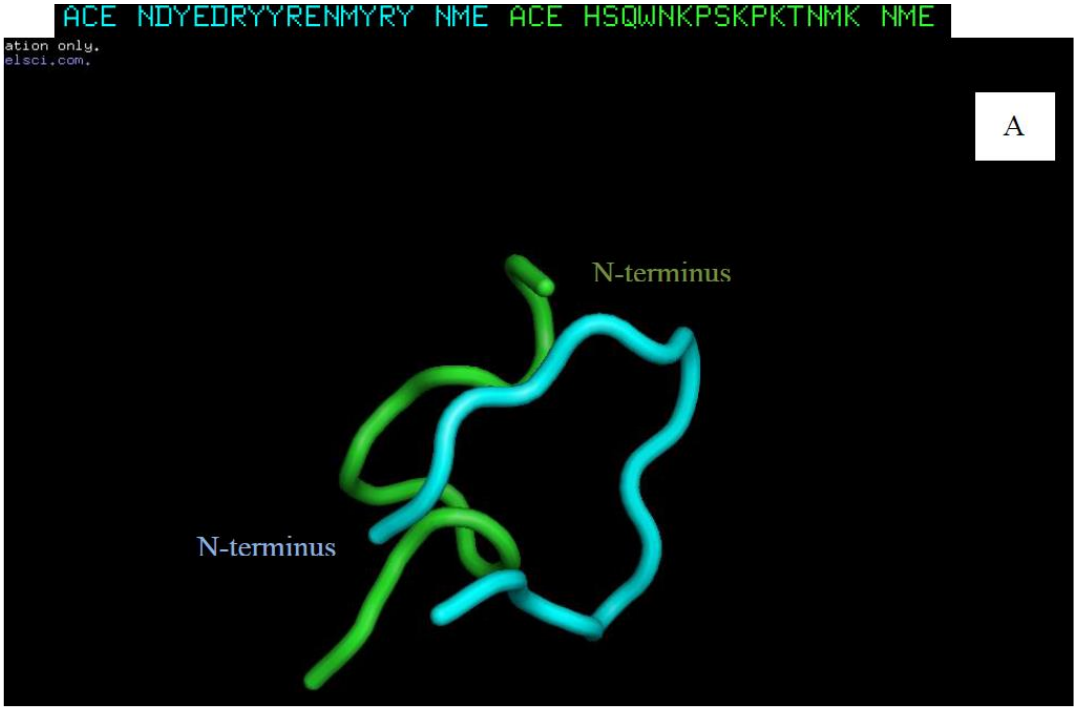

Figure 3.40: Unfolded H1 and {H^{99}SQWNKPSKPKTNMK^{113}} in anti-parallel manner.

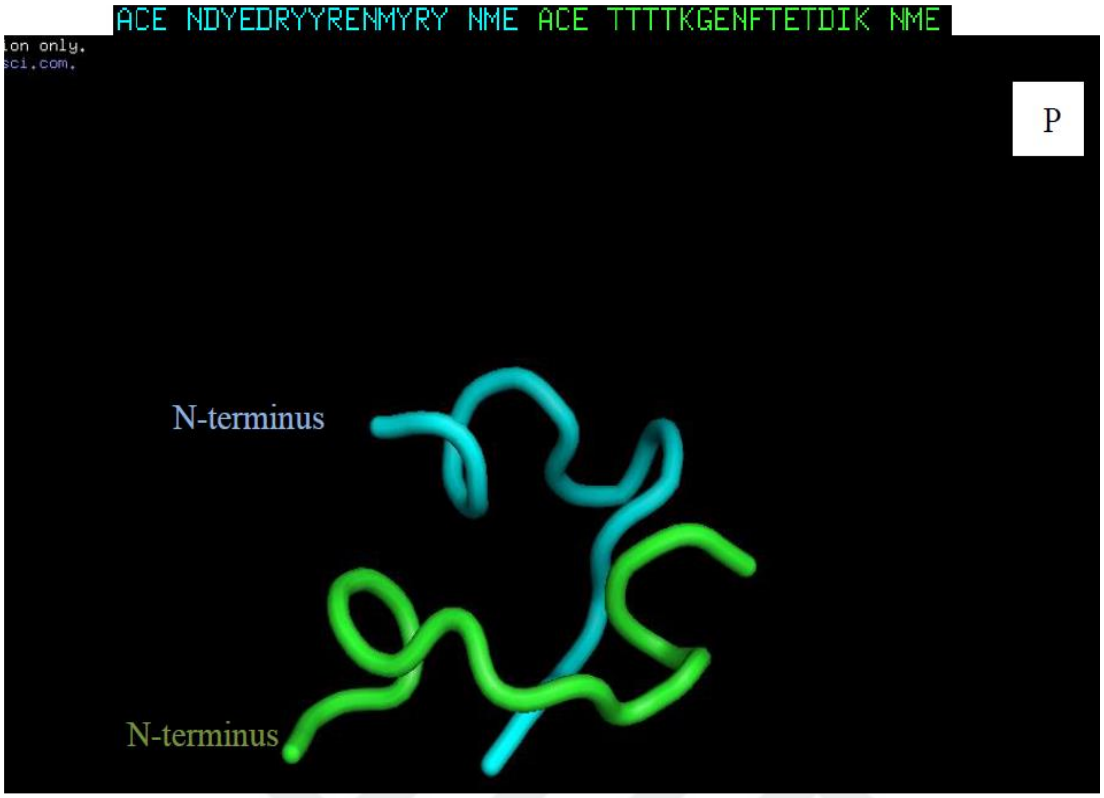

Figure 3.41: Unfolded H1 and {T^{193}TTTKGENFTETDIK^{207}} in parallel manner.

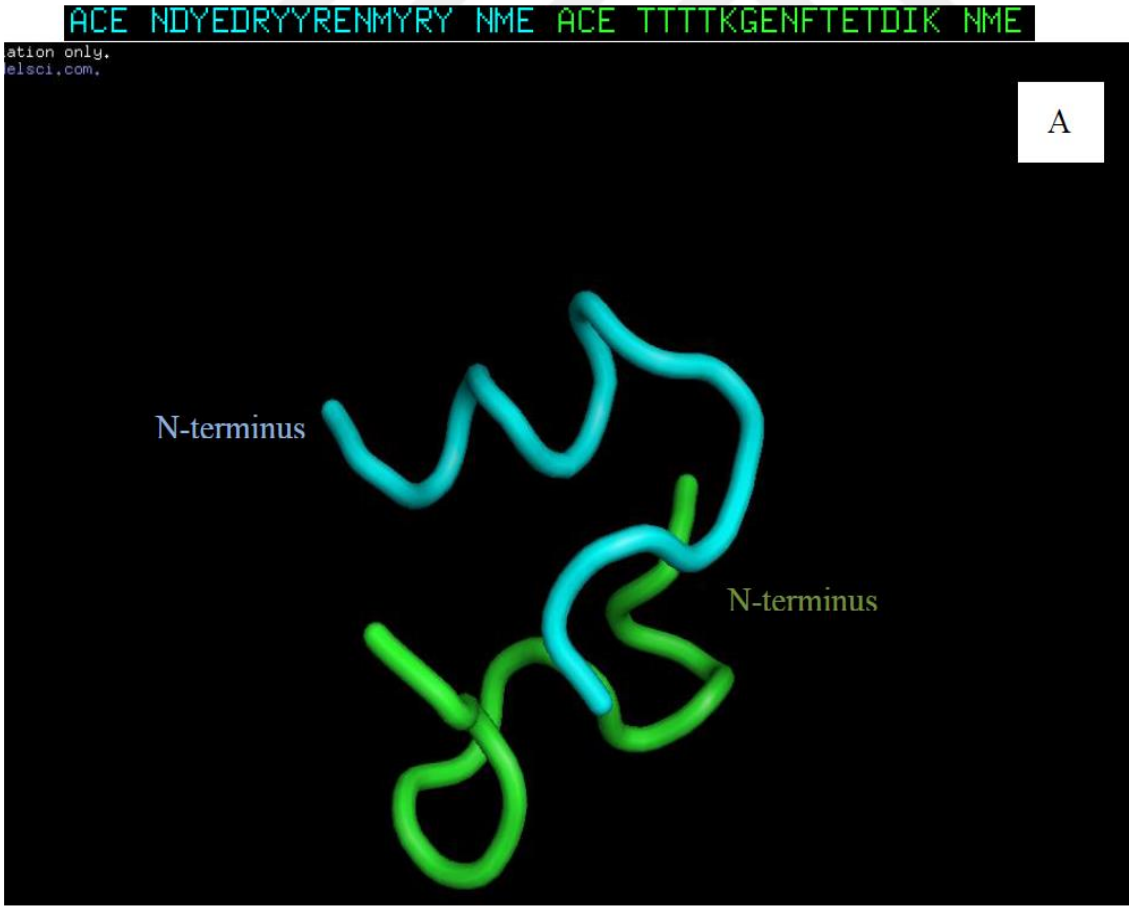

Figure 3.42: Unfolded H1 and {T^{193}TTTKGENFTETDIK^{207}} in anti-parallel manner.

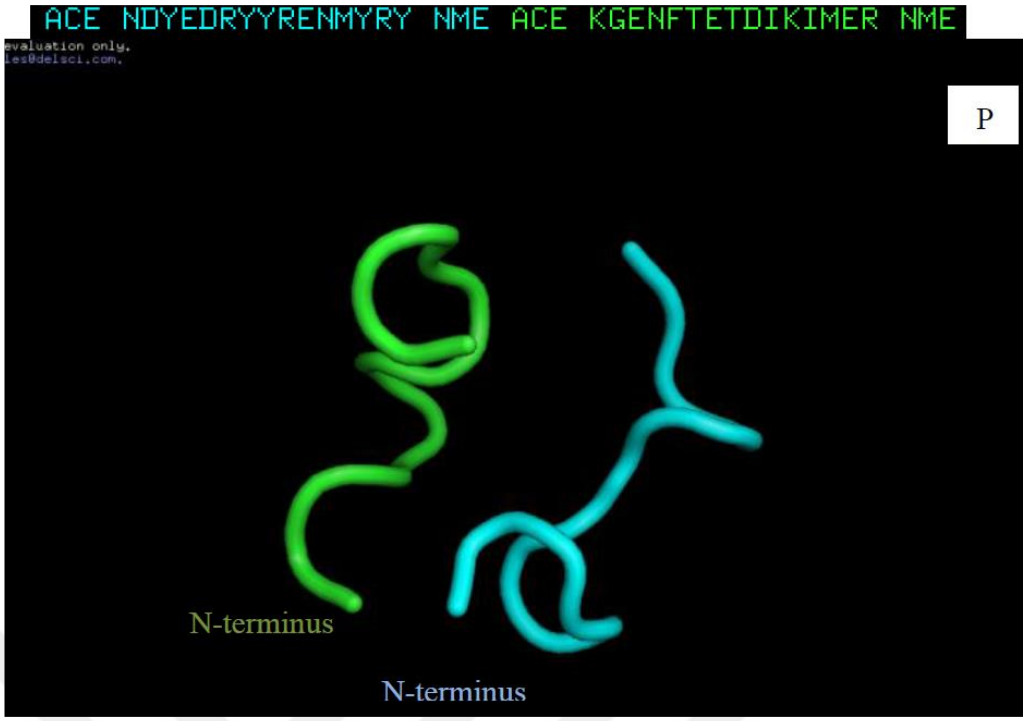

Figure 3.43: Unfolded H1 and {K^{197}GENFTETDIKIMER^{211}} in parallel manner.

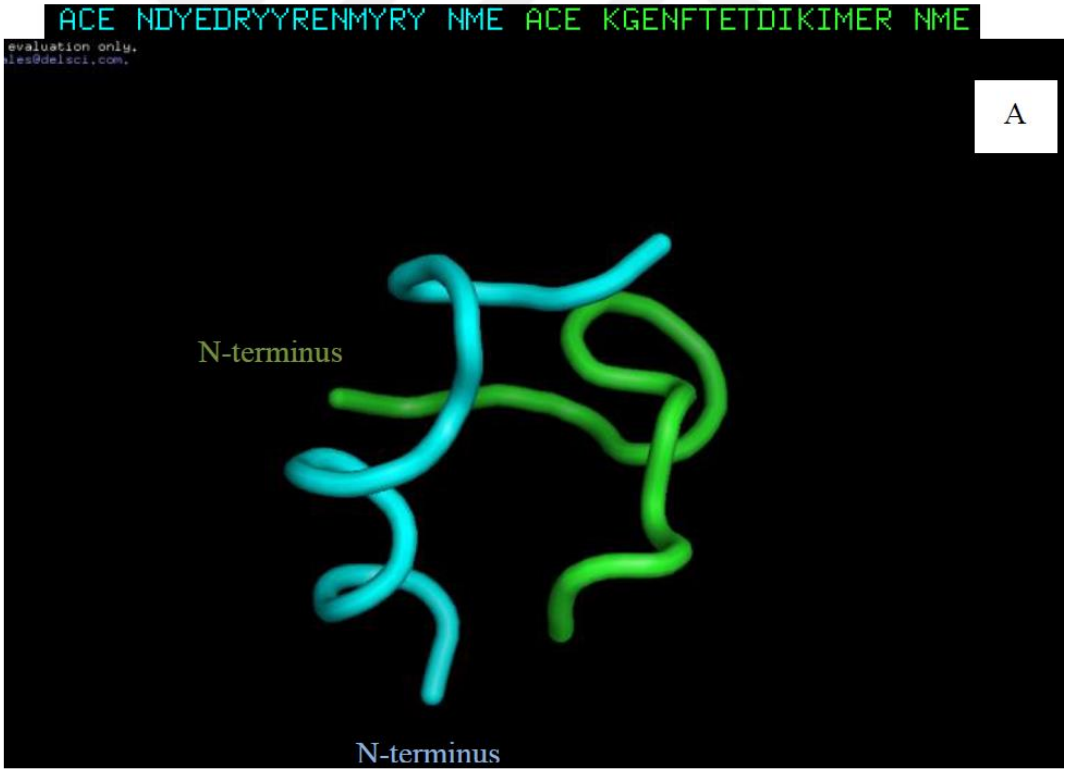

Figure 3.44: Unfolded H1 and {K^{197}GENFTETDIKIMER^{211}} in anti-parallel manner.

In Figure 3.45, helical structure and loop structure respectively were shown (blue: arginine, orange: aspartic acid, pink: glutamic acid). It can be concluded that these two

structures are separated by a high energy barrier that could not be overcome during our simulation time.

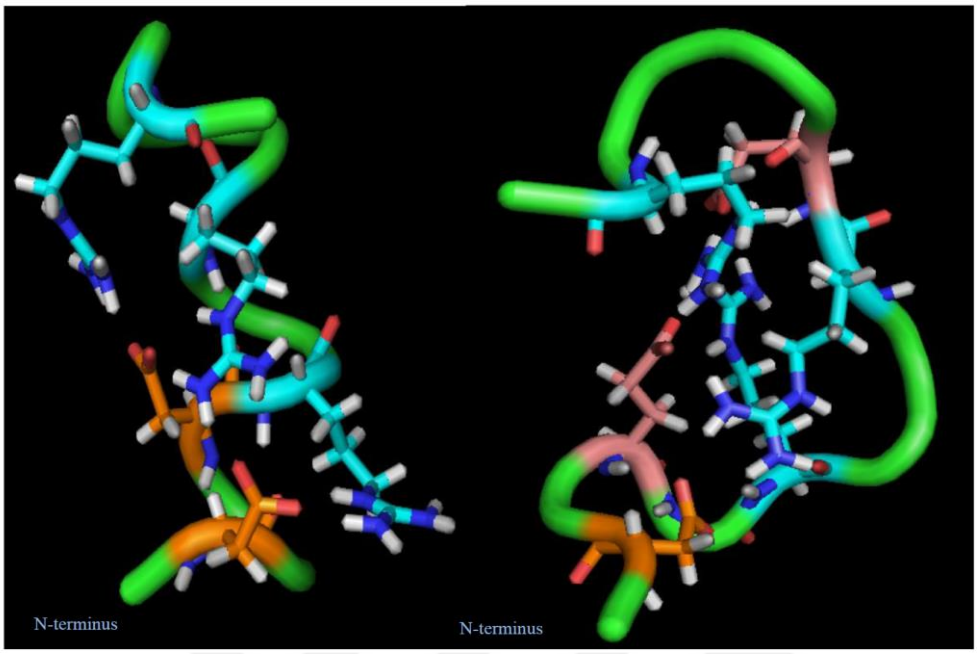

Figure 3.45: Starting structure determined the final conformation of H1.

We tried to see whether loop structured H1 was going to be able to convert into helical H1 or not, and was it going to stay in loop shape or not. So, with the help of distance restrain of 20Å between a helical H1 (pink) and loop H1 (green) (Figure 3.46), we simulated these structures for 2000ns. This simulation was conducted twice with different postioned loop H1 with respect to helical H1. As some intermolecular salt bridges formed, they did not affect the overall structure of two strands, since each strand kept most of their intramolecular salt bridge interactions; so, both of them protected their initial structure.

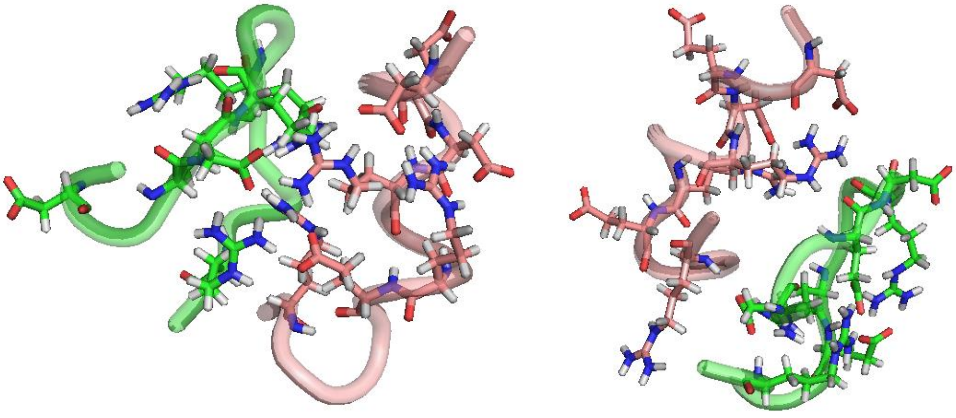

Figure 3.46: Loop structure could not unfold helical H1.

When the beginning structures were two loop H1, intermolecular salt bridges did form but still as the intramolecular salt bridges were protected no helical structure was observed (Figure 3.47).

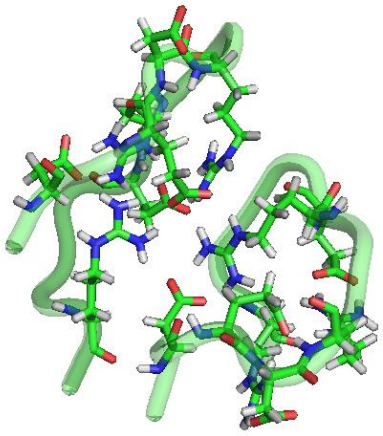

Figure 3.47: Loop structures protected their beginning position.

3.5.8.2 Replica exchange simulations of H1 and charged sequences:

Neighbouring sequence of H1 or interaction with other charged sequences might keep H1 in helical, β-strand or in loop structure. For better sampling we used REMD simulations for H1 alone, H1-H1, H1-KGENFTETDIKIMER, H1-HSQWNKPSKPKTNMK and H1-H1B1 loop, temperature ranging from 294 to 500-520K.

REMD of H1 alone, even starting from a loop structure, showed that most of the clusters are in helical shape. ~24% of the clusters were in loop shape, meaning that even the loop structure was very stable. But as the sampling continued the percentages lowered to ~10% at the end of 265ns and helical structure became dominant.

With the help of molecular mechanics with generalised Born and surface area solvation (MM/GBSA) free energy, trajectory of each cluster were undertaken. The MM/GBSA potential energy of the loop was -985.1 kcal/mol, and the most populated cluster with a helical structure was -975.1 kcal/mol. The non electrostatic part of the solvation free energy only favors the loop only by 1 kcal/mol (14.7 and 13.4 kcal/mol for the helix and loop, respectively). The helix structure might be stabilized by the entropy, but when the entropy contributions were added to the considration free energy difference reduced to 6 kcal/mol between loop and helix structure.

REMD of H1-H1B1 (residues 136-160) only showed helical structure throughout the simulation of 255ns and no loop structure was observed (96% of the simulation was in helix form). Arginine on H1B1 loop interacted with negatively charged residues like aspartic acid (Figure 3.48) that might have an affect on the helical stability of H1. Arginine of H1B1 loop made these kind of ineraction in globular protein too, so unfolding of H1 might depend on the dislocation of H1B1 away from H1. Also, hydrophobic interactions were observed between H1 and H1B1 loop to make helix more stable.

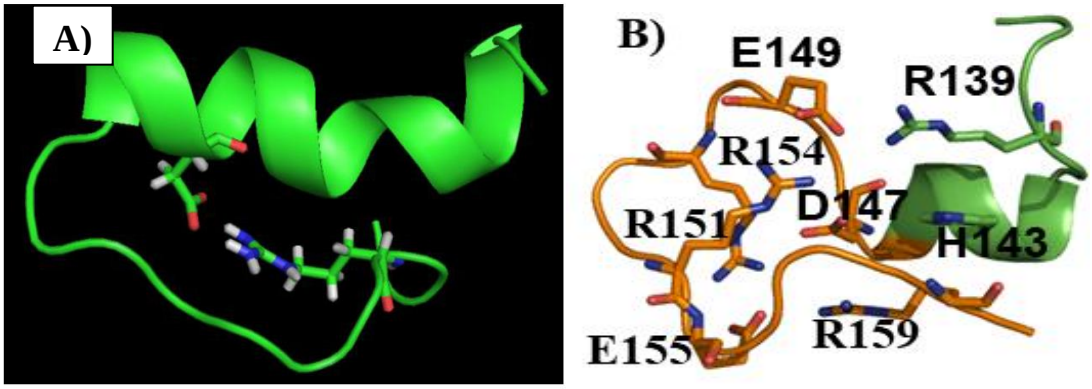

Figure 3.48: REMD result of H1 and H1B1 loop together. A) Helical structure that was dominant through the simulation, B) 4% of the simulation showed loop conformation with a helical part.

Only 4% of the simulation was on loop conformation with a helical part of H1B1 (helical structure was protected by E149-R139 salt bridge and hydrophobic contacts between H143 and R159) and this structure was the result of salt bridges between E149-R154, E149-R139, D147-R154, D147-R151, E155-R151 and E155-R159.

H1-H1 REMD simulations showed that one of them stays in helical structure, while the other one shows helical structure partially or is found unwound. No loop structure was observed. Intramolecular bridges became intermolecular but even though these changes did not have any effect on destabilization of H1; but might affect on the stabilization of helical structure (Figure 3.49: intermolecular salt bridges were shown below blue: arginine, pink: aspartic acid, orange: glutamic acid. Sticks represent residues on the same H1 and lines on the other H1 sequence).

In REMD simulaton of H1-{K^{197}GENFTETDIKIMER^{211}}, H1 kept its helical structure, where even tough intramolecular salt bridges were seen (D147-R151, D150-R154 and D150-R159), intermolecular salt bridges were also formed (R154-E199,

R151-D205, R159-E210, D147-R211): maintaining the stability of H1 (Figure 3.50 on left; blue: arginine, pink: aspartic acid, orange: glutamic acid. Sticks represent residues on the same H1 and lines on KGENFTETDIKIMER sequence; Figure 3.50 on right salt bridges).

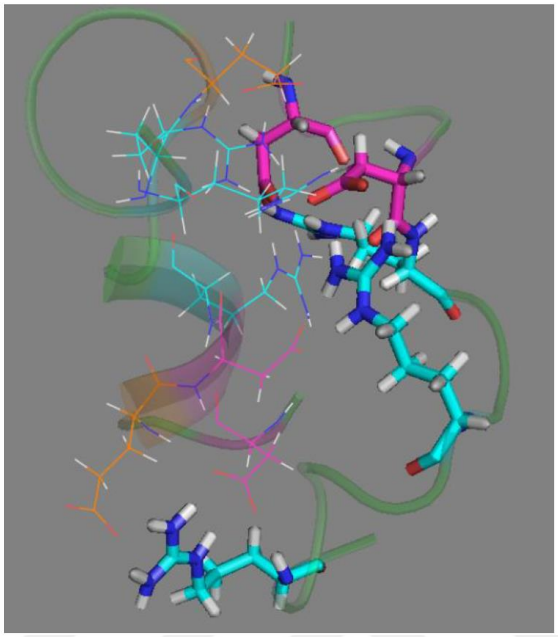

Figure 3.49: REMD result of two H1 strands.

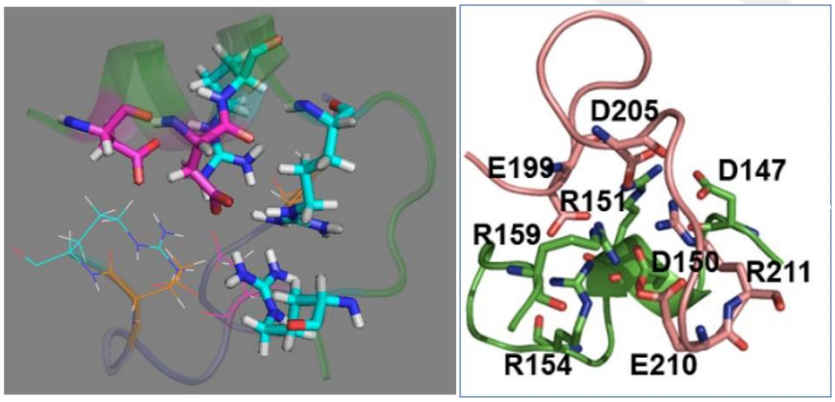

Figure 3.50: REMD result of H1-{K[197]GENFTETDIKIMER[211]}.

REMD of H1-{H[99]SQWNKPSKPKTNMK[113]} showed that loop structure was stabilized by intramolecular interactions (D147-R154, E149-R154, E149-R151, D147-R159, E149-R159 and E155-R151 salt bridges) as shown on Figure 3.51 (On left; Blue: arginine, pink: aspartic acid, orange: glutamic acid. Sticks represent residues on the same H1 and lysines shown with lines in purple on HSQWNKPSKPKTNMK sequence. On right; intramolecular interactions of H1). Lysine residues of {H[99]SQWNKPSKPKTNMK[113]} sequence did not make any interaction with H1 to make intermolecular salt bridges, which in return loop structure was protected by

intramolecular salt bridges. When lysine residues made intermolecular salt bridges with H1 residues, it would destroy the loop stability and helical structure might form. As the simulation continued, formation of intramolecular salt bridges of H1 formed again, but only ~4% of our sampling showed H1 in helical structure. The MM/GBSA free energy difference between the loop and helical structures 16.5 kcal/mol (Gloop = -1626.3 kcal/mol, Ghelix = -1609.8 kcal/mol). On the other hand, the entropy contribution is 8.7 kcal/mol in favor of the helix, meaning that the loop was favored by the potential energy, but the helix is favored by the entropy.

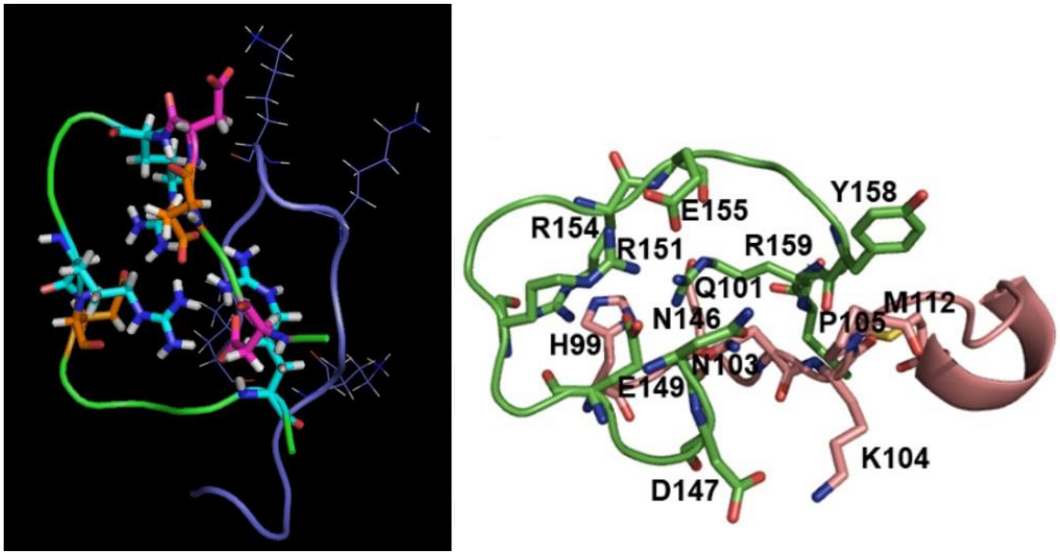

Figure 3.51: REMD result of H1-{H^{99}SQWNKPSKPKTNMK^{113}}.

To have a loop structure, H1 should not make any intermolecular salt bridges with other sequences like {K^{197}GENFTETDIKIMER^{211}} or another H1, which all seem to increase the stability of helical structure of H1. {H^{99}SQWNKPSKPKTNMK^{113}} or a similar sequence might be the region where H1 interacts to form a loop shape so that the H-bonds and hyrophobic interactions between these two strand and intramolecular salt bridges of H1 could maintain this loop stable. According to H/D exchange experiments, {H^{99}SQWNKPSKPKTNMK^{113}} is not a helix nor a β-strand, because it is an accesible region. However, {K^{197}GENFTETDIKIMER^{211}} is highly protected.

We thought that another effect of this sequence might be keeping the two ends of H1 within a suitable distance for loop formation. So, we simulated a loop shaped H1 with a restrain (≤ 9 Å), which kept C- and N-terminus at a constant distance, but unfortunately helical structure formed again, even though its sampling percentage was low ~20% (data not shown).

{H^{99}SQWNKPSKPKTNMK^{113}} only has positive charged residues when compared to other sequences mentioned above which have positive and negative residues. This might be the reason why {HSQWNKPSKPKTNMK) could not make intermolecular interaction with H1. Having postive and negative residues at the same time might provide an advantage over {H^{99}SQWNKPSKPKTNMK^{113}} sequence to make intermolecular interactions. After breaking of intramolecular salt bridges both charged residues of the adjacent sequences (whether another H1 strand or {K^{197}GENFTETDIKIMER^{211}}) could interact with H1, but when this adjacent sequence was {H^{99}SQWNKPSKPKTNMK^{113}}, arginine residues liberated from broken salt bridges could not find negative charged residues to interact with.

Besides from {H^{99}SQWNKPSKPKTNMK^{113}} sequence potential to keep H1 unfolded, we would like to see its effect in a scenerio where {H^{99}SQWNKPSKPKTNMK^{113}} and misfolded H1 interacted with a misfolded H1 of other adjacent prion protein. This interaction had been analyzed with REMD for better sampling. The result below (Figure 3.52) was the conformation with highest population throughout the 300ns REMD simulation, that both H1 stayed in loop structure ({H^{99}SQWNKPSKPKTNMK^{113}} in orange and two H1 in loop structure in green).

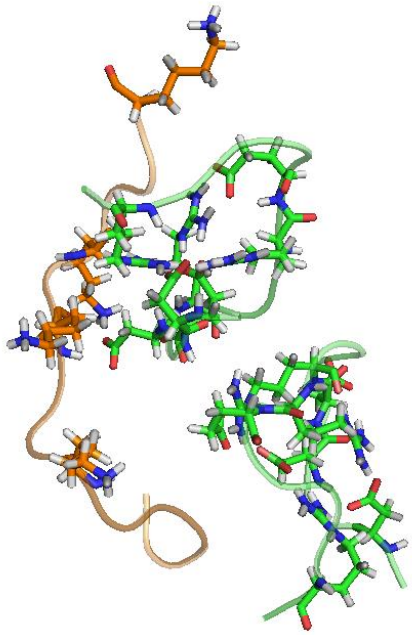

Figure 3.52: REMD result of two loop H1-{H^{99}SQWNKPSKPKTNMK^{113}}.

As the sampling elongated, helical H1 formation did observed (Figure 3.53; {H^{99}SQWNKPSKPKTNMK^{113}} in orange and one H1 in blue the other H1 in green).

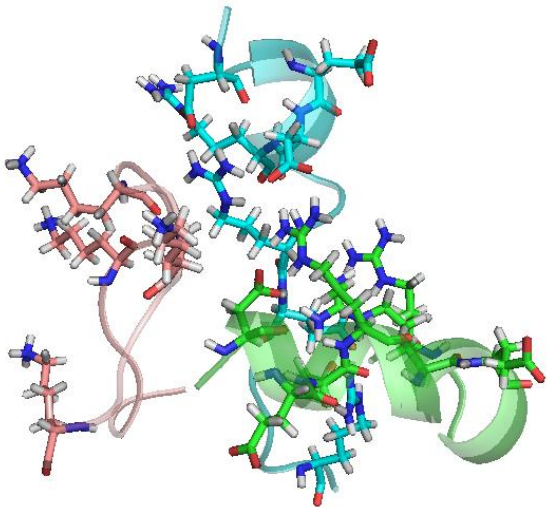

Figure 3.53: REMD result of two loop H1-{H^{99}SQWNKPSKPKTNMK^{113}}, helix formation.

Once helical structure was formed, its distribution through sampling increased.

H1 with B2 sequence showed β-hairpin structure at neutral pH (Kozin et al., 2001): but as seen in our simulations too, neighbouring squences of H1 (Ziegler et al.2003), like H1-B1 as mentioned above, did not affect the stability of H1.

Mammalian prion protein H1 stability depends on the placement of oppositely charged residues at i and i+4 (Chen and Thirumalai, 2013). These charged residues of H1 maintained helical structure under varying conditions such as high salt, pH variations and in presence of organic co-solvents; so, it was concluded that H1 actually worked as a barrier to the conformational change. Negatively charged Asp 144, Glu-146, and Asp-147 COOH terminus interactions with the positively charged residues Arg-151, His-155, and Arg-156 protect native structure (Ziegler et al.2003). Furthermore, intrahelical salt bridges might be important to stabilize helical structure (Ziegler et al.2003). However, mutations of aspartic acid residues on H1 showed that, aspartic acid-arginine salt bridges did not stabilize H1, but they stabilized the structure from converting into diseased form (Speare et al., 2003), but once the loop shape formed as seen in our simulations, these intramolecular salt bridges worked as a protector of the loop structure.

Norstrom and Mastrianni (2006) studied the charged residues of H1 and how they would affect the PrP^{Sc} conversion, secondary structure, and trafficking of PrP^{C}. They replaced these residues with oppositely charged residues, similarly, charged residues

or neutral alanine (ovine PrP numbering will be used to compare the results with our findings).

Alterations at N-terminal part of H1 were:

- D147E, D147K, D147A kept their ability to convert into PrP^{Sc},
- D147R showed a reduction in conversion when compared to wild type,
- E149D maintained conversion while E149K and E149R did not,
- E149A conversion was similar or slightly greater than the wild type,
- D150E, D150K and D150R showed similar results as D150,
- D150A resulted in different pattern of PK-resistance than the wild type,

Alterations at C-terminal part of H1 were:

- R151D, R151E inhibited the conversion, while R151K maintained the conversion,
- R151A significantly inhibited the conversion but did not completely prevent the ability,
- R154D, R154E, R154K and R154A prevented conversion,
- E155D did not show same conversion efficiency as the wild type
- E155K, E155R completely blocked conversion
- E155A restricted conversion

The stability of H1 did not depend on charges, and these alterations above did not affect the overall secondary structure or the trafficking of PrP^{C} but did affect the conversion efficiency. Loss of salt bridge interactions did not catalyze the conversion to PrP^{Sc}, however specific charge structure of H1 regulated the conversion. Besides C-terminal of H1 found to have a more critical role in PrP^{Sc} transition (Norstrom and Mastrianni, 2006).

When we replaced these residues of loop structured H1 following results were observed (data not shown):

- D147A, D147E and D147K did not change the overall loop structure of our H1,
- R151A, R151E and R151K increased the helical content of unwound H1,
- R154A, R154E and R154K also did not change the overall loop structure of H1.

H1 was found to be the determinant of PrP folding and maturation that its deletion interfered with posttranslational modifications and trafficking (ex: deletion caused the preventation of GPI anchor attachment). Also, it interfered glycosylation of PrP^{C} which in return affected PrP^{Sc} conversion (Winklhofer et al., 2003).

It seemed that hyrdophilic H1 conversion might be starting after some tertiary change in some other parts of the protein (Ziegler et al.2003), which might take place in catalyzing the aggregation of PrP^{C} to PrP^{Sc}, rather than converted into β-sheet (Watzlawik et al., 2006). Thus, H1 would be preserved in its helical shape during this transition (Liu et al., 1999).

The overall results of our H1 MD and REMD simulations can be summarized as:

-Intramolecular salt bridges are important for the integrity of H1, whether it is in helical shape or loop,

-Intermolecular salt bridges may be formed with the adjacent sequences but as long as the intramolecular salt bridges are protected, H1 would stay in its beginning structure,

-Helical and loop structure of H1 seem to be separated from each other with high energy barrier(s), that is the reason why we could not see the transition from helical to loop structure during our MD simulation or visa versa,

-But REMD simulation helped us to cross those energy barriers easily, so at the end of our REMD simulation loop turned into helical H1 structure and helical structure population through out our sampling increased,

-Positively charged sequence similar to $\{H^{99}SQWNKPSKPKTNMK^{113}\}$ seem to be important to keep H1 unfold; hydrogen bonds and hydrophobic contacts stabilize the complex D147-R154, E149-R154, E149-R151, D147-R159, E149-R159 and E155-R151 salt bridges maintained the loop structure.

3.6 REMD of H2-H3 Results

Just only two α-helices, H2 and H3, are known to be prone to fibrillization (Requena and Wille, 2014). The 3D structure model of yeast prion (protein data bank code: 2KJ3) shows that, each β-strand contains 5 amino acids in PrP^{Sc}. So, from that point of view, we decided to form 5 amino acid-longed restrained β-strands scanning through H2 and H3 sequences.

Singh et al. (2017), searched the unfolded state with lower free energy than the native structure, but results revealed that those global minima states did not have an increased β-sheet content. Also, since most of the studies had shown that H1 was very stable, they studied free energy surfaces of helical domains separately and found that H2 and H3 were inherently unstable and had the potential to form a random coil or a β-structure. Interestingly, we found that H3 was the most stable structure and hard to unfold (data not shown).

Some restrained replica exchanged simulations only show β-strand content according to our restrained amino acids. REMD studies ranging from temperature 298K-460K were analysed, but only results of 310K were shown below. The criteria for analyzation were the depletion of helix content and formation of hairpin structure or more circle-like structure with increased β-strand contents (Figure 3.54; shown as in symbols). These structures were chosen for their ease of dimerization potentials.

Figure 3.54: Circle like structure (left), hairpin structure (right).

Increased β-sheet content was considered as promising results of REMD studies. These results are shown below (Figure 3.55):

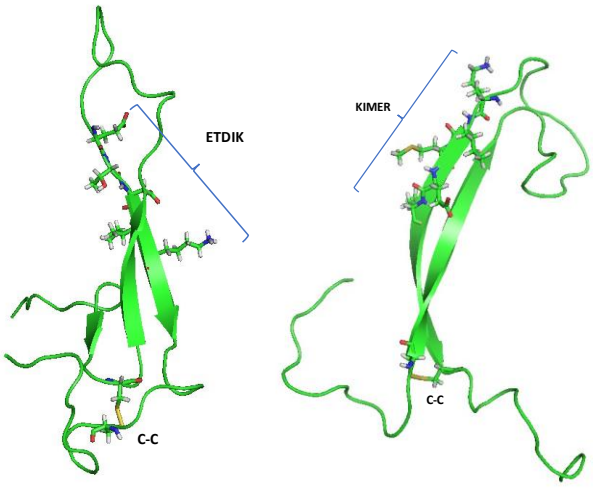

Figure 3.55: Increased β-sheet content when ETDIK, KIMER, VVEQM, ERVVE, MERVV, TKGEN, TTTKG, KQHTV residues restrained separately in different REMD simulations.

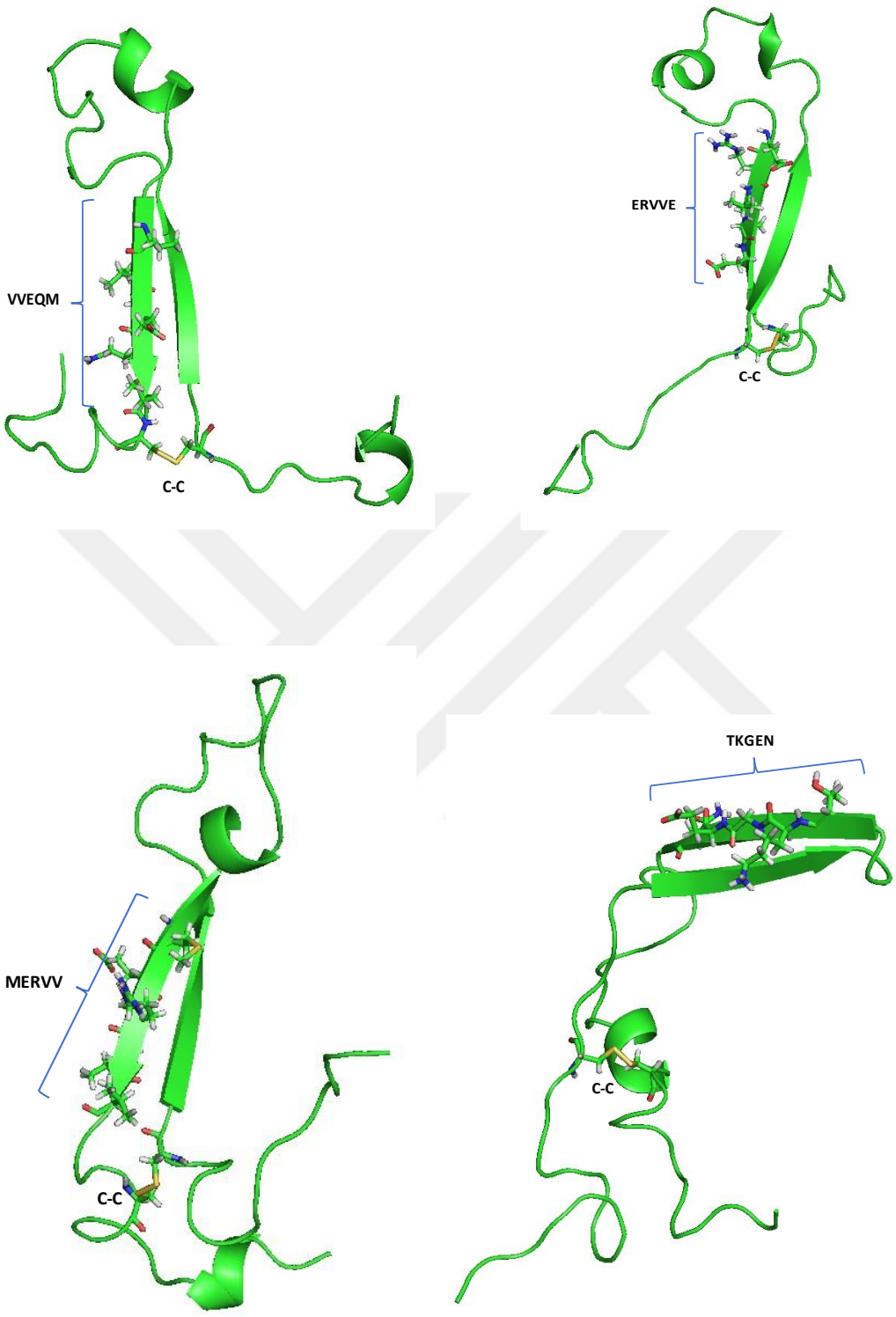

Figure 3.55 (continued): Increased β-sheet content when ETDIK, KIMER, VVEQM, ERVVE, MERVV, TKGEN, TTTKG, KQHTV residues restrained separately in different REMD simulations.

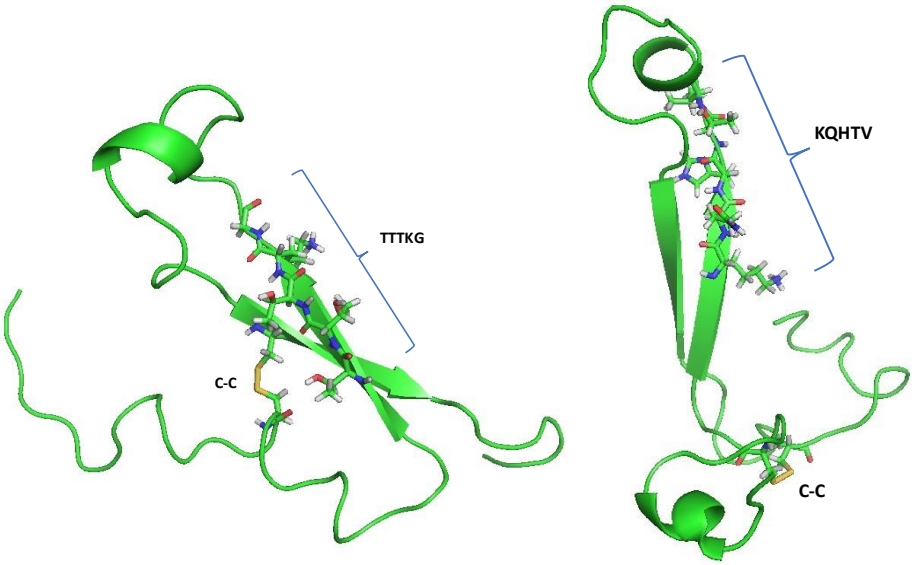

Figure 3.55 (continued): Increased β-sheet content when ETDIK, KIMER, VVEQM, ERVVE, MERVV, TKGEN, TTTKG, KQHTV residues restrained separately in different REMD simulations.

However, some restrains only formed short β-sheets as seen on Figure 3.56:

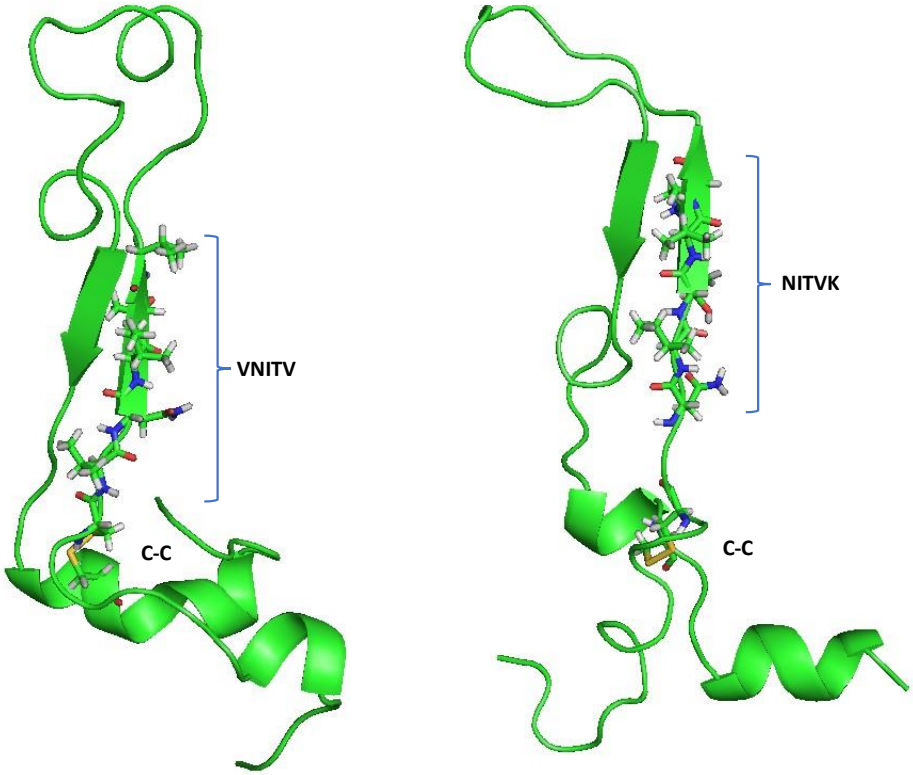

Figure 3.56: Short β-sheet formation when VNITV, NITVK, HTVTT, TTTTK, TTKGE and GENFT residues restrained separately in different REMD simulations.

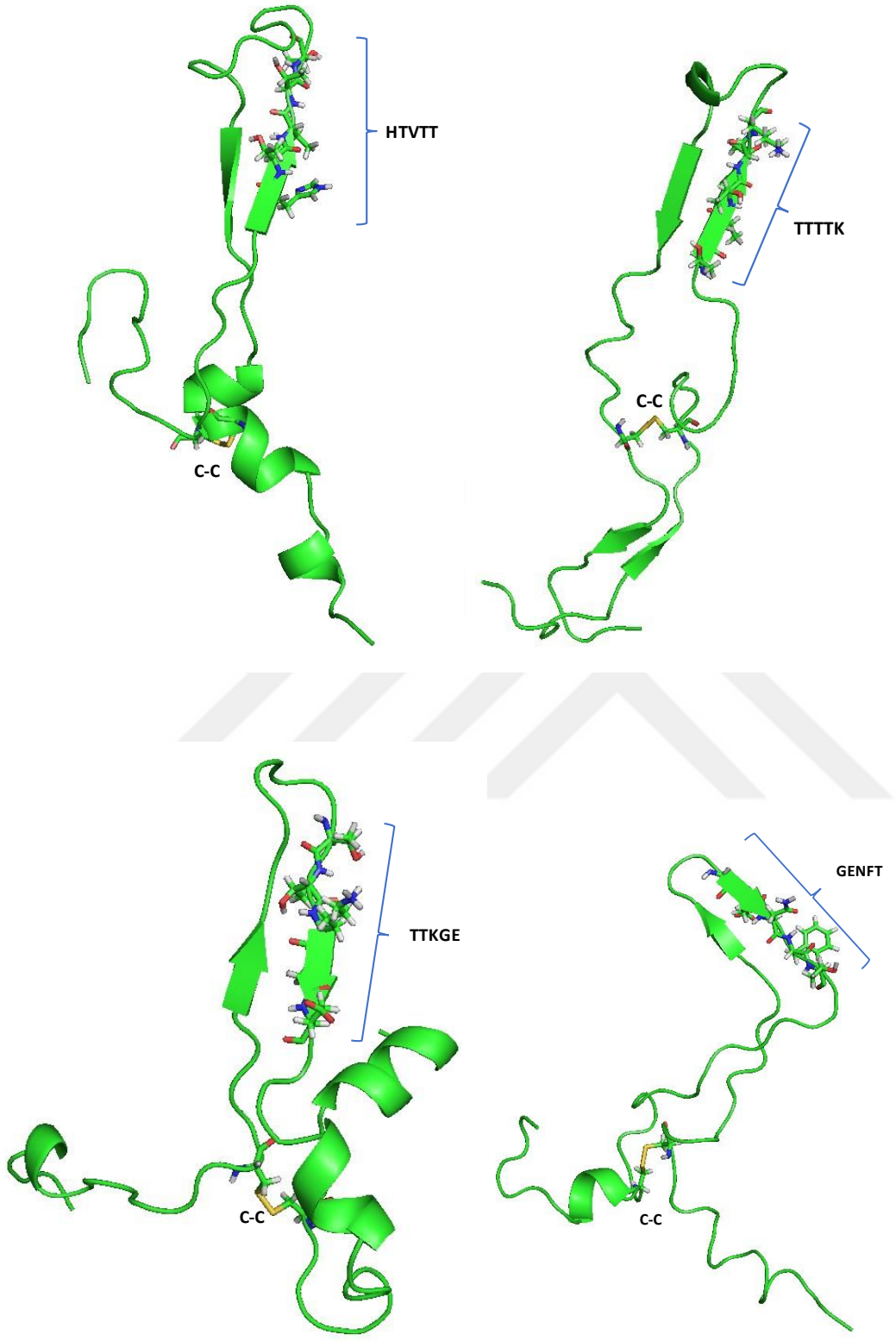

Figure 3.56 (continued): Short β-sheet formation when VNITV, NITVK, HTVTT, TTTTK, TTKGE and GENFT residues restrained separately in different REMD simulations.

Some restrained REMD simulations resulted in circle-like shape (Figure 3.57):

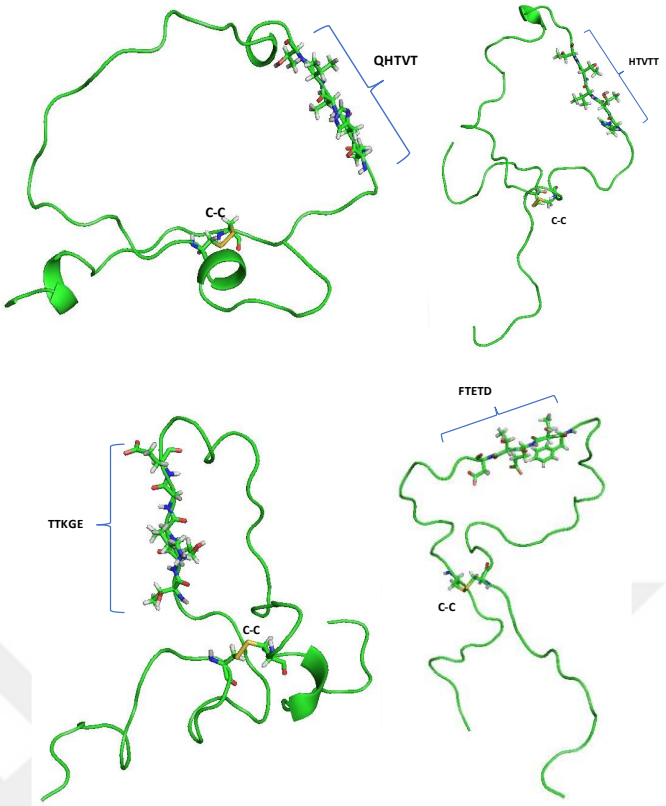

Figure 3.57: Circle-like shape when QHTVT, HTVTT, TTKGE, FTETD residues restrained separately in different REMD simulations.

On the other hand, sometimes only the sequence that we restrained showed β-strand structure, but the rest was in helical shape (Figure 3.58):

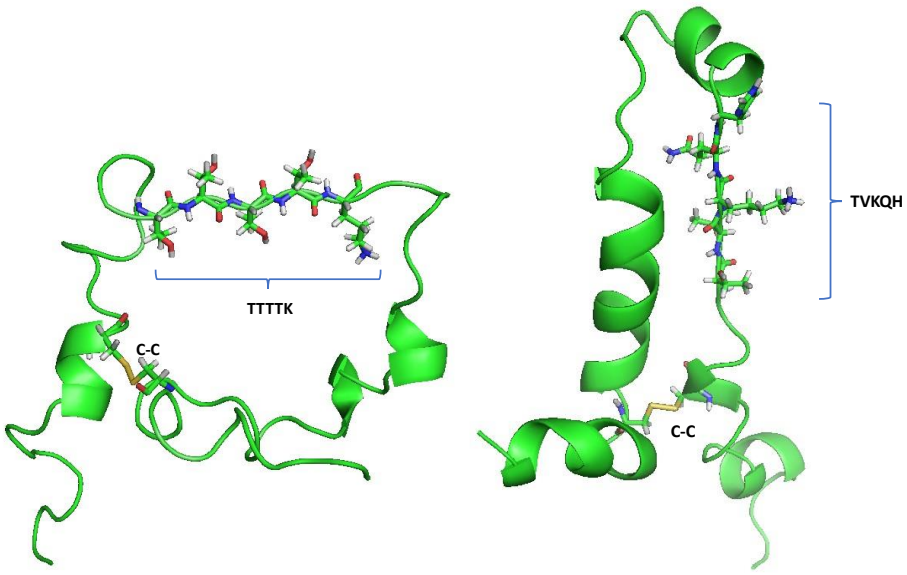

Figure 3.58: Only restrained TTTTK, TVKQH and NFTET showed β-sheet structure when restrained separately in different REMD simulations, the rest was in helical shape formation.

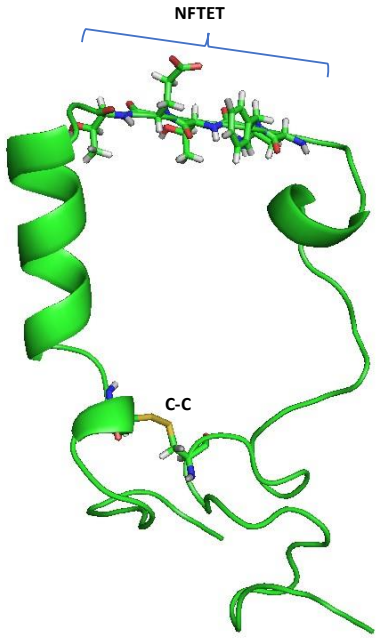

Figure 3.58 (continued): Only restrained TTTTK, TVKQH and NFTET showed β-sheet structure when restrained separately in different REMD simulations, the rest was in helical shape formation.

Instabilities in most of H3 and C-terminal end of H2, especially TTTT pattern, would determine the propensity to form aggregation prone PrP* state where the initial changes occur (Chen and Thirumalai, 2013). Our REMD studies of H2 and H3 showed that any β-strand formation at N-terminus of H2, H2-H3 loop and/or C-terminus of H3 resulted in extended formation of β-strands and β-sheet. Especially, any deformation in the integrity of H3 resulted in increased β-strand ratio. Unfolding of H3 might be the key point in the conversion of PrP^{C} to PrP^{Sc}. H3 and the loop between B2 and H1 (167-171) were found to be the candidate regions to promote transition from PrP^{C} to PrP^{Sc} (Zahn et al., 2000). Our results also confirmed that any change in H3 integrity after the bindig of diseased form might lead to this transition more easily.

PrP^{Sc} structure might be in 4-rung β-solenoid architecture (Spagnolli et al., 2019). So, dimerization potential of the two prelonged β-sheet structures, that were formed when we restrained KIMER and ETDIK sequences seperately, were also analyzed.

KIMER sequence in red color did not maintain a constant contact but instead other hydrogen bond and hyrophobic contacts were formed. ETDIK sequence in blue did not increase β-sheet contant but kept two monomers in a compact and stable structure with the help of hydrogen bonds and hydrophobic interactions between two monomers (Figure 3.59).

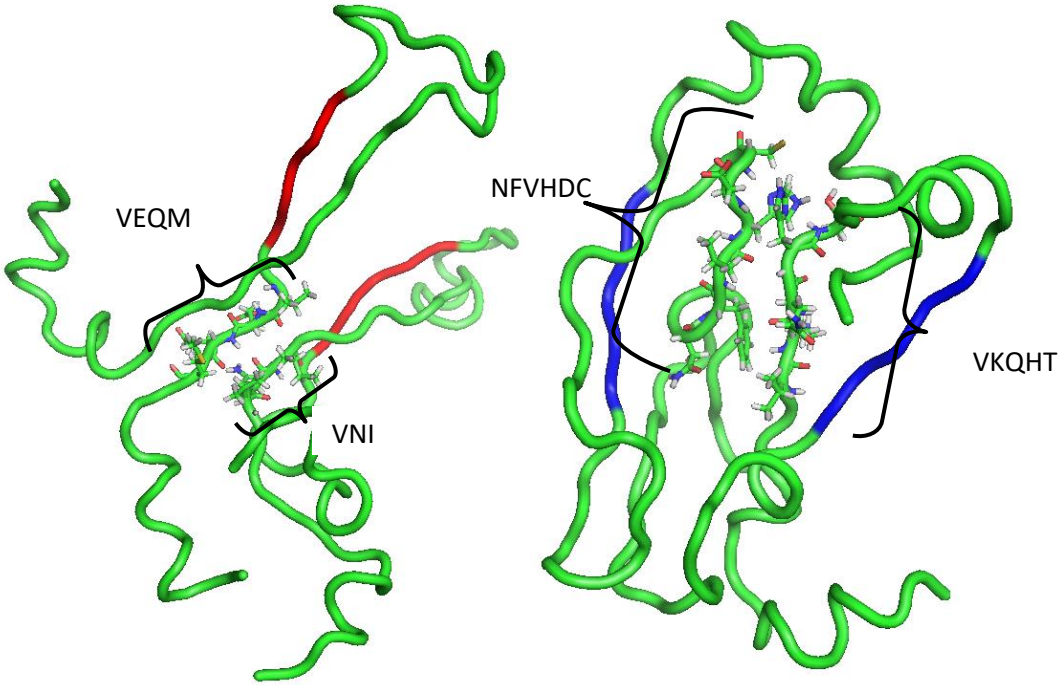

Figure 3.59: Dimerization potential of restrained KIMER and ETDIK.

4. CONCLUSION

Obtaining the misfolded structure of the prion protein is a difficult problem. The problem is complicated by the fact that PrP^{Sc} is stable only in the oligomeric form and more than one misfolded structures exist. On the other hand, experiments on the truncated prion fragments show that different parts of the protein can misfold and form fibrils. For instance, the sequence N-terminal to H1B1 loop and the sequence C–terminal to H1 give rise to fibrils even in the absence of each other. This observation suggests that interactions between these parts are limited. On the other hand, according to H/D exchange experiments, H1 and the H1B1 loop do not form an α-helix or a β-sheet in the misfolded structure whereas H1 is a very stable helix in PrP^{C}. Moreover, according to the experiments, a truncated H1 sequence also maintains a stable helical structure. Based on these experimental findings, we hypothesized that different prion regions can be studied separately or in the presence of only short fragments of other sequences. Thus, we studied using molecular dynamics simulations, the structure of H1 alone and in the presence of some hydrophilic prion sequences. Since H1 is the most hydrophilic helix in the protein data bank, we investigated its interactions only with other hydrophilic prion sequences. Our aim was to find the interactions that prevent the formation of a helical structure for the H1 sequence as in PrP^{Sc}.

To keep H1 unfolded other hydrophilic sequence like $\{H^{99}SQWNKPSKPKTNMK^{113}\}$ on the same or an adjacent prion protein might be the key for this transition to occur.

Our standard MD simulations at 310K and even at 330K showed that H1 was very stable, keeping its helical content. To do a better sampling, we continued our study with REMD. REMD simulations of H1 showed that only 0.8% of the trajectory was in a loop conformation. The structure of the helix was stabilized by salt bridges besides the usual backbone hydrogen bonds. On the other hand, the loop structure was mainly stabilized by a network of salt bridges whereas hydrogen bonds were only rarely and temporarily observed. As a result of another REMD simulation of loop H1 with the presence of the sequence $\{H^{99}SQWNKPSKPKTNMK^{113}\}$, the loop structure of H1 became abundant (96%). This sequence provided some advantage over others that we

had tried, it only contains positively charged amino acids and neutral ones, so when arginine residues of H1 liberated upon formation of salt bridges between fragments, they could not find negative charged residues to interact with. As a result, arginine residues kept their salt bridge interaction with negative residues of H1, protecting the loop structure. {H^{99}SQWNKPSKPKTNMK^{113}} sequence and H1 interacted with each other only by hydrogen bonds. However, in case of loop H1 interacting with another H1 (representing an adjacent monomer's) or another charged sequence as {K^{197}GENFTETDIKIMER^{211}}, which contain both positive and negative charges, loop structure was not protected, because those sequences had the ability to form salt bridges with charged residues of loop H1, so the loop content did not protected and lost its salt bridge network to become helix again.

As a PrP^{Sc} model, the in-register β-sheet model proposes that H1 sequences from different protomers must form β-sheet together. However, according to our results, H1 sequences from different monomers should not stack on top of each other as seen in in-register β-sheet model which will affect stability of the loop structure negatively. According to the results of our REMD of two adjacent H1 in close contact favored the helical structure.

Unfolding of prion protein seems to be eased by the low pH. Low pH conditions can be found at endosomal compartments inside the cell. So, by protonating the aspartic and/or glutamic acids of H1, we provided low pH conditions and made the helical structure more flexible. This might be the key in the unfolding process of H1, but in loop structure protonation of these residues should not occur since the stability of the loop H1 relies strictly on the salt bridges network.

As seen in our globular protein simulations, the most susceptible VRQ variant was the most unfolded structure at 330K where valine destabilized H1 with respect to H2-H3 core, but alanine did not cause such an impact. When the native β-sheet was not restrained, β1 separated from β2 in all variants but at 330K VRQ simulations, β1 dramatically moved away and did not move back to its original position. When native β-sheet was restrained, H1 moved away from H2H3 core at 330K very often but it moves back to its original position so quickly. It seems that, unstructured N-terminus of the prion protein might provide protection against the conversion by keeping β1 and H1 at their original position.

MD and REMD studies would provide valuable information about the rules of $PrP^{C} \rightarrow PrP^{Sc}$ transition, which will give ideas for designing novel therapeutic approaches that block the conversion and disease propagation. One of the the novel approaches might be to keep H1 stable in helix form to stop the progression of the transition. Also, understanding the mechanisms of aggregation and cell-to-cell transmission may provide further ideas about pharmaceutical interventions.

Stabilizing the structure of PrP^{C} by binding a drug or modifying the action of PrP^{Sc} oligomer or short polymer of PrP^{Sc} might be an option for the treatment.

Furthermore, how unfolded PrP^{C} forms dimers and turn into PrP^{Sc} should also be clarified to understand the mechanism of the disease better.

REFERENCES

Adrover, M., Pauwels, K., Prigent, S., de Chiara, C., Xu, Z., Chapuis, C., Pastore, A., and Rezaei, H. (2010). Prion Fibrillization Is Mediated by a Native Structural Element That Comprises Helices H2 and H3, *The Journal of Biological Chemistry*, **285-27**, 21004–21012.

Aguzzi, A. (2006). Prion diseases of humans and farm animals: epidemiology, genetics, and pathogenesis, *Journal of Neurochemistry*, **97**, 1726–1739.

Baillod, P., Garrec, J., Colombo, M., Tavernelli, I., and Rothlisberger, U. (2012) Enhanced Sampling Molecular Dynamics Identifies PrP^{Sc} Structures Harboring a C-Terminal β-Core, *Biochemistr*, **51**, 9891−9899.

Bocharova, O. V., Breydo, L., Salnikov, V. V., Gill, A. C., and Baskakov, I, V. (2005). Synthetic prions generated in vitro are similar to a newly identified subpopulation of PrP^{Sc} from sporadic Creutzfeldt-Jakob Disease, *Protein Science*, **14**,1222–1232.

Borgohain, G., Dan, N., Paul, S. (2016). Use of molecular dynamics simulation to explore structural facets of human prion protein with pathogenic mutations, *Biophysical Chemistry*, **213**, 32–39.

Caldarulo, E., Barducci, A., Wuthrichd, K., and Parrinello, M. (2017). Prion protein β2–α2 loop conformational landscape, *PNAS*, **114-36**, 9617–9622.

Chakroun, N., Fornili, A., Prigent, S., Kleinjung, J., Dreiss, C. A., Rezaei, H., and Fraternali, F. (2013). Decrypting Prion Protein Conversion into a β-Rich Conformer by Molecular Dynamics, *Journal of Chemical Theory and Computation*, **9**, 2455−2465.

Chebaro, Y., and Derreumaux, P. (2009). The Conversion of Helix H2 to _-Sheet Is Accelerated in the Monomer and Dimer of the Prion Protein upon T183A Mutation, *The Journal of Physical Chemistry B*, **113**, 6942-6948.

Chen K., Xu, M., Wedemeyer W. J., and Roder H. (2011). Microsecond Unfolding Kinetics of Sheep Prion Protein Reveals an Intermediate that Correlates with Susceptibility to Classical Scrapie, *Biophysical Journal*, **101**, 1221–1230.

Cheng, C. J., and Daggett, V. (2014). Molecular Dynamics Simulations Capture the Misfolding of the Bovine Prion Protein at Acidic pH, *Biomolecules*, **4**, 181-201.

Chen, J., and Thirumalai, D. (2013). Helices 2 and 3 are the initiation sites in the $PrP^{C} \rightarrow PrP^{Sc}$ transition, *Biochemistry*, **52(2)**, 310–319.

Choi, J., Cali, I., Surewicz, K., Kong, Q., Gambetti, P., and Surewicz, W. K. (2016). Amyloid fibrils from the N-terminal prion protein fragment are infectious, *PNAS*, **113-48**, 13851–13856.

Cobb, N. J., Sönnichsen, F. D., Mchaourab, H., and Surewicz, W. K. (2007). Molecular architecture of human prion protein amyloid: A parallel, in-register β-structure, *PNAS*, **104-48**, 18946–18951.

Colacino, S., Tiana, G., Broglia, R. A., and Colombo, G. (2006). The Determinants of Stability in the Human Prion Protein: Insights into Folding and Misfolding from the Analysis of the Change in the Stabilization Energy Distribution in Different Conditions, *PROTEINS: Structure, Function, and Bioinformatics*, **62**, 698–707.

Collu, F., Spiga, E., Chakroun, N., Rezaei, H., and Fraternali, F. (2018). Probing the early stages of prion protein (PrP) aggregation with atomistic molecular dynamics simulations, *The Royal Society of Chemistry*, **54**, 8007-8010.

Cosseddu, G. M., Agrimi, U., Pinto, J., and Schudel, A. A. (2007). Advances in scrapie research, *Rev. sci. tech. Off. int. Epiz.*, **26(3)**, 657-668.

De Simone, A., Zagari, A., and Derreumaux, P. (2007). Structural and Hydration Properties of the Partially Unfolded States of the Prion Protein, *Biophysical Journal*, **93**, 1284–1292.

Deleault, N. R., Harris, B. T., Rees, J. R., and Supattapone, S. (2007). Formation of native prions from minimal components in vitro, *PNAS*, **104-23**, 9741–9746.

DeMarco, M. L., and Daggett, V. (2004). From conversion to aggregation: Protofibril formation of the prion protein, *PNAS*, **101:8**, 2293–2298.

Diaz-Espinoza, R., and Soto, C. (2012). High-Resolution Structure Of Infectious Prion Protein: The Final Frontier, *Nature Structural & Molecular Biology*, **19/4**, 370-377.

Dima, R. I., and Thirumalai, D. (2004). Probing the instabilities in the dynamics of helical fragments from mouse PrP^{C}, *PNAS*, **101:43**, 15335–15340.

Ding, H., Schauerte, J. A., Steel, D. G., and Gafni, A. (2012). β-Amyloid (1–40) Peptide Interactions with Supported Phospholipid Membranes: A Single-Molecule Study, *Biophysical Journal*, **103**, 1500–1509.

El-Bastawissy, E., Knaggs, M. H., Gilbert, I. H. (2001). Molecular dynamics simulations of wild-type and point mutation human prion protein at normal and elevated temperature, *Journal of Molecular Graphics and Modelling*, **20**, 145–154.

Frost, B., and Diamond, M. I. (2010). Prion-like Mechanisms in Neurodegenerative Diseases, *Nature Review Neuroscience*, **11(3)**, 155–159.

Garrec, J., Tavernelli, I., Rothlisberger, U. (2013). Two Misfolding Routes for the Prion Protein around pH 4.5, *PLOS Computational Biology*, **9/5**.

Groveman, B. R., Dolan, M. A., Taubner, L. M., Kraus, A., Wickner, R. B., and Caughey, B. (2014). Parallel In-register Intermolecular β-Sheet Architectures for Prion-seeded Prion Protein (PrP) Amyloids, *The Journal of Biological Chemistry*, **289-35**, 24129–24142.

Groveman, B. R., Kraus, A., Raymond, L. D., Dolan, M. A., Anson, K. J., Dorward, D. W., and Caughey, B. (2015). Charge Neutralization of the Central Lysine Cluster in Prion Protein (PrP) Promotes PrP^{Sc}-like Folding of Recombinant PrP Amyloids, *The Journal of Biological Chemistry*, **290-2**, 1119–1128.

Guitart, K., Loers, G., Buck, F., Bork, U., Schachner, M., and Kleene, R. (2016). Improvement of Neuronal Cell Survival by Astrocyte-derived Exosomes Under Hypoxic and Ischemic Conditions Depends on Prion Protein, *GLIA*, **64**, 896-910.

Guo, B. B., Bellingham, S. A., and Hill, A. F. (2015). The Neutral Sphingomyelinase Pathway Regulates Packaging of the Prion Protein into Exosomes, *The Journal of Biological Chemistry*, **290-6**, 3455–3467.

Guo, J., Ren, H., Ning, L., Liu, H., Yao, X. (2012). Exploring structural and thermodynamic stabilities of human prion protein pathogenic mutants D202N, E211Q and Q217R, *Journal of Structural Biology*, **178**, 225–232.

Hartmann, A., Muth, C., Dabrowski, O., Krasemann, S., and Glatzel, M. (2017). Exosomes and the Prion Protein: More than One Truth, *Frontiers in Neuroscience*, **11.**

Head, M. W., and Ironside, J. W. (2012). Review: Creutzfeldt–Jakob disease: prion protein type, disease phenotype and agent strain, *Neuropathology and Applied Neurobiology*, **38**, 296–310.

Hosszu, L. L. P., Tattum, M. H., Jones, S., Trevitt, C. R., Wells, M. A., Waltho, J. P., Collinge, J., Jackson, G. S., and Clarke, A. R. (2010). The H187R Mutation of the Human Prion Protein Induces Conversion of Recombinant Prion Protein to the PrP^{Sc}-like Form, *Biochemistry*, **49**, 8729–8738.

Hsiao, K., Meiner, Z., Kahana, E., Cass, C., Kahana, I., Avrahami, D., Scarlato, G., Abramsky, O., Prusiner, S. B., and Gabizon, R. (1991).mMutation of the Prion Protein in Libyan Jews with Creutzfeldt–Jakob Disease, *The New England Journal of Medicine*, **324**, 1091-1097.

Jucker, M., and Walker, L. C. (2013). Self-propagation of pathogenic protein aggregates in neurodegenerative diseases, *Nature*, **501**(7465), 5–51.

Kaimann, T., Metzger, S., Kuhlmann, K., Brandt, B., Birkmann, E., Höltje, H. D., and Riesner, D. (2008). Molecular Model of an α-Helical Prion Protein Dimer and Its Monomeric Subunits as Derived from Chemical Cross-linking and Molecular Modeling Calculations, *Journal of Molecular Biology*, **376**, 582–596.

Kozin, S. A., Bertho, G., Mazur, A. K., Rabesona, H., Girault, J., Haertlé, T., Takahashi, M., Debey, P., and Hoa, G. H. B. (2001). Sheep Prion Protein Synthetic Peptide Spanning Helix 1 and β-Strand 2 (Residues 142–166) Shows β-Hairpin Structure in Solution, *The Journal of Biological Chemistry*, **276-49**, 46364–46370.

Kuwata, K., Li, H., Yamada, H., Legname, G., Prusiner, S. B., Akasaka, K., and James, T. L. (2002). Locally Disordered Conformer of the Hamster Prion Protein: A Crucial Intermediate to PrP^{Sc}, *Biochemistry*, **41**, 12277-12283

Larda, S. T., Simonetti, K., Al-Abdul-Wahid, M. S., Sharpe, S., and Prosser, R. S. (2013). Dynamic Equilibria between Monomeric and Oligomeric Misfolded States of the Mammalian Prion Protein Measured by 19F NMR, *Journal of American Chemical Society*, **135**, 10533−10541.

Lau, A. L., Yam, A. Y., Michelitsch, M. M. D., Wang, X., Gao, C., Goodson, R. J., Shimizu, R., Timoteo, G., Hall, J., Medina-Selby, A., Coit, D., McCoin, C., Phelps, B., Wu, P., Hu, C., Chien, D., and Peretz, D. (2007). Characterization of prion protein (PrP)-derived peptides that discriminate full-length PrP^{Sc} from PrP^{C}, *PNAS*, **104-28**, 11551–11556.

Lin, Y., and Pande, V. S. (2012). Effects of Familial Mutations on the Monomer Structure of Aβ42, *Biophysical Journal*, **103**, 47–49.

Linden, R. (2017). The Biological Function of the Prion Protein: A Cell Surface Scaffold of Signaling Modules, *Frontiers in Molecular Neuroscience*, **10**.

Liu, A., Riek, R., Zahn, R., Hornemann, S., Glockshuber, R., Wüthrich, K. (1999). Peptides and Proteins in Neurodegenerative Disease: Helix Propensity of a Polypeptide Containing Helix 1 of the Mouse Prion Protein Studied by NMR and CD Spectroscopy, *John Wiley & Sons Biopolymers*, **51**, 145–152.

Mead, S. (2006). Prion disease genetics, *European Journal of Human Genetics*, **14**, 273–281.

Morrissey, M. P., and Shakhnovich, E. I. (1999). Evidence for the role of PrP^{C} helix 1 in the hydrophilic seeding of prion aggregates, *PNAS*, **96**, 11293–11298.

Munoz-Montesino, C., Sizun, C., Moudjou, M., Herzog, L., Reine, F., Chapuis, J., Ciric, D., Igel-Egalon, A., Laude, H., Béringue, V., Rezaei, H., Dron, M. (2016). Generating Bona Fide Mammalian Prions with Internal Deletions, *Journal of Virology*, **90-15**.

Norstrom, E. M., and Mastrianni, J. A. (2006). The Charge Structure of Helix 1 in the Prion Protein Regulates Conversion to Pathogenic PrP^{Sc}, *Journal of Virology*, **80-17**, 8521–8529.

Novitskaya, V., Makarava, N., Bellon, A., Bocharova, O. V., Bronstein, I. B., Williamson, R. A., and Baskakov, I. V. (2006). Probing the Conformation of the Prion Protein within a Single Amyloid Fibril Using a Novel Immunoconformational Assay, *The Journal of Biological Chemistry*, **281-22**, 15536–15545.

Okur, A., Roe, D. R., Cui, G., Hornak, V., and Simmerling, C. (2007). Improving Convergence of Replica-Exchange Simulations through Coupling to a High-Temperature Structure Reservoir, *Joural of Chemical Theory and Computation*, **3**, 557-568.

Osborne, K. L., Bachmann, M., and Strodel, B. (2013). Thermodynamic analysis of structural transitions during GNNQQNY aggregation, *Proteins*, **81**,1141–1155.

Prusiner, S. B. (1998). Prions, *Proceedings of the National Academy of Sciences USA*, **95**, 13363–13383.

Requena, J. R., and Wille, H. (2014). The structure of the infectious prion protein, *Prion*, **8:1**, 60–66.

Ribeiro, A. A. S. T., and de Alencastro, R. B. (2013). Mixed Monte Carlo/Molecular Dynamics simulations of the prion protein, *Journal of Molecular Graphics and Modelling*, **42**, 1–6.

Riek, R., Hornemann, S., Wider, G., Billeter, M., Glockshuber, R., and Wutrich, K. (1996). NMR Structure of the mouse prion protein domain PrP (121-231), *Nature*, **382**, 180-182.

Roitberg, A. E., Okur, A., and Simmerling, C. (2007). Coupling of Replica Exchange Simulations to a Non-Boltzmann Structure Reservoir, *Journal Physical Chemistry B*, Vol. **111**, No. 10.

Ross, C. A., and Poirier, M. A. (2004). Protein Aggregation and Neurodegenerative Disease, *Nature Medicine*, **10-17**.

Rossetti, G., and Carloni, P. (2017). Structural Modeling of Human Prion Protein`s Point Mutations, *Progress in Molecular Biology and Translational Science, Elsevier Inc.*, **150**, 1877-1173.

Sakudo, A., Xue, G., Kawashita, N., Ano, Y., Takagi, T., Shintani, H., Tanaka, Y., Onodera, T., and Ikuta, K. (2010). Structure of the Prion Protein and Its Gene: An Analysis Using Bioinformatics and Computer Simulation, *Current Protein and Peptide Science*, **11**.

Sepulveda, M., Rozas, P., Hetz, C., and Medinas, D. B. (2016). ERp57 as a novel cellular factor controlling prion protein biosynthesis: Therapeutic potential of protein disulfide isomerases, *Taylor and Francis*, **10**, 50–56.

Shamsir, M. S., and Dalby, A. R. (2005). One Gene, Two Diseases and Three Conformations: Molecular Dynamics Simulations of Mutants of Human Prion Protein at Room Temperature and Elevated Temperatures, *PROTEINS: Structure, Function, and Bioinformatics*, **59**, 275–290.

Silva, C. J., Vázquez-Fernández, E., Onisko, B., Requena, J. R. (2015). Proteinase K and the structure of PrP^{Sc}: The good, the bad and the ugly, *Virus Research*, **207**, 120–126.

Silveira, J. R., Raymond, G. J., Hughson, A. G., Race, R. E., Sim, V. L., Hayes, S. F., and Caughey, B. (2005). The most infectious prion protein particles, *Nature*, **437**, 257-261.

Singh, J., and Udgaonkar, J. B. (2013). Dissection of Conformational Conversion Events during Prion Amyloid Fibril Formation Using Hydrogen Exchange and Mass Spectrometry, *Elsevier Journal of Molecular Biology*, **425**, 3510–3521.

Singh, J., and Udgaonkar, J. B. (2015a). Molecular Mechanism of the Misfolding and Oligomerization of the Prion Protein: Current Understanding and Its Implications, *Biochemistry*, **54**, 4431−4442.

Singh, J., and Udgaonkar, J. B. (2015b). Structural Effects of Multiple Pathogenic Mutations Suggest a Model for the Initiation of Misfolding of the Prion Protein, *Angew. Chem. Int.Ed.*, **54**, 7529–7533.

Singh, J., Kumar, H., Sabareesan, A. T., and Udgaonkar, J. B. (2014). Rational Stabilization of Helix 2 of the Prion Protein Prevents Its Misfolding and Oligomerization, *Journal of American Chemical Society*, **136**, 16704−16707.

Singh, J., Sabareesan, A. T., Mathew, M. K., and Udgaonkar, J. B. (2012). Development of the Structural Core and of Conformational Heterogeneity during the Conversion of Oligomers of the Mouse Prion Protein to Worm-like Amyloid Fibrils, *Journal of Molecular Biology*, **423**, 217–231.

Singh, R. K., Chamachi, N. G., Chakrabarty, S., and Mukherjee, A. (2017). Mechanism of Unfolding of Human Prion Protein, *Journal of Physical Chemistry B*, **121**, 550−564.

Smirnovas, V., Kim, J., Lu, X., Atarashi, R., Caughey, B., and Surewicz, W. K. (2009). Distinct Structures of Scrapie Prion Protein (PrP^{Sc})-seeded Versus Spontaneous Recombinant Prion Protein Fibrils Revealed by Hydrogen/Deuterium Exchange, *The Journal of Biological Chemistry*, **284-36**, 24233–24241.

Soto, C. (2012). Transmissible Proteins: Expanding the Prion Heresy, *Cell*, **149**, 968-977.

Spagnolli, G., Rigoli, M., Orioli, S., Sevillano, A. M., Faccioli, P., Wille, H., Biasini, E., and Requena, J. R. (2019). Full atomistic model of prion structure and conversion, *PLOS Pathogens*.

Speare, J. O., Rush III, T. S., Bloom, M. E., and Caughey, B. (2003). The Role of Helix 1 Aspartates and Salt Bridges in the Stability and Conversion of Prion Protein, *The Journal of Biological Chemistry*, **278-14**, 12522–12529.

Stahl, N., Baldwin, M. A., Teplow, D. B., Hood, L., Gibson, B.W., Burlingame, A. L., and Prusiner, S. B. (1993). Structural studies of the scrapie prion protein using mass spectrometry and amino acid sequencing *Biochemistry*, **32**, 1991-2002.

Stöhr, J., Weinmann, N., Wille, H., Kaimann, T., Nagel-Steger, L., Birkmann, E., Panza, G., Prusiner, S. B., Eigen, M., and Riesner, D. (2008). Mechanisms of prion protein assembly into amyloid, *PNAS*, **105/7**, 2409–2414.

Taguchi, Y., and Schätzl, H. M. (2013). Identifying critical sites of PrP^{C}-PrP^{Sc} interaction in prion-infected cells by dominant-negative inhibition, *Prion*, **7:6**, 452–456.

Turnbaugh, J. A., Unterberger, U., Saa, P., Massignan, T., Fluharty, B. R., Bowman, F. P., Miller, M. B., Supattapone, S., Biasini, E., and Harris, D. A. (2012). The N-Terminal, Polybasic Region of PrP^{C} Dictates the Efficiency of Prion Propagation by Binding to PrP^{Sc}, *The Journal of Neuroscience*, **32(26)**, 8817– 8830.

Van der Kamp, M. W., and Daggett, V. (2009). The consequences of pathogenic mutations to the human prion protein, *Protein Engineering, Design & Selection*, **22-8**, 461–468.

Van der Kamp, M. W., and Daggett, V. (2011). Molecular Dynamics as an Approach to Study Prion Protein Misfolding and the Effect of Pathogenic Mutations, *Topics in Current Chemistry*, **305**, 169–198.

Vila-Viçosa, D., Campos, S. R. R., Baptista, A. M., and Machuqueiro, M. (2012). Reversibility of Prion Misfolding: Insights from Constant-pH Molecular Dynamics Simulations, *The Journal of Physical Chemistry B*, **116**, 8812−8821.

Wadsworth, J. D. F., Hill, A. F., Beck, J. A., and Collinge, J. (2003). Molecular and clinical classification of human prion disease, *British Medical Bulletin*, **66**, 241–254.

Wang, F., Wang, X., Yuan, C., Ma, J. (2010). Generating a Prion with Bacterially Expressed Recombinant Prion Protein, *Science*, **327**.

Watzlawik, J., Skora, L., Frense, D., Griesinger, C., Zweckstetter, M., Schulz-Schaeffer, W. J., and Kramer, M. L. (2006). Prion Protein Helix1 Promotes Aggregation but Is Not Converted into β-Sheet, *The Journal of Biological Chemistry*, **281-40**, 30242–30250.

Winklhofer, K. F., Heske, J., Heller, U., Reintjes, A., Muranyi, W., Moarefi, I., and Tatzel, J. (2003). Determinants of the in Vivo Folding of the Prion Protein, *The Journal of Biological Chemistry*, **278-17**, 14961–14970.

Yang, C., Lo, W., Kuo, Y., Sang, J. C., Lee, C., Chiang, Y., and Chen, R.P. (2015). Revealing Structural Changes of Prion Protein during Conversion from α-Helical Monomer to β-Oligomers by Means of ESR and Nanochannel Encapsulation, *American Chemical Society*, **10**, 493−501.

Zahn, R., Liu, A., Lührs, T., Riek, R., von Schroetter, C., Garcia, F. L., Billeter, M., Calzolai, L., Wider, G., and Wüthrich, K. (2000). NMR solution structure of the human prion protein, *PNAS*, **97-1**, 145–150.

Zhang, J., Wang, F., and Chatterjee, S. (2016). Molecular dynamics studies on the buffalo prion protein, *Journal of Biomolecular Structure and Dynamics*, **34:4**, 762–777.

Zhang, J., Wang, F., and Zhang, Y. (2015). Molecular dynamics studies on the NMR structures of rabbit prion protein wild type and mutants: surface electrostatic charge distributions, *Journal of Biomolecular Structure and Dynamics*, **33-6**, 1326–1335.

Ziegler, J., Sticht, H., Marx, U. C., Müller, W., Rösch, P., and Schwarzinger, S. (2003). CD and NMR Studies of Prion Protein (PrP) Helix 1, *The Journal of Biological Chemistry*, **278-50**, 50175–50181.

CURRICULUM VITAE

Name Surname **:** Ayşenaz TAVŞANLI

EDUCATION **:**

- **B.Sc.** **:** 2008, Istanbul University, Faculty of Science and Literature, Biology Department
- **M.Sc.** **:** 2011, Istanbul Technical University, Faculty of Science and Literature, Molecular Biology-Genetics and Biotechnology Department

PROFESSIONAL EXPERIENCE AND REWARDS:

- 2018-2022 Onkim Stem Cell Technologies-Chief of Production
- 2015-2018 Onkim Stem Cell Technologies-Laboratory Personnel

PUBLICATIONS, PRESENTATIONS AND PATENTS ON THE THESIS:

- **Tavşanlı A.**, Keskin F. E., Balta B. 2017: 11th Triennial Congress of the World Association of Theoretical and Computational Chemists. International Congress, August 27 – September 1, 2017 Munich, Germany.
- **Tavşanlı A.**, Balta B. (2023). Conversion of Helix 1 into a Loop in Prion Protein Misfolding, *American Chemical Society Omega*, **8(7)**, 7191-7200. (DOI: 10.1021/acsomega.3c00212)